AN ABSTRACT OF THE THESIS OF

George F. Hall for the degree of Master of Science in Civil Engineering presented on May 21, 2012.

Title: Tidal Range Changes in the Delaware Bay: Past Conditions and Future Scenarios

Abstract approved:

_____

David F. Hill

Throughout the Holocene, appreciable changes in bathymetry are hypothesized to have resulted in large changes to tidal datums in coastal and estuarine areas. An understanding of tidal change is an important contribution to the knowledge of relative historical sea-level change and future coastal planning. To test this hypothesis, the Advanced Circulation (ADCIRC) model was used, with representative bathymetric grids based on glacial isostatic adjustment models and semi-empirical sea level rise predictions, in order to model the time-varying tidal behavior of the Delaware Bay. Model runs were conducted at various time slices between 10,000 years before present and 300 years into the future on high resolution grids that allowed for inundation moving forward in time. Open boundary tidal forcing was held constant in time to highlight the effect of the changing regional bathymetry. With each change in sea level, the shape of the Delaware Bay was considerably altered, leading to changes in the tides. Resonance and shallow water dissipation appeared to be the primary mechanisms behind these changes. Results showed that tidal ranges have nearly doubled in the upper Delaware Bay over the past 3000 years, while decreasing in the lower bay by 8%. Tidal range change represents a possible correction to past sea level rise estimates from the geologic record. Scenarios incorporating future sea level predictions primarily showed a small decrease in tidal range, potentially impacting future water levels and tidal sediment transport. Trends modeled were consistent with field measurements of relative change over similar time periods.

Tidal Range Changes in the Delaware Bay: Past Conditions and Future Scenarios

by

George F. Hall

A THESIS

submitted to

Oregon State University

in partial fulfillment of

the requirements for the

degree of

Master of Science

Presented May 21, 2012

Commencement June 2012

Master of Science thesis of George F. Hall presented on May 21, 2012.

APPROVED:

_____

Major Professor, representing Civil Engineering

_____

Head of the School of Civil and Construction Engineering

_____

Dean of the Graduate School

I understand that my thesis will become part of the permanent collection of Oregon State University libraries. My signature below authorizes release of my thesis to any reader upon request.

_____

George F. Hall, Author

ACKNOWLEDGEMENTS

I would like to expresses sincere appreciation for the wisdom and insight provided by Dr. David Hill throughout the process of this thesis as well as the postgraduate school experience. Contributions from Dr. Stephen Griffiths of Leeds University, UK, and Dr. Ben Horton and Dr. Simon Engelhart of the University of Pennsylvania, USA made this study possible and I would also like to acknowledge their assistance in interpreting these results. I would like to thank my committee members; Dr. Dan Cox, Dr. Jim Lerczak and Dr. Peter Ruggiero for their participation. I would also like to thank fellow graduate students John Dawson, Aaron Porter, Kyle Landon and Wei-Cheng Wu for their feedback both in drafting this work and throughout my postgraduate career in Coastal and Ocean Engineering at Oregon State University. Finally, I would like to acknowledge the U.S. Coast Guard's Officer Advanced Education Program in Ocean Engineering for allowing me to continue my education and further use it in a capacity to serve my country.

TABLE OF CONTENTS

TABLE OF CONTENTS (Continued)

TABLE OF CONTENTS (Continued)

LIST OF FIGURES

LIST OF FIGURES (Continued)

LIST OF TABLES

LIST OF ABBREVIATIONS, ACRONYMS AND SYMBOLS

Symbol	Description
ADCIRC	Advanced Circulation Model of Luettich and Westerink (1991)
ETOPO1	Topography data of NOAA (2011c)
f	Coriolis parameter
Fort.14	ADCIRC input grid file
Fort.15	ADCIRC input control file
Fort.53	ADCIRC output global harmonic analysis file
g	Acceleration due to gravity
GIA	Glacial Isostatic Adjustment
GT	Great diurnal range (mean higher high water less mean lower low water)
GWCE	Generalized wave continuity equation
H	Total depth of water column
ICE-(3G, 4G, 5G, 6G)	Model series of global ice sheet coverage found in Tushingham and Peltier (1991); Peltier (1994); Peltier (2004); Peltier (2010); Toscano, Peltier and Drummond. (2011), respectively.
K_1	Lunisolar diurnal tidal constituent
kyr	Thousand years
ka	Kilo-annum; thousand years before present
LGM	Last glacial maximum
M	Horizontal mixing term from Kolar and Grey (1990)
M_2	Lunar semidiurnal tidal constituent
M_4/M_6	Higher frequency overtides of the M_2 constituent
MHHW	Mean higher high water
MHWST	Mean high water spring tide
MLLW	Mean lower low water
MTL	Mean tide level
MSL	Mean sea level
NAVD88	North American vertical datum of 1988
NED	National elevation dataset of USGS (2011)
NGDC	National Geophysical Data Center

LIST OF ABBREVIATIONS, ACRONYMS AND SYMBOLS
(continued)

Symbol	Description
NOAA	National Ocean and Atmospheric Association
PADCIRC	Parallel ADCIRC
P_s	Atmospheric pressure at free surface
RMSE	Root mean squared error
RSLR	Relative sea level rise
S_2	Solar semidiurnal tidal constituent
SLIPs	Sea level index points
SLR	Sea level rise
SMS	Surface water Modeling System
t	Time
TPXO	Tide model of Egbert, et al. (1994)also called OSU model.
U	Depth integrated velocity in x direction
USGS	United States geological survey
V	Depth integrated velocity in y direction
VM (1, 2, 5a, 5b)	Model series of earth's mantle viscosity found in Tushingham and Peltier (1992), Peltier (2004), Toscano, Peltier and Drummond (2011), Engelhart, Peltier and Horton (2011), respectively.
WNAT	Western Atlantic Ocean grid of Mukai, et al. (2002)
+0.1kyr, +0.3kyr	100 and 300 years into the future
ζ	Distance between still water and free surface
ρ_0	Reference density of water
τ_0	Dissipative factor in the GWCE (also called tau0)
τ_b	Bottom stress

TIDAL RANGE CHANGES IN THE DELAWARE BAY: PAST CONDITIONS AND FUTURE SCENARIOS

Chapter 1 – Introduction

Studies of sea level from the past and predictions for the future reflect changes that are appreciable enough to alter the behavior of the tides. The premise of this study is that tides change in response to altered bathymetric depths associated with sea level changes and crustal deformations. These changes can have a regional impact but are often pronounced in estuaries and coastline areas where the effects of bathymetry on the tidal waves are amplified. A tidal signal must be accounted for when resolving sea levels from gauges or the geologic record; tidal changes therefore represent an important correction to estimates of past sea level change over century to millennial time scales. Tidal changes can also have direct impacts on the nearshore environment, such as increased inundation, so it is important to examine potential future scenarios and implications.

1.1 Tides and Tidal Range

Barotropic ocean tides are forced by the gravitational interactions and motions of the earth, moon and sun, and are heavily influenced by the shape of the basins in which they act. Distinguishing tides from other shorter time-scale water surface changes (i.e. waves, storm surge, temperature differences), these periodic oscillations in sea level occur on the order of hours, but cyclical changes in the tidal forcing are known to produce patterns up to 18.6 years long. Over periods on the order of many thousands of years, tides can change due to changes in external gravitational forcing. For example, the moon and earth have been said to be separating at 0.04m per year leading some to speculate that the tides are slowly decreasing with this separation (Pugh 1987).

Tides can be characterized by the measured or observed height of their wave, called tidal range. A known tidal range at a given location can be used to infer information about sea levels and currents. In order to examine the spatial patterns of tides at multiple locations, both the forcing and bathymetry must be properly accounted for. In shallow water areas, tidal behavior also depends on friction and other nonlinear actions. With sea level and bathymetric changes, tidal ranges are temporally variable, at intervals between their shorter cyclical or longer astronomical changes.

1.2 Sea Level Change

Geologic records indicate that there has been a temporally variable rise in global sea level since the most recent point at which a maximum amount of water was entrained in ice age glaciers, called the last glacial maximum (LGM), 20-21 thousand years ago (ka) (Milne, et al. 2009; Tushingham and Peltier 1991). Global and relative sea level changes since the LGM came from the exchange of mass between melting glaciers and the ocean, in addition to a process called glacial isostatic adjustment (GIA). While mass exchange is a global process, GIA is spatially variable; geographic areas that were once forced down by direct glacial coverage rise as the force decreases with a reduction in glacial weight. Adjacent areas of land subside as the crust of the earth seeks equilibrium in the region. This process is slowed in time by the viscosity of the earth's mantle allowing GIA to act over thousands of years after changes to the glacial mass.

The first mean sea level (MSL) measurements were made in Brest, UK in 1807; however high and low water tidal marks were measured as far back as 1682-1774 in Amsterdam and Stockholm (Pugh 1987). Modern sea levels and tides are measured using tide gauges, which are often placed in sheltered harbors, away from the influence of higher frequency waves and near areas of marine traffic interest. Information about the sea and tide levels also comes from satellite observations. These combined measurements show that sea level changes are spatially variable even on a shorter time scale than GIA (Cazenave and Llovel 2010). While GIA still impacts the present day sea levels, changes in gauge data reflect other processes as the sea level, coastline shapes and nearshore bathymetry are altered by human actions. On a larger scale, observations of modern sea level, coupled with measurements of global temperature increase, indicate that we are currently in a period of accelerated sea level rise with predictions of a further global rise on the order of one meter in the next 100 years (Rahmstorf, Perrette and Vermeer 2011).

1.3 Tidal Range Change

While many climate change studies reflect the changes in sea level as the cornerstone measure of future sea conditions, other processes can be impacted. The sea level changes associated with periods of the past and future represent changes to the ocean basins on a global, regional and local scale. It should then follow that tides would change in association.

However, data to support these changes in tidal range are not easily read from gauges or geologic record.

Recent advancements have been made in satellite imaging, but most present day tides are only measured at certain gauge locations; the historical records of which often only go back several decades. To close this coverage gap, numerical models of the components of tides have been advanced to the point that they accurately predict the tidal signal of present day. The Western Atlantic tidal database (WNAT), (Mukai, et al. 2002) and the TPXO series (Egbert, Bennett and Foreman 1994) are two examples of verified present day regional and global tidal models. For these models to function properly, they are run over a grid representing bathymetry at an appropriate scale; often one of high resolution.

Since tide gauge data is not available on the millennia scale, nor are gauges able to predict the future, hydrodynamic models can be run over bathymetric grids that are representative of the shape of a given body of water at certain times. Using a grid with present day bathymetry as a starting point, sea levels can be raised or lowered. While spatially uniform sea level changes can be imposed to coincide with estimates, a better understanding of the effects of spatial variability can be obtained by basing the changes on a model of GIA. Certain hydrodynamic models use wetting and drying algorithms; allowing for the horizontal waterline retreat or inundation associated with vertical sea level changes. Moving forward in time, locations dry at some point can become part of the intertidal zone and then fully inundated. Inundation can be defined as when a location is submerged throughout the tidal cycle enabling a model to resolve the tidal range. The results of these models can then be used to analyze past or future tide scenarios. At times other than present day, however, verifications of these models are difficult due to the lack of measured data.

Model and gauge water surface elevation time-series data analysis can give more information about the tides. Harmonic analysis consists of deconstructing the tidal signal wave into individual waves that consist of an amplitude and frequency. These individual waves are known as tidal constituents, each representing the influence of a specific interaction. Constituents of lower frequency (i.e. K_1, M_2) represent the interactions of the celestial bodies and earth (diurnal and semidiurnal, respectively). Higher order, and higher

frequency, constituents are based on other, often non-linear interactions of constituents and themselves or their boundary conditions. In a semi-diurnal tidal environment, the M_4 and M_6 constituents often have the strongest signal of the higher order tides, and are based on nonlinear interactions of M_2 waves with themselves and friction, respectively (Parker 1991). These constituents have periods that are exact multiples of that of the M_2 and are also called overtides. Overtides become more important in coastal and estuarine zones, and can be assumed negligible in the open ocean. In many cases, models will use only specific constituents to represent tidal forcing. Constituents can be used to calculate otherwise measurable datums such as mean higher high water (MHHW), mean lower low water (MLLW). From these datums, tidal range can be calculated; in the case of the difference between MHHW and MLLW, this is referred as the great diurnal range (GT).

1.4 Impacts of Tidal Range Change

With future tidal range changes, relative water levels would also change; shifting the extent to which water reaches the land and potentially impacting the coastal system. Coincidence of future storm events with higher high tide levels may result in further inland inundation. Pickering, et al. (2012) claimed that future climate change driven coastal planning should take tidal range change into effect when calculating flood risk and storm surge, while others have said that changes in surge and tides may actually offset (Sterl, et al. 2009). Similar changes tidal range may cause shifts in the low tide that could impact harbor depths required for port operations and/or dredging requirements. Tidal range change can be a mechanism for bay formation when a bathymetric response is considered. Here, small basins near tidal resonance with a shallow depth have larger tidal ranges and therefore larger magnitude tidal currents. These currents may directly induce sediment transport in one direction or another allowing for coastal erosion until the basin became larger and the basin falls out of resonance with the tides (Pugh 1987). Gerritsen and Berentsen (1998) developed a method for modeling the variations on erosional patterns caused by changes in tidal behavior. Changes in the spatial distribution of the tides may also affect internal waves and vertical mixing, potentially affecting the salinity of the environment (Jay 2009). Green (2010) proposed that future sea level changes could have exponentially large effects on regional shelf tides altering the chemistry, biology and sediment transport in the coastal environment.

The study of past tidal range change provides a baseline for understanding these tidally influenced processes prior to major anthropogenic influences. Past tidal ranges also play a major role in sea level rise estimates from the time period of the Holocene, or 10ka until today. Geologic records of sea level at individual locations often come from sea level index points (SLIPs). A SLIP must have a geographic location, age and a vertical relationship with respect to some tidal datum, this relationship is called indicative meaning (Van De Plassche 1986). Often, SLIPs are established from found organic matter that is known to grow at or around a tidal datum. The majority of samples used to reconstruct Holocene sea level change form close to mean high water at spring tide (MHWST), but a variety of other datums are used with different samples (Shennan, et al. 2000). Specific samples are located, dated and then used to eventually form a network of SLIPs. With different indicative meaning, a relating tidal datum must be used to connect multiple points and observe trends (I. Shennan 1986).

Figure 1 is a sketch of a beach and offshore vertical tide marker. An example cross section of organic matter that is known at present day to reside at the MHHW datum is shown as the upper green box. Present day reference datums can be observed or measured and are shown; MLLW, mean tidal level (MTL) and GT with the solid lines and subscript "0". Suppose that the same type of organic matter is found at the same geographic location at a lower elevation and dated to 5ka, as in the lower green box. Without the understanding of tidal range change in many localities, it is common to assume that GT *has not* changed. When this is the case, tidal datums are simply shifted down based on present day GT (dotted lines, subscript 5(a)). These dashed lines provide information on the sea level at 5ka. Using MTL to relate the two measurements, relative sea level rise ($RSLR_{5(a)}$) can be calculated as the difference between the two datums.

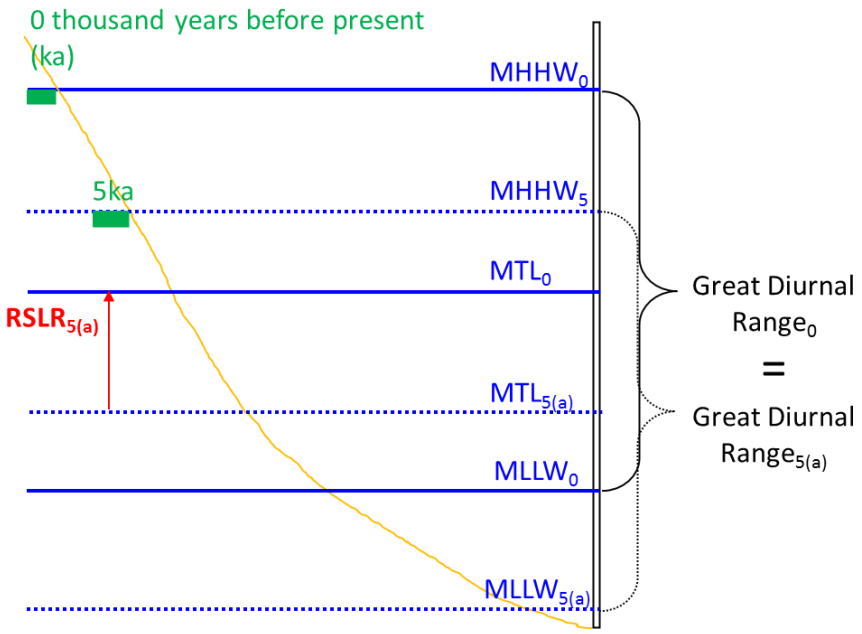

Figure 1: Sketch of tidal datums based on an example sea level index point assuming no GT change between 5 and 0ka.

If GT *has* changed, the relationship between the MTL_0 and MTL_5 can change significantly. Figure 2 shows an example of the case where tidal range at 5ka is smaller than present day. Here, the MTL datum formed by the smaller GT (denoted with subscript 5(b) and dashed lines), is closer to the MTL_0 datum indicating a smaller RSLR. In this case, the RSLR difference between constant GT (a), and changing GT (b) is half of the difference between the respective GTs. Depending on the datums involved for a given location with multiple SLIPs, the difference in RSLR estimates can be anywhere from no change to the total amount of GT difference. Among other errors in the assessment of SLIPs, an improperly accounted for GT can have an especially large effect in macrotidal environments (I. Shennan 1986). Holocene tidal range change is therefore best implemented as a spatially variable corrective factor to individual SLIPs (Shennan and Horton 2002)

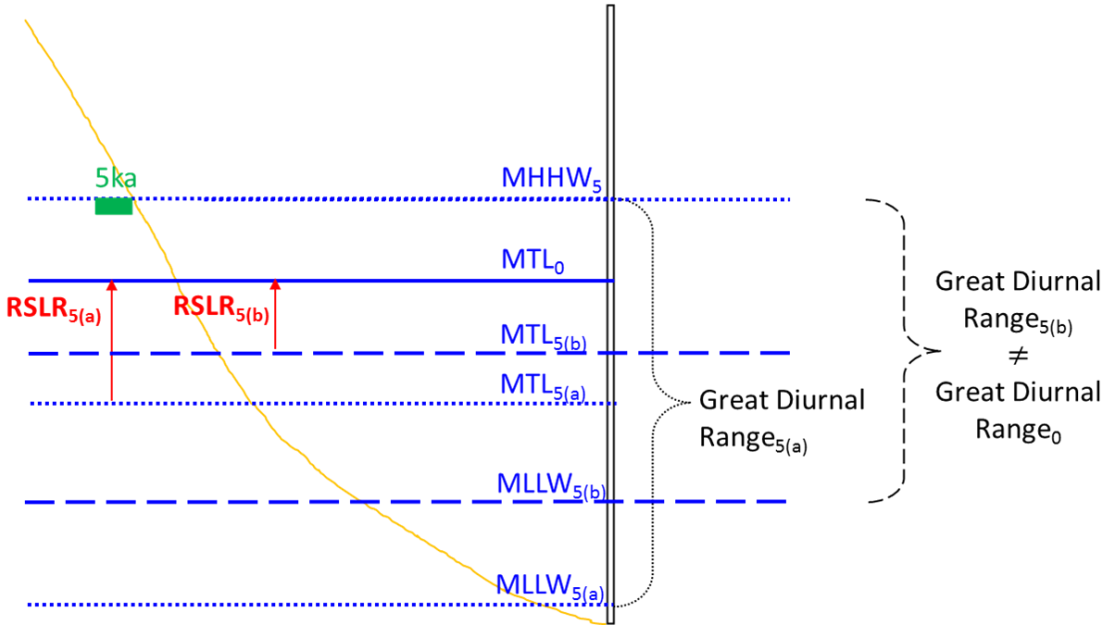

Figure 2: Sketch of tidal datums based on an example sea level index point with GT change between 5 and 0ka.

Chapter 2 – Literature Review

2.1 Study Area

This study modeled the regional and local effects of SLR on GT change. The Delaware Bay represented the subject study area, but this study used an expanded coverage to examine trends in the Northwest Atlantic Ocean as well. The Delaware Bay is a large coastal plain estuary located on the Mid-Atlantic coast of the United States. Figure 3 shows the geographic location of the estuary and adjacent regional area of the Atlantic Ocean. The bay is formed between the Delaware River and Atlantic Ocean and can be divided into lower bay, upper bay and river sections based on cross sectional areas and locations chosen based on Walters (1997) and Fletcher, Knebel and Kraft (1990) (Figure 3). The bay has a shallow average depth of less than 5m but a deeper relict river channel runs through the center with areas of depth greater than 10m (Walters 1997).

Within an estuary of moderate depth like the Delaware, independent tides, caused by cosmic forcing on the body of water itself, are often much less important than co-oscillating tides caused by communication with the ocean through the inlet (Officer 1976). In the Delaware Bay, these co-oscillating tidal influences in the river reach as far north as Trenton, NJ (Fletcher, Knebel and Kraft 1990). With a mostly progressive tidal wave in the upper bay, the Delaware behaves like a classic funnel shaped 'long estuary' (Wong and Sommerfield 2009). The M_2 constituent represents the dominant tidal forcing within the bay. The Delaware Bay tidal range is amplified, larger than that of the adjacent continental shelf as opposed to the Chesapeake Bay which has a smaller range than the shelf (Zhong, Li and Foreman 2008).

At present day, the Delaware Bay is a semidiurnal mesotidal environment with variable GT between the upper and lower portions, 1.8m and 1.4m, respectively. Similar findings of tidal amplification in the bay head are found in other estuaries with a funnel shape close to a natural resonance period with semidiurnal or diurnal tides such as the Bay of Fundy and Gulf of California (Zhong, Li and Foreman 2008). Estuary tidal resonance can be estimated from a simple geometric representation, but depends on more complex geometries as well as bottom friction (Officer 1976). Walters (1997) used a frequency response model to show that the Delaware Bay estuary has a complex resonance with the

tides, varying between the river, upper and lower bay. This pattern results in diurnal tides being small and evenly distributed across the bay, while the semidiurnal tides show the larger amplification. Semidiurnal constituents are also generally greater moving west to east in the lower bay.

In the Delaware Bay, a large portion of the frictional damping in the river and upper bay is due to overtides and residual flows (Walters 1997). Bottom friction in the bay is not large enough to attenuate sea level between the upper and lower bay, but is important in the tidal dynamics (Wong and Sommerfield 2009). Friction is important in tidal analysis as it reduces the tidal range by shortening its wavelength and slowing wave propagation. With linear friction, higher frequency constituents would decrease more in amplitude while the propagation speed of lower frequency constituents is slowed; however, friction is non-linear (Parker 1991). The relationship of the M_6 overtide amplitude to that of the M_2 can be used to show the impact of bottom friction (Parker 1991).

Parker (1991) focused on the nonlinearities of an estuary; tides, wind and river inflow. The author used data and models of the Delaware Bay and, among other nonlinearities, showed the importance of friction terms in the momentum balance. His study showed that the $2MS_2$, $2MN_2$, M_2, N_2 and S_2 constituents were amplified moving from the bay mouth to river; however, the $2MS_2$ and $2MN_2$ constituents experience much greater amplification from non-linear effects. A major source of the present day M_4 tide in the Delaware Bay is nonlinear generation between interacting M_2 waves in the lower river (Walters 1997). Physically, the M_4 constituent acts to distort the tidal profile. Amplitude and phase relationships of the M_4 constituent can indicate the strength of dominance by either flood or ebb tidal currents in an estuary (Parker 1991).

The Delaware Bay is well mixed, but stratification can also play an important role in the hydrodynamics (Walters 1997). The tidal volume flux within the bay is nearly two orders of magnitude greater than that caused by either the mean river inflow or atmospheric effects such as wind generated setup (Wong and Sommerfield 2009).

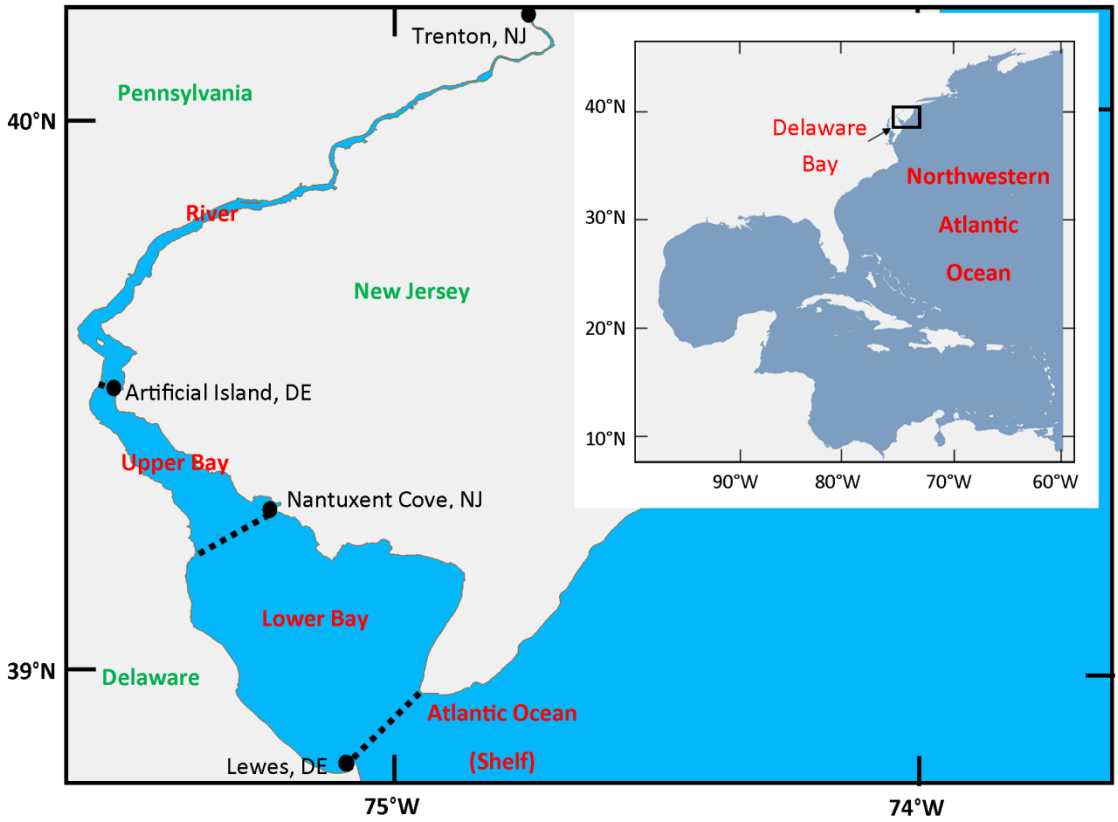

Figure 3: Sketch of Delaware Bay separated into general areas of river, upper, lower, shelf based on bay width.

2.2 Sea Level

In order to examine tidal range changes in the past and future, sea level scenarios corresponding to different times must be explored. These scenarios are important as they form the differing boundaries that the tidal hydrodynamics are subject to. Understanding the sea level estimates also allows the implementation of tidal range change corrections in SLIP data.

2.2.1 Holocene Sea Level Rise

Engelhart, et al. (2009) converted multiple Holocene SLIPs from different time slices into local SLR rates at 19 locations on the U.S. coast. The study used indicator information, making corrections for methodology, sample thickness, compaction and relation to the NAVD

88 vertical datum, but not tidal range change or GIA. From these results, trends of SLR rates at locations from 4 to 0ka indicate a significant amount of spatial variability. The maximum RSLR of 1.7+/- 0.2 mm/yr was recorded in the inner Delaware Bay as compared to 1.2+/- 0.2mm/yr in the outer bay. These locations are only about 50km apart, yet show this significant difference of 0.5mm/yr in SLR rates (Figure 4). This spatial variability highlights the importance of understanding processes such as GIA and tidal range change that act in conjunction with global SLR and may help account for the spatial differences.

Between the LGM and present day, the global sea level has risen approximately 120-125m from the effects of warming temperatures and changes in ice coverage (Peltier 1999; 2004). The global rise over this 20kyr period has been nonlinear, and can be generally divided into periods where the mechanisms and corresponding rates of sea level rise changed. Between 20 and 10ka, atmospheric temperature was unsteadily increasing; sea level change was marked by rapid spikes and dominated by the melting of ice that directly fed into the global oceans. During the Holocene, the rate of the initial melt off from the end of the LGM continued until 6ka when temperatures began to stabilize. From 6ka through the 19th century, with stable temperatures, mass exchange between the glaciers and ocean was significantly reduced, and the global rate of sea level rise was steady and small (Milne, et al. 2009). After 6ka and before recent increases in temperature, GIA became the dominant process in relative sea level rise in some locations (Peltier 1999).

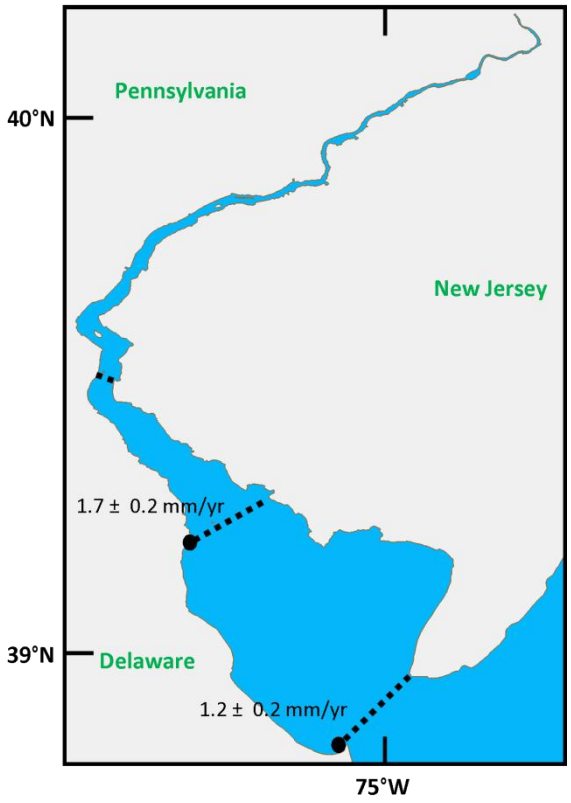

Figure 4: Sketch of Delaware with sea level rise rates in upper and lower bay (from Engelhart, et al. 2009).

2.2.2 Glacial Isostatic Adjustment Models

Models of paleo-bathymetry that account for glacial mass transfer and GIA offer robust solutions that can contribute to the understanding of the behavior of the Holocene ocean. These models can be further used to examine the GIA component of present day sea level changes. One such model is the combination of the ICE and VM series, where ICE represents global ice sheet reconstruction and VM refers to the modeling of the radial variation of the viscosity of the sub-lithospheric mantle. These models are based primarily on the Sea Level Equation as described in Peltier (1999). This equation takes into account the time dependent relationships of ocean, ice and land. ICE/VM models are used in combination to provide results for RSL predictions with the ICE coverage forcing the VM

response (Peltier 2004; Argus and Peltier 2010). Through the availability of new data, understanding, and technological improvements, a series of adjustments to each model have been made.

The VM viscosity models define the material properties of separate layers within the earth's mantle, which respond to the forcing of the ice sheets. VM1 was presented as a two layer model of the mantle with a lower viscosity value twice that of the upper (Tushingham and Peltier 1992; Argus and Peltier 2010). VM2 offered an improvement by using Holocene RSL data, mostly from northern Europe, to draw out a larger range of mantle viscosity values through the two layers (Peltier 2004). The VM5 model, also called VM5a, (Toscano, Peltier and Drummond 2011) was updated to address misfits of the VM2 model to GPS data of horizontal and vertical land motion. The VM5a model accounts for the stratification within a two layered lithosphere with both a highly viscous and elastic layer. It further separates the deeper portion of the mantle into three areas of different viscosity to form five total layers (Peltier and Drummond 2008). VM5b departed from VM5a in that its upper mantle layer and transition zone viscosity were reduced by a factor of 2 (Engelhart, Peltier and Horton 2011).

ICE-3G was created from RSL data sets that covered previously glaciated areas (Tushingham and Peltier 1991). It was then verified by combining it with VM1 to model response, and then comparing the results to indicators in non-glaciated areas (Tushingham and Peltier 1992). Important improvements to this model were based on data obtained on glacial coverage in northern America and Europe. ICE-4G improved on ICE-3G by incorporating different temporal variability in the Laurentide ice sheet and spatial variability in the Fennoscandian ice sheet, where the behavior of the Laurentide ice sheet dominated the GIA of the U.S. Atlantic Coast (Peltier 1994; Peltier 1996; Engelhart, Peltier and Horton 2011). ICE-5G departed significantly from the previous versions, by adding land-based ice mass on the North American continent, resulting in a modeled net eustatic, or uniform, SLR of 125m since the LGM, 5m more than previously estimated (Peltier 2004). The ICE-5G model was further verified with satellite observations (Peltier 2009) and improvements were made to adjust to further misfits. In Argus and Peltier (2010), more extensive comparisons of ICE-5G to data obtained from the satellite projects showed some misfits, specifically regarding the spatial variability of sheet thicknesses and a distribution of the Laurentide

glacier that was too small. The ICE-6G model made these corrections for a better fit (Toscano, Peltier and Drummond 2011).

The most recent combination of the ICE-6G/VM5b series was also specifically fit to the sea level data in the U.S. Atlantic Coast. Engelhart, Peltier and Horton (2011) offered a comparison of 686 sea level indicators to the four combinations of the VM5a and VM5b with the ICE-5G and ICE-6G with the combination of ICE-6G and VM5b providing the best correlation to the indicators. This data was obtained from SLIPs, but again *not* corrected for tidal range change. While the reduction in the viscosity of the VM5b performed better in the mid-Atlantic region of the U.S., the ICE-5G and 6G only offered small improvements due to the limited amount of present day influence. The discrepancies noted between the index points and VM5b model in Engelhart, Peltier and Horton (2011) showed variability between the inner and outer Delaware Bay similar to those in Engelhart, et al. (2009). The inner bay index points showed a strong correlation with the VM5b model while in the outer bay location, the model under-predicted the RSL from the index points. ICE-6G/VM5b and ICE-6G/VM5a will be further referenced as VM5b and VM5a, respectively, where the ICE-6G component is the same in both models.

2.2.3 Modern Sea Level Rise

An understanding of sea level history is important in making predictions about future SLR; however, measured changes in temperature are leading many to conclude that we are in a new era of accelerated SLR caused by anthropogenic influence (Cazenave and Llovel 2010). Contemporary global temperature rise and associated sea level fluctuations are items of current interest in the scientific community. A complete review of SLR hypotheses and potential scenarios will not be presented here. Instead, acknowledging that the mechanisms and predictions for the changes are heavily debated, the focus will be on a specific scenario that falls within a range of estimates.

When compared to prior estimates, recent models have projected increasingly higher rates of SLR based on an acceleration of ice melt and thermal expansion due to warming temperatures (Cazenave and Llovel 2010). In one such study, Rahmstorf, Perrette and Vermeer (2011) built on the work of similar predecessors, and examined a semi-physical relationship between sea level rise acceleration and temperature rise (predicted to be 1.8°C

by 2100). A model based on this relationship was then tuned to sea level data sets including SLIPs from 1 to 0ka, gauge data and satellite altimetry. In this scenario, the authors estimated that SLR by 2100 to be 101, 84, and 128 cm for median, 5^{th} and 95^{th} percentiles, respectively. Several other contemporary works give similar estimates with slightly lower and higher bounds (Cazenave and Llovel 2010). Others, such as Houston and Dean (2011), suggest a much lower bound of ~15cm SLR or less based on their findings of little evidence of SLR acceleration in gauge data.

2.3 Models of Tidal Range Change

Sea level changes drive tidal behavior through physical mechanisms that can be thought of in terms of resonance and energy damping. The dissipation of global tidal energy is considered primarily due to damping in shallow waters but can also be due to baroclinic internal tides and turbulence (Egbert and Ray 2000; Griffiths and Peltier 2009). At the LGM, with a reduced sea level of 120-125m from present day, the continental shelf was mostly dry (Peltier 2004; Egbert, et al. 2004; Uehara, et al. 2006; Griffiths and Peltier 2009; Green 2010). This suggests that the open ocean was then subject to less damping effects by these shallow water areas, allowing for greater tidal amplitudes and dissipation farther offshore. Damping of this type can also be caused by similar dissipation sites such as the Hudson Bay that may have, at some point in time been cut off, as described by Egbert and Ray (2000) and Arbic, et al. (2009). Moving forward into future SLR scenarios, wider shelf seas would add areas of relatively shallow water, which may then continue to reduce global tidal range.

Larger scale basin changes affect their natural frequencies and resonances with tidal waves. From a regional perspective, changes in the phase speed of a tidal wave can affect the location of amphidromic points, or node locations of zero tidal oscillation (Pickering, et al. 2012). Since tides are shallow water waves, their celerity is proportional to the square root of the depth, where celerity is speed, or a relationship of frequency and wavelength. Tides have constant frequency, so their wavelength is proportional to the square root of the depth. Simplified, amphidromic points can be related to standing waves in a basin where the nodal locations of no oscillation depend on the wavelength distance to the boundary (Pugh 1987). Changes in wavelength could then cause changes to these points, shifting the waves

themselves. Tidal range change models have previously been explored on global and regional scales. In these studies, simulations of past, present and future tides reveal location-specific changes in the tidal range.

2.3.1 Global Models

While several models of global paleo-tides have been constructed, here, we focus on studies of tidal range change on time scales on the order of hundreds to thousands of years. Several of these studies have used GIA models to drive the bathymetry over which their model is run. Thomas and Sündermann (1999) created a global M_2 constituent tide model, run over bathymetry representative of time slices since the LGM. Applying spatially variable changes in sea level rise, they used ICE-4G estimates. In their study, they noted the nonlinear changes of the M_2 tide in response to sea level changes. They also saw an increase in the global M_2 tidal dissipation between 15 and 8ka, where the dissipation signaled an increase in the global amplitude. Egbert, et al. (2004) also used ICE-4G transformations in a global tide model and found similar results. Their study emphasized the accuracy of the bathymetry as an important part of the proper solution; using perturbations and present day bathymetry tests, they determined that the results are highly sensitive to the bathymetry inputs.

Griffiths and Peltier (2009) included the tides of the polar oceans as well as the K_1 constituent in their model as opposed to Egbert, et al. (2004). They found that these oceans show amplifications in tidal ranges at the LGM from present day at the polar coasts. They showed that a higher resolution global model works better to account for dissipation using the ICE-5G transformations. A general agreement with other studies in higher dissipation at the LGM was seen.

Green (2010) created a global model focusing on the changes in tides due to varying bathymetry, sea levels, and bed friction in the continental shelf areas, exploring several damping scenarios. His study employed LGM and 0ka past conditions as well as future SLR scenarios of 1, 5, and 60m on the global ocean. Using model run results of sea level increases with and without shelf seas, he argued that larger tides during the LGM were due to the basin resonance allowed by decreased damping and not by changing propagation speed associated with shifts in amphidromic points. For future SLR scenarios, Green (2010) found that rises in 10s of meters of sea level had a significant effect on global dissipation rates.

Even the 1m SLR scenario had notable results for tidal range changes including areas of decrease in Severn and St. Malo on the European shelf. An increased sea level on the shelves led to weaker currents, weaker damping and higher tidal ranges. He also proposed that future tidal range change models should incorporate land topography to allow for dissipation instead of setting vertical walls as boundaries.

2.3.2 Regional Models

Several regional models have studied the Gulf of Maine in the northwestern Atlantic Ocean. This system has strongly amplified tides from the adjacent shelf, and contains the Bay of Fundy with the largest tidal range in the world. Scott and Greenberg (1983) presented a regional model of Holocene tidal range by modeling the M_2 constituent over bathymetries interpolated from past sea level curves. Their use of the M_2 constituent as representative of the tidal range was justified by their claim that it comprised 90% of the tidal signal in the system. Similar to global models, these authors found that tidal range response to SLR was non-linear. They further developed a method from which the sea level curves (based on SLIPs) could be corrected for tidal range change. Gehrels, et al. (1995) imposed changes to present day bathymetry based on sea level curves, and then forced their model with a temporally constant M_2 tide. An additional uniform raised sea level from present simulated a future scenario. Similar findings of non-linear response to the changes in elevation were prevalent as the tidal range increased from 5ka to present day as well as for the future estimate.

Other regional models focused on the macro-tidal environments in northern Europe. Hinton (1996) modeled the tidal range changes in the Northeast Atlantic Ocean and used the results to force smaller scale tidal models in Britain. His study modeled the M_2, S_2, μ_2, M_4, MS_4 and M_6 tidal constituents in sea levels that were uniformly lowered by up to 30m and raised by up to 5m from the present bathymetry, deciding not to assign ages to these levels. The author noted that the changes shifted the locations of numerous amphidromic points that also represented larger scale changes in the characteristics of the tidal wave. Changes in the tidal range were spatially variable showing a dependence on bathymetry and resonance. His study highlighted the importance of model grid size in regional and local tidal models (less than 1km was recommended) and the need to model multiple constituents and overtides as

opposed to just the M_2 due to the potential for a shift in dominance caused by the nonlinear behavior of tidal constituents in response to basin shape.

Shennan, et al. (2000) noted that Hinton (1996) was limited by the spatially uniform surface rising and lowering of the sea level. Instead, they based their bathymetric transformations on models of GIA for their analysis of the North Sea and found close correlation with the geological record. They additionally improved upon previous tidal models by using 26 constituents in their harmonic analysis. Their findings showed a nonlinear increase in tidal range throughout time. Shennan and Horton (2002) updated a sea level database taken from SLIPs around Great Britain noting areas of subsidence and uplift. They used paleo-bathymetries to model Holocene tidal range changes, noting that there are areas of small change on the open coast but significant changes in the large estuaries of the Humber and the Wash. In some areas, the difference between MHWST and MTL was nearly than 2.5m from that of present day. They applied these changes to the SLIPs, noting that for the most part, the tidal range changes and GIA models agreed. However, there were areas of conflicting results leading the authors to conclude that some estimates of GIA subsidence were over-estimated. Shennan, et al. (2003) made further improvements in the present day bathymetric information of the specific area. Both of these studies used temporally constant open boundary forcing.

Uehara, et al. (2006) modeled a larger region in the European shelf over paleo-bathymetries derived from different models including VM2 ICE-5G (Peltier 2004). These authors used both temporally fixed present day tidal forcing and temporally varying forcing obtained from global models. The impact of using temporally varying forcing was seen clearly in this region, leading the authors to conclude that evidence of major tidal range change on the shelf was a likely indication of changing oceanic tides instead of local bathymetry.

Pickering, et al. (2012) imposed a eustatic SLR of 2m and 10m to simulate future scenarios, modeling the M_2 tide on the northwest European Continental Shelf. They imposed a land, or vertical wall, boundary, not allowing inundation to occur assuming that engineered structures would act in opposition to inundation. Their results showed nonlinear interactions of SLR and tidal range changes with areas of increased and decreased tidal range. These

authors also used modern tide gauge data for comparison, finding spatial consistency with the trends modeled. In their regional focus, as opposed to Green (2010), they noted that increases and decreases in tidal range were primarily seen due to increases in phase speed and shifting amphidromic points while damping in shallow waters played a slightly less-significant role. They found tidal range changes smaller in magnitude than SLR, but large enough to have their own impact. These authors concluded that grid spacing was important in climate change studies noting that other studies were perhaps too coarse.

Hill, et al. (2011) explored a nested global and regional model of the northwestern Atlantic Ocean to examine Holocene tidal range changes. Global and regional bathymetries were transformed based on the ICE-5G/VM5a models at 1kyr intervals back to 10ka. Global results were similar to the findings in Griffiths and Peltier (2009), finding significant change in the semidiurnal components of global tides that coincided with the period of initial warming and eustatic sea level rise in the Holocene (10 to 6ka). Barotropic regional results were obtained by using the Advanced Circulation model (ADCIRC) (Luettich and Westerink 1991). In their regional results, they found that tidal ranges in the Northwestern Atlantic Ocean were 2 to 3 times greater than the ranges of present day, reflecting an amplitude change of the M_2 constituent and comparing well with other global models. They showed that the natural frequency of the Atlantic Ocean at 9ka was reduced bringing it closer to the period of the M_2 tide. Aside from the large spike around 9ka, little significant change in either the global or regional tides was seen in this study.

2.3.3 Local Models

In a shallow estuary, resonance with the tides again depends on the shape characteristics of the basin while damping can occur on smaller scales in areas such as tidal flats (Officer 1976). In these cases, sea level changes on the order of meters represent large relative changes to otherwise moderate estuary depths. It is hypothesized in this study that mechanisms linking tidal range change and sea level rise in an estuary act similarly to, but scaled down from, global and regional effects. Smaller sea level changes can therefore have large effects on the tidal characteristics of estuaries by both changing the resonance as well as the areas of dissipation (Zhong, Li and Foreman 2008).

Due to its long shape and shallow bathymetry, with a 48 hour period of resonance that is well away from major constituent frequencies, the tidal amplitudes of the present day Chesapeake Bay are lower than those of the adjacent shelf. Zhong and Li (2006) found that in the Chesapeake Bay at present day, 60% of tidal energy was dissipated in the bottom boundary layer and 40% in four spots of sills, headlands and constrictions. Zhong, Li and Foreman (2008) presented a local tide model of the Chesapeake Bay and compared it to another model of the bay given a future eustatic SLR of 1M. This model only allowed for changing depths and did not account for inundation beyond the coastline boundary. The effect of the SLR decreased the resonant period of the bay to 36 hours, bringing it closer to resonance with diurnal tides and displaying a nonlinear relationship with the tidal range. This allowed the authors to propose that the tidal range in the Chesapeake Bay would noticeably increase, even with 1m SLR scenario.

Looking to the past, Leorri, et al. (2011) modeled local tidal M_2 constituent changes in the Delaware Bay from 4ka to present day. Their discussion centered on the application of tidal range change corrections to Holocene SLR estimates since GIA models had not been able to fully explain the spatial variability between certain estimates that were geographically close (e.g. Engelhart, et al. 2009 as shown in Figure 4). These authors ran the Delft3D model for the M_2 tide over two grid scenarios representing 0.1ka (present day bathymetry less 0.33m) and present day bathymetry lowered by 5m to simulate 4ka. This 5m decrease was based on sea levels determined in Leorri, et al. (2006). Their sea level decrease caused the bay to change shape from a funnel to a wide-river estuary, noticeably changing the hydrodynamics. Here, they found that at 4ka, the M_2 amplitude at a location in the upper bay was significantly lower than the same location at present day, while the amplitude in the lower bay was slightly higher in the past. The authors used M_2 amplitude as a proxy for tidal range and applied corrections to the SLIPs in Engelhart, et al. (2009). Without accounting for spatial variability from GIA, they found that modeled tidal range changes could account for at least 25% of the difference in SLR estimates between the upper and lower Delaware Bay.

2.4 Tidal Range Change Measurements

Tide gauge data offer additional, but time limited, observations of tidal range change and sea level in the modern era. Observations of RSLR using tide gauges can lead to more

direct studies of impacts due to recent climate change. Gauge records of sufficient time to ensure that tidal cycles are fully captured; 20 years without interruption, according to Flick, et al. (2003), should be able to show local behavior, however, the results must be examined with caution. Global surveys of tidal gauge data, such as that done by Woodworth (2010) showed that spatially redundant records generally display the same trends, but are difficult to quantify due to the variability in sampling capability and human induced changes near the gauge locations (i.e. dredging, construction). Furthermore, gauge instruments and observation techniques have changed over time causing some concern for discontinuity. It is important to note that these gauge records only represent the local relative tidal records. Correction of global tide gauge readings for GIA may be necessary to extract needed information on modern SLR due to other factors like climate change Peltier (1996). Even on the time scale of a tidal gauge, GIA still has a measurable effect on the sea level. Based on the VM5b model used here, in the lower Delaware Bay, GIA has caused the sea level to rise 1.6mm/yr compared to an estimated 10-11mm/yr median value of global SLR in the next century due to warming (Rahmstorf, Perrette and Vermeer 2011).

Flick, et al. (2003) presented a study tide gauge histories for locations along the U.S. coasts. Based on measurements that have been taken on the order of tens of years, these authors were able to note trends in tidal range at each station and along the coasts as a whole. The trends on the east coast were mostly localized and depended somewhat on the north-south orientation of the local coasts. Exceedingly high tidal range change was found at Wilmington, N.C. while surrounding stations displayed much different behavior. Measurements within the outer Delaware Bay were analyzed, but no comparison to points within the bay was made. In the Chesapeake Bay, present trends show an increase in tidal amplitude toward the upper end of the bay with a decrease in amplitude in the lower portion.

Through harmonic analysis, trends of tidal constituents can be further extracted from raw data to develop a better understanding of the change. Ray (2006) showed a strong increase in the M_2 amplitude within the gulf of Maine over the course of the 20^{th} century. He noted that this area is highly susceptible to changes in the shape of the bay due to GIA but the changes observed in the M_2 amplitude were much larger than those documented in

Holocene tidal models. Ray (2009) further examined the S_2 constituent on the east coast of the U.S., finding patterns of amplitude decrease at most stations. On the U.S. Pacific coast, Jay (2009) documented an overall increase in the M_2 and K_1 amplitudes in areas outside of harbors that should not be primarily affected by direct bathymetric changes.

Müller, et al. (2011) offered studies of selected tidal constituent changes based on tide gauge readings and harmonic analysis. These authors also found a general trend of rise in the K_1 constituent along the east coast of the U.S. This work compared several models of tides based on the changing bathymetry due to GIA models, including VM2/ICE-5G. Here, they sought to explain changes in tidal range from gauges by examining the global changes in the water column. Based on low resolution models, they found that on the U.S. Atlantic coast up to 40% of recorded tidal range changes and up to 30% of phase changes could be attributable to GIA driven or eustatic SLR by magnitude, but the modeled changes did not agree in sign with the observations, with each showing different trends.

Aside from tidal range changes due to the geometry of the seas, other hypotheses for the causes of tidal range changes on this century scale have been made by several of the previous studies. Jay (2009) discussed two possible driving mechanisms; stratification changes or modification to the internal tidal wave caused by baroclinic changes, as well as atmospheric or wind shifts leading to surface shear stress changes that could affect tides of given frequencies. Müller, et al. (2011) added that the potential effects of seasonal changes, ocean circulation leading to nonlinear effects, arctic ice coverage changes, and error due to tide gauge instrumentation could also contribute to this change.

An important common conclusion from these observations was that the observed tidal range changes were *not* insignificant compared to SLR and should be further explored due to their potential impacts (Flick, et al. 2003; Jay 2009; Woodworth 2010, Müller, et al. 2011). The authors of the local tidal models (Zhong, Li and Foreman 2008; Leorri, et al. 2011) echoed these statements, noting that further numerical modeling could help to further the understanding of these changes.

Chapter 3 - Materials and Methods

3.1 Purpose

The primary objective of this study was to model the response of local tidal amplitudes to bathymetric changes in time, in both past and future scenarios. Development of a general method for modeling local GT change that could be applied to other geographic areas was a corollary goal, with this analysis focused on the tidal behavior in the Delaware Bay, USA.

Comparisons of this study's results to prior local (Leorri, et al. 2011) and regional (Hill, et al. 2011) works were sought to contrast methods, look for similarities in the results, and help identify the different physical processes for GT change in time. The analysis was also conducted to highlight processes that may have contributed to the findings of sea level change studies in the Delaware Bay (Engelhart, et al. 2009) as well as studies of general GT changes in the modern era (Flick, Murray and Ewing 2003).

3.2 ADCIRC Description

Tide driven water surface elevations, depth averaged velocities, and harmonic constituents were obtained by applying the two dimensional (2-D) depth integrated Advanced Circulation model, ADCIRC-2DDI (Luettich and Westerink 1991). Model output was subsequently used in the calculation of GT changes. ADCIRC is an established set of programs and has been particularly effective in modeling long wave processes such as storm surge and tides. Hill, et al. (2011) successfully used ADCIRC in their study of regional GT change in the Atlantic Ocean, Gulf of Mexico, and Caribbean Sea during the Holocene. Given the well accepted documentation of the workings and theory of ADCIRC only a brief description of the model will be presented in this study.

ADCIRC-2DDI is based on continuity and conservation of momentum equations that retain all non-linear terms and makes shallow water, Boussinesq approximation, and hydrostatic assumptions (Luettich and Westerink 2004). The governing continuity equation is given by

$$\frac{\partial H}{\partial t} + \frac{\partial}{\partial x}(UH) + \frac{\partial}{\partial y}(VH) = 0 \qquad \textbf{(Eqn. 1)}$$

where H is the total depth of the water column, equal to (ζ+h) where h is the depth to the still water line and ζ is the distance between still water and the free surface. U and V are the depth integrated velocities in the x and y directions, respectively (Luettich and Westerink 2004). ADCIRC uses the generalized wave continuity equation (GWCE) form to obtain water surface elevations. The GWCE modifies the continuity equation by applying small time weighting dissipative factors as well as a constant, or spatially varying, factor, τ_0 (also called tau0). These weak weighting factors work to suppress unstable oscillations that would otherwise come from formulating the GWCE on a finite element mesh. Instabilities lead to unrealistic solutions and may cause the model results to exceed certain threshold values and halt equation solution.

With no surface stress, the conservation of momentum equations used are of the form

$$\frac{\partial U}{\partial t} + U\frac{\partial U}{\partial x} + V\frac{\partial U}{\partial y} - fV = -gH\frac{\partial\left[\zeta + \frac{P_s}{g\rho_0} - \alpha\eta\right]}{\partial x} - \frac{\tau_{bx}}{H\rho_0} + \frac{M_x}{H} \qquad \textbf{(Eqn. 2)}$$

and

$$\frac{\partial V}{\partial t} + U\frac{\partial V}{\partial x} + V\frac{\partial V}{\partial y} - fU = -gH\frac{\partial\left[\zeta + \frac{P_s}{g\rho_0} - \alpha\eta\right]}{\partial y} - \frac{\tau_{by}}{H\rho_0} + \frac{M_y}{H} \qquad \textbf{(Eqn. 3)}$$

where *f* is the Coriolis parameter, g is acceleration due to gravity, P_s is the atmospheric pressure at the free surface, ρ_0 is the reference density of water, α is the earth elasticity factor, η is the Newtonian equilibrium tidal potential, and τ_b is the bottom stress (calculated as determined by model input). M is the horizontal mixing term as given by the eddy viscosity equations of Kolar and Gray (1990) where a coefficient of mixing is specified by the user.

ADCIRC has the ability to conduct harmonic analysis locally at specified locations or globally throughout the mesh, enabling tidal constituent extraction and eventual datum calculation. Model time series of both water surface elevations and velocities can be analyzed for constituents based on specified amplitudes and phases.

3.3 Domain Creation

A finite element mesh (described by the fort.14 model input file) that best represented the bathymetry of the area of study while not commanding excessive computational power was important for accuracy and time. With a sea level not constant in time, the ADCIRC model needed to be run over multiple grids representative of bathymetry at different time slices throughout the Holocene and the future. It was determined that creating one grid of connected elements from present day data could provide a baseline structure of horizontal nodal locations (latitude, longitude) with vertical values (depth) that could be manipulated corresponding to the changes in sea level for past and future scenarios. Focusing on the primary objective of modeling GT change, the process beginning with grid generation was separated into 1) Holocene Runs, or model runs with grids built based on bathymetric features characteristic of previous time periods, and 2) Future Runs similarly based sea level predictions extrapolated into the near future.

3.3.1 Delaware Bay Grid

The first step for both processes was to generate a new local-scale Delaware Bay grid to focus results within the area of study. For other ADCIRC applications, grids are often created with finer resolution in shallow water and coarser resolution in deep water areas to save computational time and to allow nearshore results to be more highly resolved. In this study, the geographic location of the coastline changed, moving further offshore with each sea level transformation going back in time. With this, a highly resolved baseline grid throughout the local domain, even in the deeper portions of the bay, was chosen. This allowed the mesh resolution in shallow areas to be maintained as the bay changed shape in accordance with time slices.

The Delaware Bay grid coastline data was downloaded from the National Geophysical Data Center (NGDC), National Ocean and Atmospheric Association (NOAA) coastline extractor tool (NOAA 2011a) using the NOAA Medium Resolution database at a 1:70,000 resolution. The extended coastline was selected from New York Harbor to the end of the Delmarva Peninsula and downloaded in the “Arc/Info Ungenerate” format. The current bathymetric data was obtained from the NGDC’s hydrographic surveys, available online (NOAA 2011b). Posted surveys within the Delaware Bay and Atlantic Ocean immediate vicinity were used

with dates ranging from the 1950's to present. The data was downloaded in two separate XYZ ASCII files; surveys prior to and post 1970. The bathymetry data was transformed to a common datum using the VDatum Software (NOAA 2011c). The two sets of data, pre/post 1970, were transformed to the NAVD88 datum using their appropriate input datum, MLW/MLLW, respectively.

Surface water Modeling System (SMS) version 10.0 was used to generate the mesh from the raw data. Through a layered, visual approach, SMS allows the user to interpolate raw input coastline and bathymetry data to finite element meshes for fluid models such as ADCIRC. Using SMS, manual modifications and transformations to the coastline were made in order to create a usable mesh. Smaller rivers, piers, islands and other features within the domain that were defined in less than 100-200 meter lengths were removed. This ensured that false solutions were not provided for features with resolutions beyond the model's capability. Downloading the next lowest resolution coastline data from the extractor (NOAA 2011a) would have minimized work involved in this step, but this resolution was too coarse for the desired model. To focus only on the area of tidal influence in the Delaware Bay, the coastline boundary was truncated at Trenton, NJ (Fletcher, Knebel and Kraft 1990). In addition to the coastline boundary, a semi-circular ocean boundary, extending beyond the continental shelf outside of the Delaware Bay was selected, which completed the domain extent definition and provided deep water positions from which tidal forcing was to be imposed for trial runs. Since the model was forced with only diurnal and semidiurnal tidal constituents from a global database, a deep water boundary was necessary to minimize the impact of higher order constituents that are amplified in shallow water. Using SMS's paving function for generation; mesh node placement and variable element size throughout the grid were determined by the boundary spacing.

3.3.2 Delaware Bay Grid Water Surface Elevation Verification

Grid spacing was manipulated through a trial and error approach where a mesh was generated based on a given arrangement and an ADCIRC model was run over the grid, subjecting it to the tidal forcing of a measured time series along the open boundary. Model results were set to output water surface elevation times series and then analyzed in comparison to NOAA predictions (6-minute resolution). Focusing on the minimization of the

root mean squared error (RMSE) between the gauge and model values of water surface elevation time series, optimal grid spacing was selected that balanced error with acceptable computational time

Boundary forcing for these tests was obtained from the TPXO7.2 global tidal database which provided 8 constituent amplitudes and phases that were input into the mandatory forcing fort.15 file for ADCIRC (TPXO 2011; Egbert, Bennett and Foreman 1994; see section 3.6 for description of the tidal database comparisons). Runs consisted of 6 days of total simulation time with three days of ramp time, with a beginning date of 18 May 2011. Nodal factors and Equilibrium arguments were obtained from the Tide_Fac Fortran code provided as an ADCIRC utility program (ADCIRC 2011). Time series of data from eleven NOAA tidal gauge locations within the Delaware Bay were used for this comparison. Figure 5 shows the distribution of the NOAA stations around the bay (NOAA 2011d). Similar model runs also served as verification, enabling comparisons of different baseline grids, offshore forcing databases and model parameters.

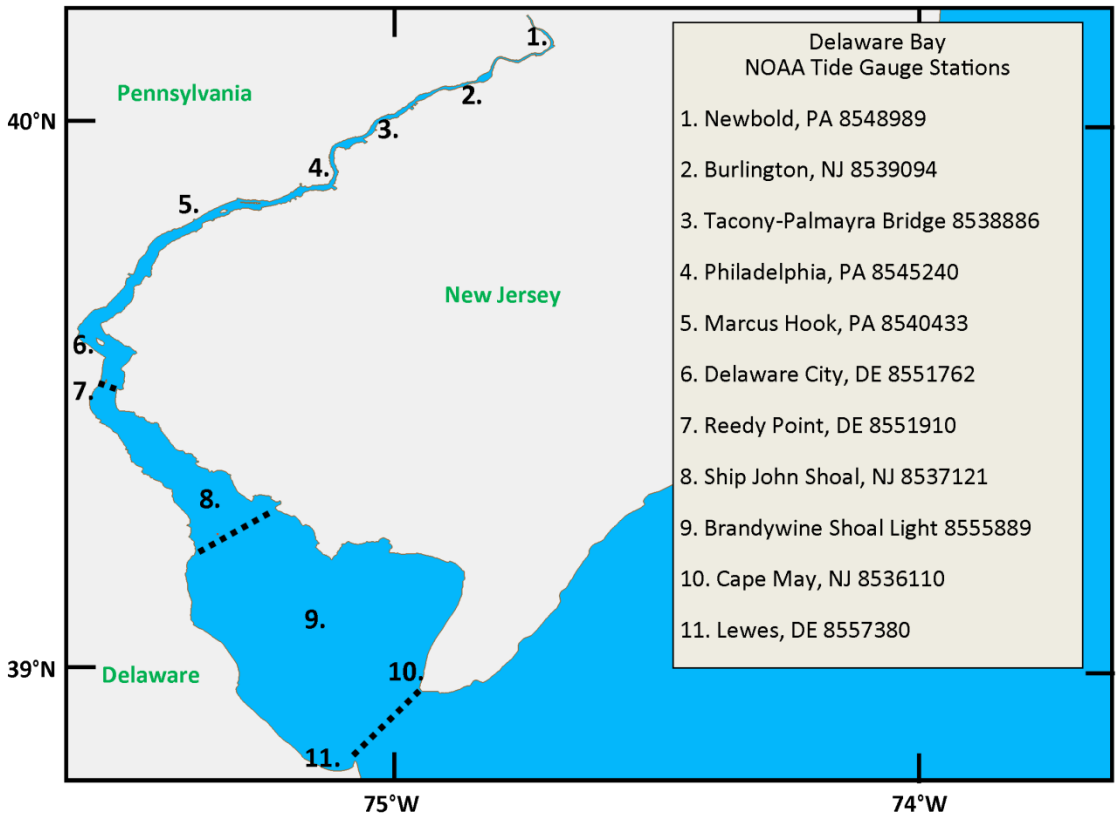

Figure 5: Sketch of 11 NOAA tide gauge locations in the Delaware Bay.

As a sample model output Figure 6 shows the comparison of the tide gauge elevation time series to model results for Reedy Point, DE. The NOAA prediction was used for the RMSE comparison as the NOAA measurement included non-tidal residual effects, which were not modeled. This example plot, while showing a low RMSE in elevation data between the model and NOAA predictions, shows the model time series discontinuous below elevation values of -0.3. This truncation represents model 'drying' whereby the location of the point is in the intertidal zone and dries at certain times in the tidal cycle. NOAA tide gauges in the field are in deep enough water to measure the full tidal range, but their placement at or near nearshore features may preclude them from being resolved by the model. Importantly, model data from truncated tidal locations in the intertidal zone provide unusable results for harmonic analysis.

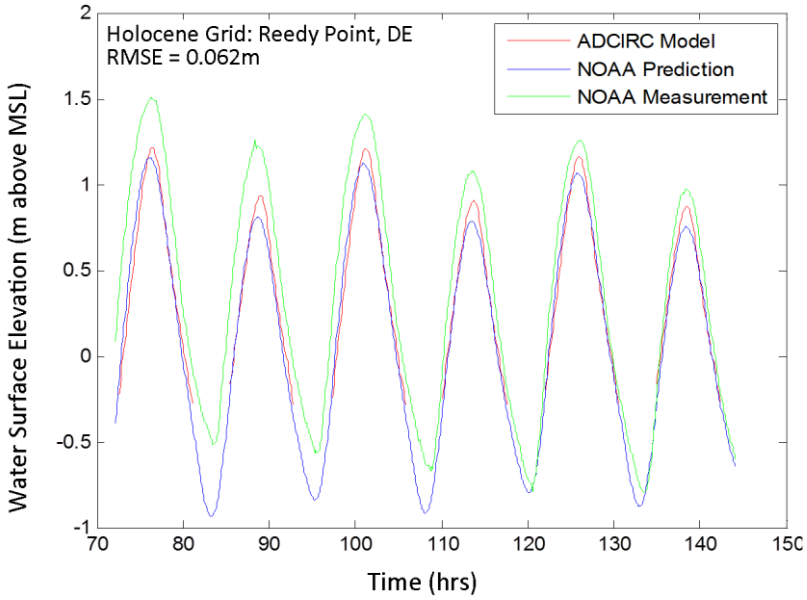

Figure 6: NOAA data compared to the Holocene Grid model of 0ka. Water surface elevation time series comparison for Reedy Point, DE.

Based on these trials for the Delaware Bay grid, coastline element sizes of 80m in the Delaware River, increasing to 175m at the mouth of the Bay, and further expanding to 2.5km at the outermost edges of the mesh were selected (Figure 7). The transitions between the grid point spacings spacings were smoothed for model stability. Bathymetry data were imported into SMS as scatter points, from which the elevations of the mesh nodes were spatially interpolated.

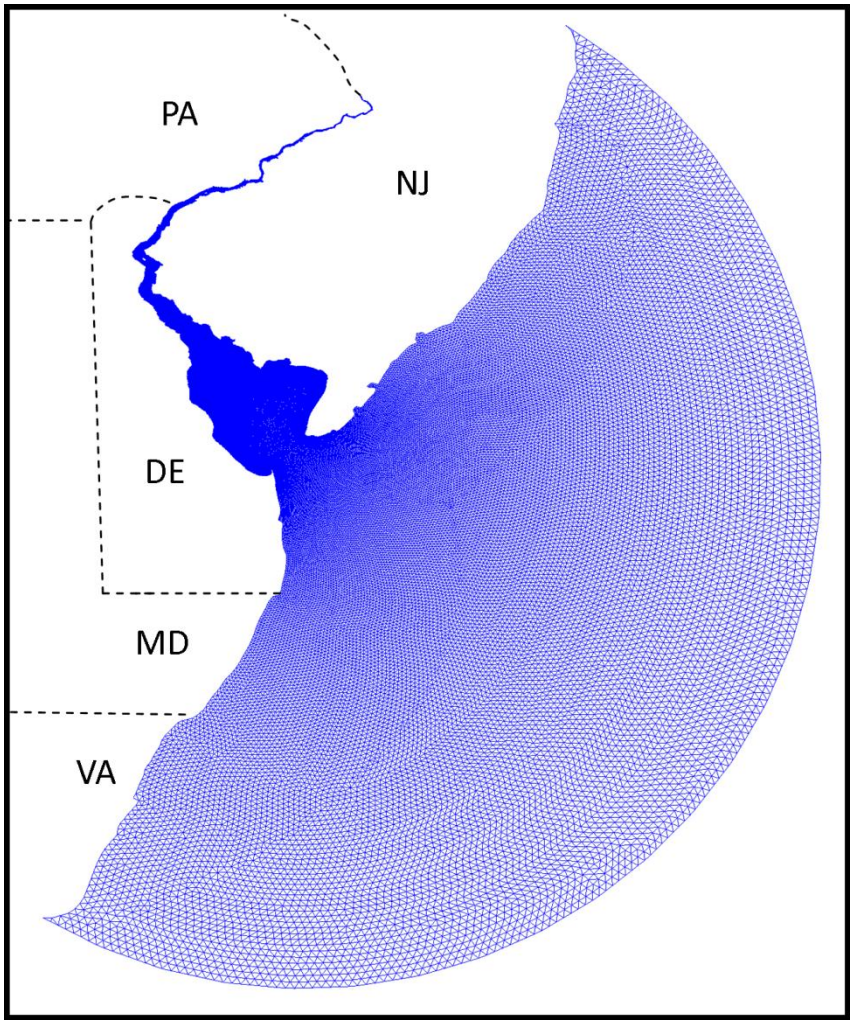

Figure 7: Delaware Bay Grid element structure.

3.3.3 Holocene Grid

To provide a regional coverage for the Holocene Runs and further reduce the error between the NOAA tidal gauge data and the model data, the Delaware Bay Grid was combined with a coarser resolution grid representing the Western Atlantic Ocean. The previously created Western Atlantic East Coast 2001 Grid (WNAT) from Mukai, et al. (2002) was selected as it had already been shown to be accurate in present day tidal modeling cases. Mukai, et al. (2002) described the sources of the coastline and bathymetry, which are similar to the sources used in the Delaware Bay Grid. While the Delaware Bay Grid's

resolution depended on the coastline boundary, the WNAT was only slightly different in that it had resolution mostly dependent on bathymetric features. This similarity in grid generation techniques allowed the two grids to work well together.

The area representing the Delaware Bay was removed from the WNAT grid and the Delaware Bay Grid was stitched in using features in the SMS software, providing a single Holocene Run grid that transitioned from regional to local resolution in the Delaware Bay (Figure 8).

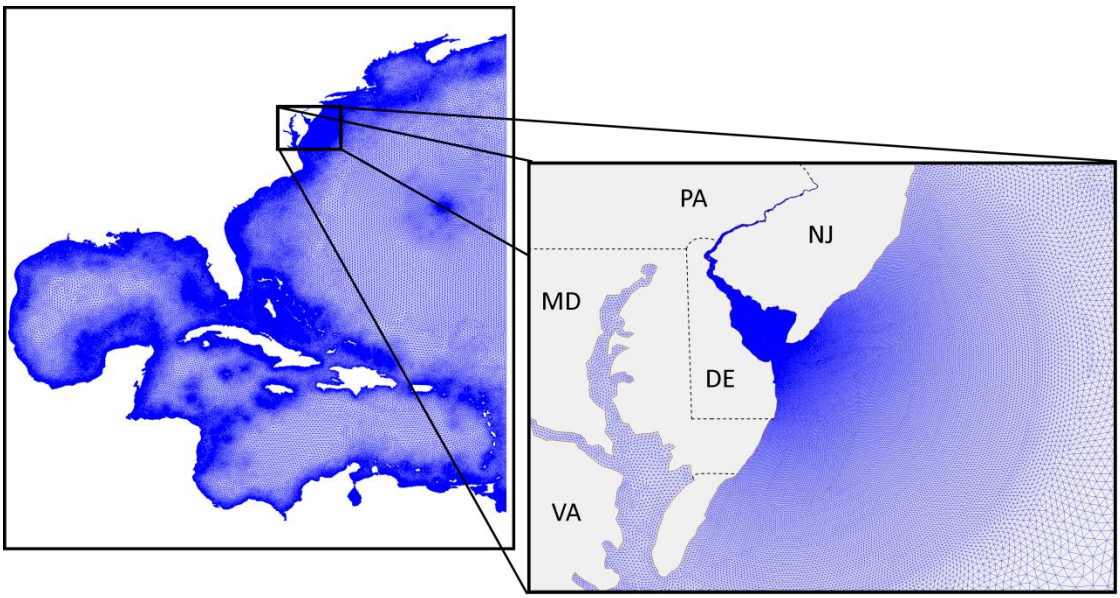

Figure 8: Holocene Grid element structure.

The resolution of the open ocean boundary of the Delaware Bay Grid (2.5 km) (See Figure 8) allowed a smooth transition to the same portion of the WNAT grid (3-5km). Then, for the merged grid, the open ocean tidal forcing was imposed at the open boundary of the WNAT grid, which was at the 60th meridian. The placement of this boundary allowed for more accurate results than the Delaware Bay grid, having almost no effect from higher order constituents, and being significantly far away from the area of concentration. The verification process described in section 3.3.2, was repeated for this grid, where the area of

transition between the two grids was manipulated to find the best fit corresponding to the same NOAA data.

3.3.4 Future Grid

In order to conduct Future Runs, land elevation data was added to supplement the original grid area, thus enabling the inundation associated with a continuing sea level rise to be modeled. Data from the NGDC ETOPO1 (NOAA 2011e) and the US Geological Survey (USGS 2011) National Elevation Dataset (NED) were combined to form a scatter set for the grid. Additional scatter points were included from the previously used hydrographic survey data in the immediate Delaware Bay region. These data included the bathymetry of the rivers and lakes that were cut out and not included in the original Holocene Grid. ETOPO1 is referenced to mean sea level, provides a regional 1-arc minute coverage and was therefore used outside the primary area of concern for a coarse resolution in the western Atlantic domain. ETOPO1 was able to be directly downloaded from its source site (NOAA 2011e), but was not transformed to NAVD88. The NED is a frequently updated representation of US elevation data with a grid size of 1 arc second or 30 m in the Delaware Bay (USGS 2011). The NED data from the web download required manipulation in ArcGIS in order to convert from a Raster to ASCII for use in SMS. It was also down sampled to 80m and, in conjunction with the ETOPO1 data, loaded as scatter points, forming the elevation background for a new grid. With these scatter points as a vertical reference; an elevation contour of greater than 15 meters, inland of the previously defined coast was drawn to represent a new inland boundary. The additional grid used the feature point spacing and location of the previously completed Holocene Grid's previous land boundary to frame and size the elements. A new Future Run grid was created that stitched the Holocene Run grid to this additional land grid (Grid 3 in Figure 9). As with previous grids, trial model runs were conducted for water surface elevation verification from the method used in section 3.3.2.

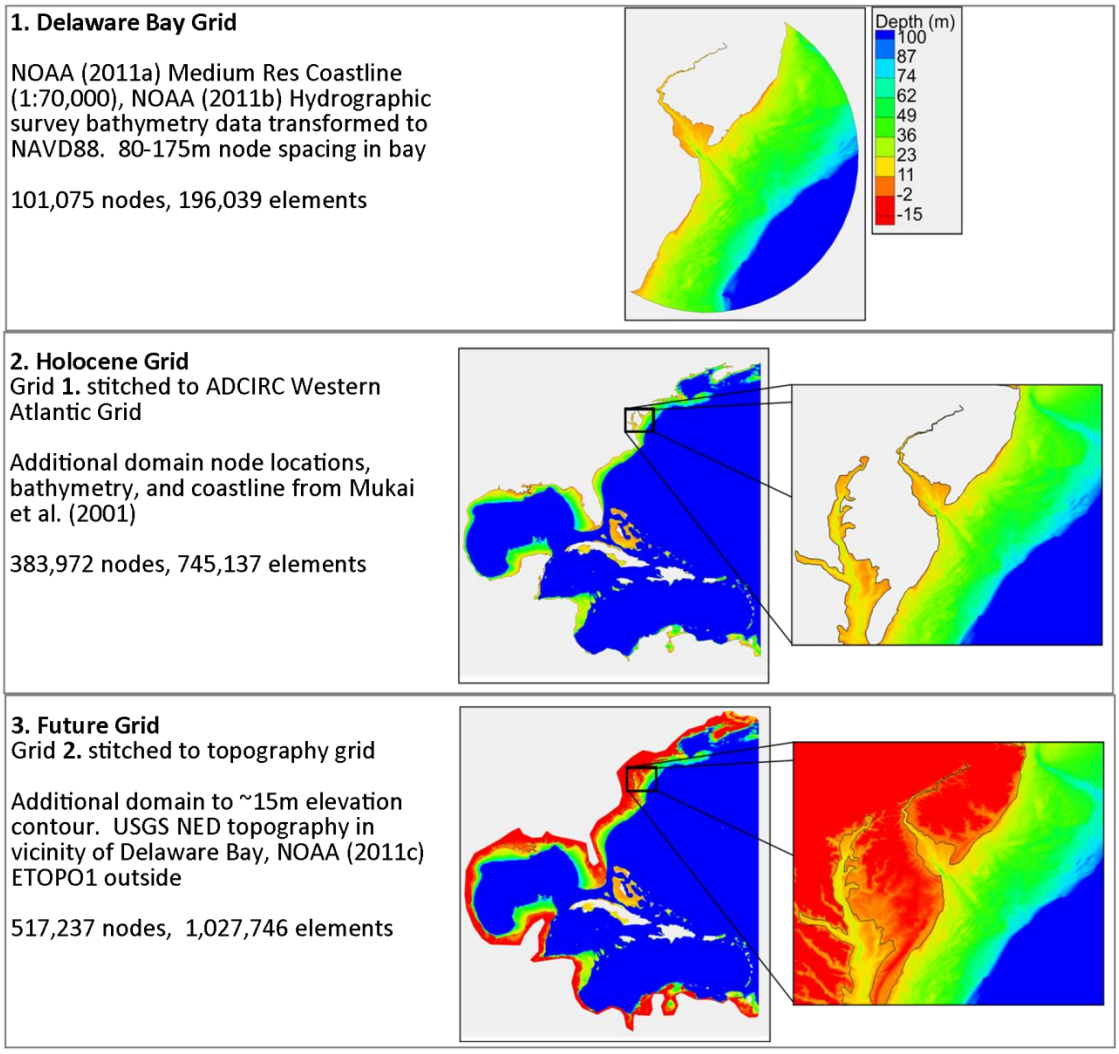

Figure 9: Bathymetric plots and characteristic comparisons of Delaware Bay, Holocene and Future baseline grids.

Table 1 shows the root mean squared errors (RMSE) in meters between the NOAA data and model predictions for 11 tidal stations in the vicinity of the Delaware Bay from the process described in section 3.3.2. Across the three grids, the lowest errors are highlighted in bold. Each grid has certain stations for which it performs better, with errors generally decreasing moving from the northernmost gauge on the Delaware River to the mouth of the bay (stations 1 to 11). Based on these present day verification runs, the use of the Holocene Grid (Grid 2) over the Delaware Bay Grid (Grid 1) reduced the total error between model and

NOAA 6-minute predicted water level data by 19.5% (Table 1). The inclusion of the topography information in the Future Grid actually increased this error from Holocene Grid. Based on the information in Table 1, present day grids 2 and 3 were determined to be acceptable to be used as baselines for the depth transformations of the Holocene and Future Runs, respectively.

Table 1: RMSE of water surface elevation time series data between NOAA tide gauge station predictions and corresponding model locations of the three grids created.

	RMSE, model to NOAA (m)		
NOAA Tidal Gauge Station (No.)	1. Delaware Bay Grid	2. Holocene Run Grid	3. Future Run Grid
1. Newbold, PA (8548989)	0.21	**0.14**	0.23
2. Burlington, NJ (8539094)	0.24	0.19	**0.17**
3. Tacony-Palmayra Bridge (8538886)	0.21	**0.14**	0.14
4. Philadelphia, PA (8545240)	0.14	**0.12**	N/A
5. Marcus Hook, PA (8540433)	**0.17**	0.18	0.18
6. Delaware City, DE (8551762)	**0.11**	0.11	0.23
7. Reedy Point, DE (8551910)	0.07	**0.05**	N/A
8. Ship John Shoal, NJ (8537121)	0.16	**0.14**	0.10
9. Brandywine Shoal Light (8555889)	0.14	0.12	**0.11**
10. Cape May NJ, (8536110)	0.09	0.07	**0.06**
11. Lewes, DE (8557380)	0.09	**0.06**	0.07
Mean across all stations	0.15	**0.12**	0.14

3.4 Transformations

3.4.1 VM5b Holocene Transformations

To represent bathymetric changes in time, transformations were applied to present day (0ka) depth/elevation values to create grids that represented time slices at specified intervals in relation to present day. The change values came from the VM5b (ICE-6G) model

as highlighted in Engelhart, Peltier and Horton (2011). Based on the VM5b model, bathymetric plots of time slices were produced at 0.5kyr intervals from 10 to 0ka at a spatial resolution of ten arc-minutes, which is approximately 15 kilometers in the Delaware Bay region. From these plots, depth changes with respect to 0ka were calculated for each time slice. Over a regional area, these were spatially variable with larger changes occurring in the northern portion of the grid due to more significant glacial activity (Figure 10). Note that the difference between present day bathymetry and the time slices in Figure 10 do not represent linear changes as there are periods of modeled acceleration in ice melting since the LGM, 20-6ka, and deceleration after 6ka (Milne, et al. 2009).

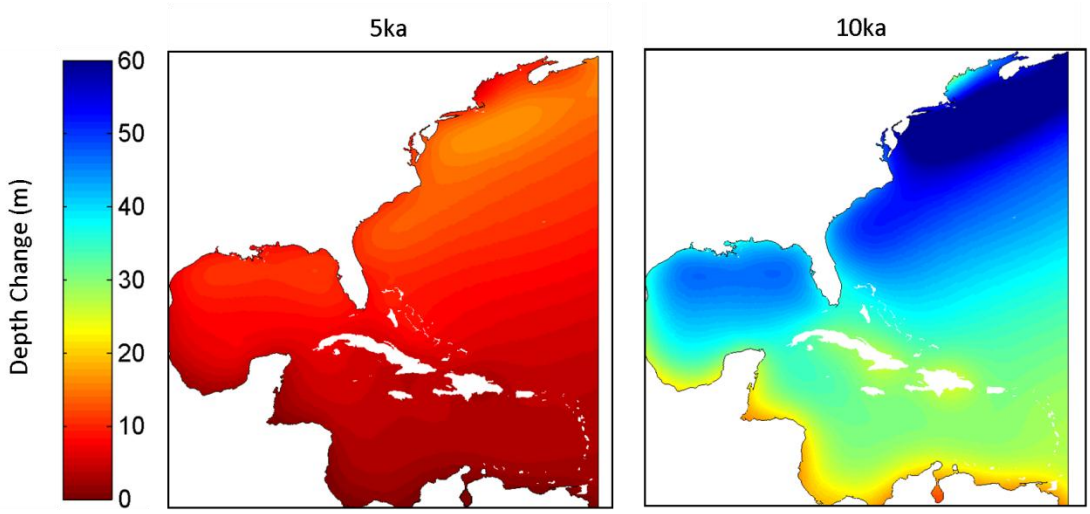

Figure 10: VM5b calculated depth changes from present day to time slices of 5 and 10ka.

Beginning with Thomas and Sündermann (1999), the use of GIA models for spatially variable bathymetric transformations improved information in regional studies, however, previous local studies had only used uniform changes in sea level (Zhong, et al. 2008; Leorri, et al. 2011). In these studies, the spatial variability of GIA on smaller scales was assumed negligible. Here, the 15km VM5b results were significantly lower resolution than the Delaware Bay portion of the Holocene Grid, which had grid spacing on the order of 100

meters, so judging by these spatial scales, this assumption could have been upheld. However, the VM5b results in this study, interpolated over the baseline grid, did in fact show a significant spatial non-uniformity on a local level. Figure 11 shows the VM5b resolution and associated interpolation to the Holocene Grid; from 0 to 1ka, the depth changes differ by as much as 0.6m between the upper and lower Delaware Bay. A spatially uniform change to sea level would not capture this variability and would be less accurate; hence, the use of the GIA model was required.

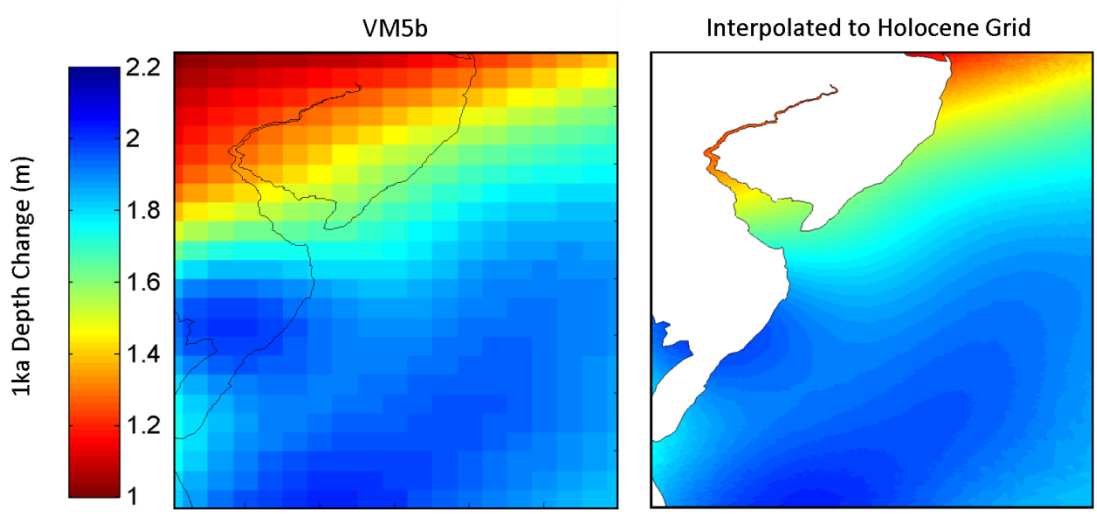

Figure 11: VM5b calculated depth change from 0 to 1ka (left) and that change interpolated to the Holocene Grid (where positive depth increase is equivalent to sea level decrease).

Regional scale morphologic changes to shorter-term forcing such as non-tidal wave driven energy, river inflow and human impact, such as dredging, were not incorporated. Relative to processes modeled by the VM5b, these processes are not yet well documented on the longer time scales being studied here.

For the Holocene Runs, the VM5b transformations were applied to the baseline mesh by finding the difference between present day depth (0ka) and the desired time slice depth (i.e. 2ka) at all locations provided in the GIA plots, and interpolating this difference to nodal locations and corresponding depths in the chosen baseline grid domain. A total of 19 runs were conducted over grids representing different time slices. For the Holocene, these

intervals were selected based on initial findings where grids at 1kyr intervals between 0 and 10ka were prepared. In applying the VM5b transformations, it was noted that the Delaware Bay was completely dry prior to 7ka and only began to resemble an estuary from 4ka to present (Figure 12). Four additional runs were therefore carried out at 0.5k intervals from 0.5ka to 3.5ka in order to better constrain the results from 0.5 to 3.5ka. The models experienced two instabilities at 7 and 8ka (See Appendix A), so runs at 7.5 and 8.5ka were conducted. Table 2 summarizes the different grids created from each combination of transformation and baseline grid.

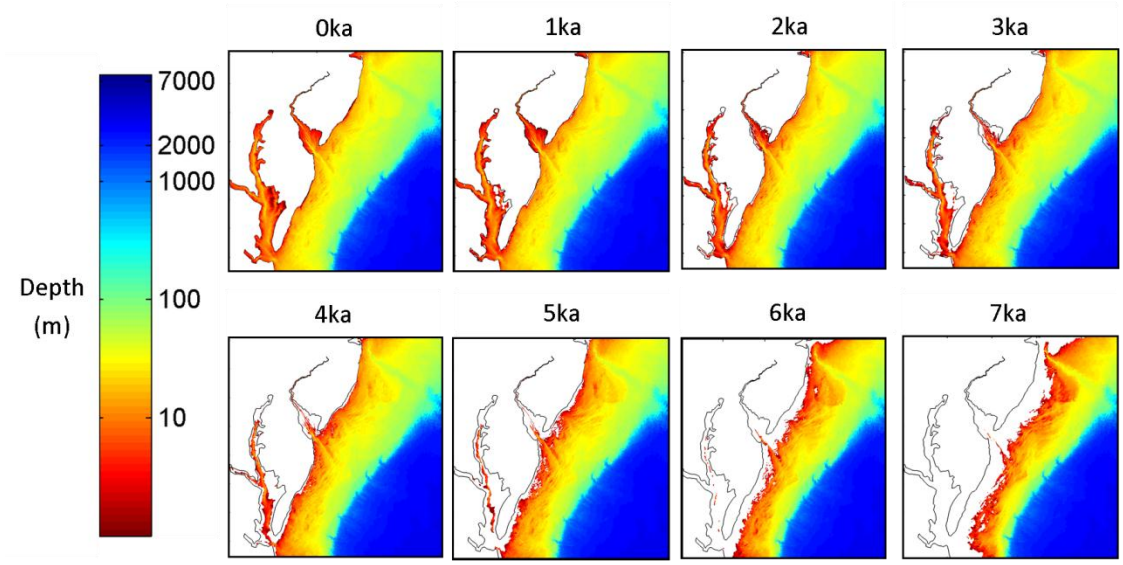

Figure 12: Depth after Holocene VM5b transformations were applied to the Delaware and Chesapeake Bays at time slices of 7 to 0ka.

3.4.2 VM5a Holocene Transformations

An additional 9 runs using the VM5a model of the Holocene bathymetry at specified time slices were conducted. These runs mirrored the important time slices in the Delaware Bay from the VM5a runs; 0.5, 1, 1.5, 2, 2.5, 3, 3.5, 4 and 5ka intervals were selected (Table 2). Significant differences between the VM5a and VM5b were noted in the temporal bathymetric changes. The VM5a and VM5b transformations from 0 to 1ka in the Delaware Bay are shown in Figure 13 where all changes represent increases in depth, or decreases in

water levels. The VM5a model shows a higher rate of change in the depths from 0 to 1ka; 2.5-3m compared to 1.5-2m in VM5b. Although the VM5a and VM5b models are non-linear with respect to time, the VM5a data showed consistently higher magnitudes of change from 0.5 to 5ka. In other words, at a given time before present, the sea level in the VM5a model was lower than that of the VM5b (Engelhart, Peltier and Horton 2011). Where the VM5b modeled Delaware Bay is dry at 7ka, the VM5a model dries the bay at 6ka indicating that, at that point in time, the change rates of the models differ by 1KYR.

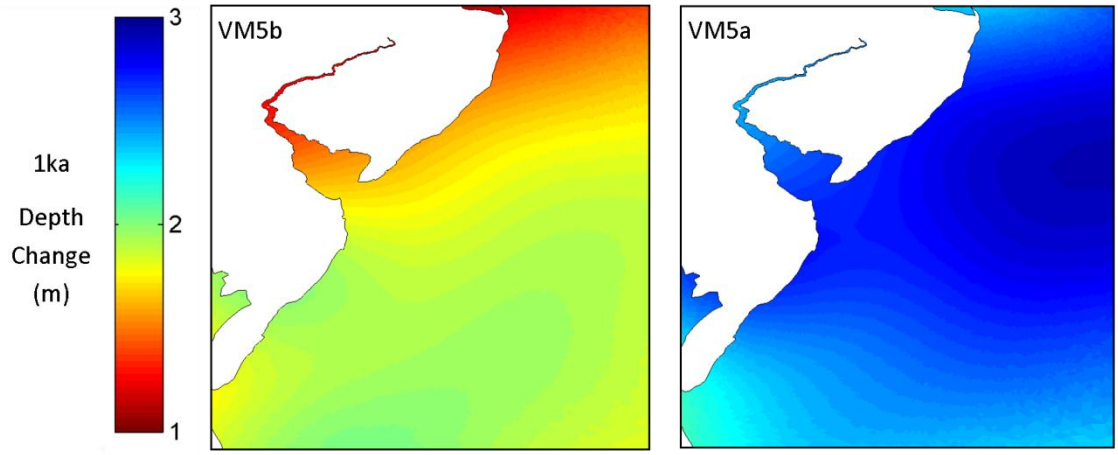

Figure 13: Depth change from 0 to 1ka comparing VM5b and VM5a.

Figure 13 also illustrates a different spatial distribution between the models within the local depth changes from 0 to 1ka. The contours of the VM5b model in the shelf area outside the bay show an increased change moving south, while the VM5a model has an increase followed by a decrease in magnitude. Within the Delaware Bay itself, the change in the VM5b and VM5b models show a smaller increase in the upper bay and a larger increase in the lower bay. Both range on the order of 0.25-0.4M over the 1KYR interval, but are somewhat different. These spatial differences impact the evolving shapes of the bay between the VM5a and VM5b, but to a smaller extent than the temporal differences.

3.4.3 Future Transformations

For Future Runs, two additional grids were created at 0.1 and 0.3 thousand years after present (+_kyr) to represent potential scenarios. Transformations consisted of two components; first, previously calculated GIA values from 0.5 to 0ka were linearly extrapolated, forward to the additional time slices. Then, an additional eustatic sea level rise was applied based on predictions of accelerated temperature increase; 1.01 m for +0.1kyr (Rahmstorf, Perrette and Vermeer 2011), and 3.5m for +0.3kyr (Rahmstorf, personal correspondence). These estimates were chosen because they were provided as semi-empirical results and represent what some consider median values in terms of estimates of SLR in the future.

In using the VM5b transformations, the intention was to model the spatially variable change in sea level accounting for mantle elasticity and GIA based on data throughout the Holocene (Peltier 2004). Since the eustatic rises were primarily based on ocean thermal expansion and glacial-ocean mass exchange due to temperature increase (Rahmstorf, Perrette and Vermeer 2011), the use of only the most recent interval of VM5b results (0.5 to 0ka), meant that ice melt mass exchange with the ocean was minimally modeled (Engelhart, Peltier and Horton 2011). Given the multiple possible outcomes of SLR, these future transformations were intentionally rough pictures of accelerated sea level rise in the modern era.

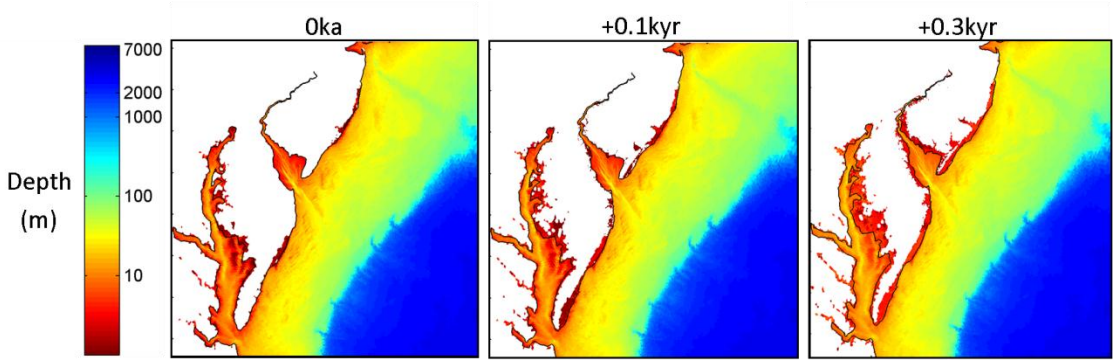

Figure 14: Depth after Future transformations were applied to Delaware and Chesapeake Bays.

Table 2: Grids created and runs conducted using each combination of transformation and baseline grid.

Baseline Present Day	Transformation Model	Representative Bathymetry Runs (KY)
2. Holocene Run Grid	VM5b (ICE-6G)	0, 0.5, 1, 1.5, 2, 2.5, 3, 3.5, 4, 5, 6, 7, 7.5, 8, 8.5, 9, 10, 12.5, 15 (BP)
2. Holocene Run Grid	VM5a (ICE-6G)	0.5, 1, 1.5, 2, 2.5, 3, 3.5, 4, 5 (BP)
3. Future Run Grid	VM5b (ICE-6G) + Eustatic Estimate	0, 0.1, 0.3 (AP)

3.5 Model Parameters

ADCIRC was set up to run on each time slice grid using a similar control file (fort.15) for the model parameters and forcing. Each run consisted of 90 total model days, 20 of which were ramp time, which slowly applies forcing and minimizes errors that may be induced by transients. The last 60 days of model simulation time were then used for harmonic analysis.

Convective and finite amplitude terms were enabled, meaning that Equations (1-3) were solved in full as described in section 3.2. The allowance of model wetting and drying was perhaps the most significant non-linearity for this study. This setting allowed nodes to be classified as 'dry' when the water depth reached a minimum value (set as 0.05m in this study). Wetting and drying effectively allows previously fixed land boundaries to be changed based on water level. It was integral to this study in that it allowed the body of water to change shape as it passed over the grids with the same horizontal layout but different depth values. Without wetting and drying, completely new grids with different node configurations would have to be created for each time slice. Dietrich, et al. (2004) described an assessment of this algorithm noting accurate results once the model is stable with this feature enabled. Coriolis forces were relevant to the region and were computed by ADCIRC.

Several parameters in the model governing equations (section 3.2) were tuned in order to achieve stable and accurate model results. Verifications of these parameters were

conducted with NOAA water surface elevation time series data as described in section 3.3.2, but some were further manipulated after initial results or instabilities of 90 day harmonic analysis runs. In the momentum balance equation, bottom friction in all cases was calculated from the quadratic equation,

$$\tau_b = C_f \rho_0 \left(\sqrt{u^2 + v^2}\right) v \qquad \textbf{(Eqn. 4)}$$

where u and v are the x and y components of velocity and the coefficient of friction, C_f was selected as 0.003 throughout the domain. An eddy viscosity mixing coefficient of 5.0 was found to allow stable results, given that this is a non-physical term, this value was chosen for the model. From the GWCE, comparisons of trials with recommended settings found that a spatially variable τ_0 calculated using the ADCIRC utility tau0_gen.exe based on grid information provided the most stable results for this parameter (ADCIRC 2011).

For each time slice run, harmonic analysis was conducted by ADCIRC globally (at all grid points) based on water surface elevation data. The amplitudes and phases of 23 tidal constituents were extracted at each grid point and output to a file (fort.53). ADCIRC version 49 also automatically output files that provide global maximum water surface elevations and maximum horizontal velocity magnitudes throughout the model time period. For selected portions of runs, water surface elevation and velocity time series data were output globally for verification.

The Courant condition for numerical equation solving is based on a relationship between model space discretization and time, where for a given grid spacing, a time step above a certain value will be insufficient to allow information to move through the grid. Since the grid was so finely resolved in the Delaware Bay, a short model time step of 3 seconds was found to satisfy the Courant condition and otherwise achieve stable results in most cases. Differences in the wetted shapes throughout the time slices caused certain grids to require time steps of 2 seconds as determined through trial runs (See Appendix A). Heavily dependent on the time step and amount of wet nodes, individual runs required 500-900 processor hours. Since this represented a large amount of computational power, the parallel version of ADCIRC (PADCIRC) was used. PADCIRC has additional code that

decomposes the grid into sub-grids (one per processor), runs the model on each piece individually, and transfers the information between them at each time step, eventually forming a solution that is the same as the serial version of ADCIRC. PADCIRC was run on a web enabled account with the LONESTAR computer cluster, hosted by the Texas Advanced Computing Center at the University of Texas, Austin, with access provided by a grant through the XSEDE portal (formerly Teragrid) project (NSF 2011).

3.6 Model Forcing

Hill, et al. (2011) used ICE-5G bathymetric changes as well as open boundary forcing that was taken from global tidal models to model GT change on a similar regional scale. Their model, with both spatially and temporally variable tidal forcing at the open boundary, showed significant change in the GT of the Western Atlantic Ocean from 6 to 9ka, but little change between 0 and 6ka. They demonstrated a pronounced resonance in the Bay of Fundy, commencing around 5ka but otherwise no significant changes in the GTs of local estuaries (Hill, et al. 2011). Based on these results, and since the Delaware Bay was dry prior to 7ka (Figure 12), the impact of using temporally variable vs. constant open boundary forcing in this study would be minimal.

To determine the forcing to be used at the 60th meridian open ocean boundary, two global tidal databases; ADCIRC WNAT (Mukai, et al. 2002) and TPXO 7.2 (Egbert, Bennett and Foreman 1994) were compared. Output from each database was interpolated to the open ocean boundary of the Holocene Grid. The same verification method described in section 3.3.2 was then used twice; for the grid with forcing from each of the databases. A comparison of the RMSE in water surface elevation time series between the model results forced by each database and NOAA data shows that the TPXO 7.2 forced results are closer to NOAA data at each location. The present day forcing from the TPXO 7.2 model was selected for all of the Holocene and Future models, providing the spatially variable, temporally constant tidal forcing.

Table 3: Comparison of RMSE in water surface elevation time series relating model data to NOAA predictions, TPXO to WNAT open boundary tidal forcing

	RMSE, model to NOAA (m)	
NOAA Tidal Gauge Station (No.)	TPXO	WNAT
1. Newbold, PA (8548989)	**0.14**	0.16
2. Burlington, NJ (8539094)	**0.19**	0.20
3. Tacony-Palmayra Bridge (8538886)	**0.14**	0.15
4. Philadelphia, PA (8545240)	**0.12**	0.13
5. Marcus Hook, PA (8540433)	**0.18**	0.18
6. Delaware City, DE (8551762)	**0.11**	0.12
7. Reedy Point, DE (8551910)	**0.05**	0.07
8. Ship John Shoal, NJ (8537121)	**0.14**	0.14
9. Brandywine Shoal Light (8555889)	**0.12**	0.13
10. Cape May NJ, (8536110)	**0.07**	0.08
11. Lewes, DE (8557380)	**0.06**	0.07
Mean across all stations	**0.12**	0.13

3.7 Data Reduction

For both the Holocene and Future Runs, the harmonic analysis model output was compared to present day NOAA data at tide gauge stations throughout the domain to verify accuracy. The 0ka model constituent phases and amplitudes at locations of 7 of the 11 NOAA tidal gauges were analyzed for error paying particular attention to the 4 major constituents contributing to the tides in the bay (M_2, S_2, K_1, and S_2).

Once it was determined that the accuracy was acceptable, the harmonic analysis files were combined with grid files and the global amplitudes and phases of the individual tidal constituents were analyzed to determine their change at the different time intervals. Major contributing constituent amplitudes and phases were plotted over the latitude and longitude of the grid points. For comparison, amplitude ratios were calculated as the amplitude of a constituent at a respective time slice to the amplitude of the same constituent at present day.

Using the HCD method described by Mofjeld, et al. (2004), constituent amplitudes and phases were used to calculate tidal datums; MHHW, MHW, MTL, MSL, MLW and MLLW at each grid node. For the purposes of this study, great diurnal range, abbreviated GT, was calculated as the difference between MHHW and MLLW. For further analysis, GT ratio was defined as the ratio of the GT of a given time slice to the GT at 0ka. The constituents, datums and ratios were calculated for each node and each time slice, plotted, and analyzed to provide a picture of GT changes in the regional and local areas of study.

Chapter 4 – Results

4.1 Present Day Constituent Verification

Figure 15 and Figure 16 show model verifications of constituent amplitudes and phases at seven NOAA tide gauge locations. NOAA constituents (blue) were compared to the harmonic analysis model results from the Holocene Grid (Figure 15) and Future Grid (Figure 16) runs at 0ka with TPXO open boundary forcing (red) with percentage error or degrees off (black). Generally, for both amplitude and phase, errors were small but show a spatial pattern; increasing at locations further into the bay and river away from the open ocean.

Like the water surface elevation time series trials, the 0ka Holocene Grid run showed less amplitude error than the Future Grid run when comparing constituents. The Future Grid had exceedingly large errors in constituent amplitudes at Cape May, NJ and Philadelphia, PA. The additional error at these two gauges was due to the coverage area and can be seen from plots of the locations within the grid (not shown). In the Holocene Grid with a coastline boundary, datums at gauge locations were interpolated from areas of the grid that were inundated with full solutions at present day. Since the Future Grid had resolution landward of the previous coastline boundary, the locations of certain tide gauges were interpolated to areas were dry or in the intertidal zone, providing incomplete data and meaningless harmonic solutions. The remaining gauge locations in the Future Grid show amplitude errors that were only slightly larger than those seen in the Holocene Grid. The phase errors of the constituents on both grids are comparable.

Holocene Grid
Present Day K1,N2,M2,S2 Tidal Constituent Amplitudes (m)
NOAA Tide Gauge Station vs. **Model, % Difference**

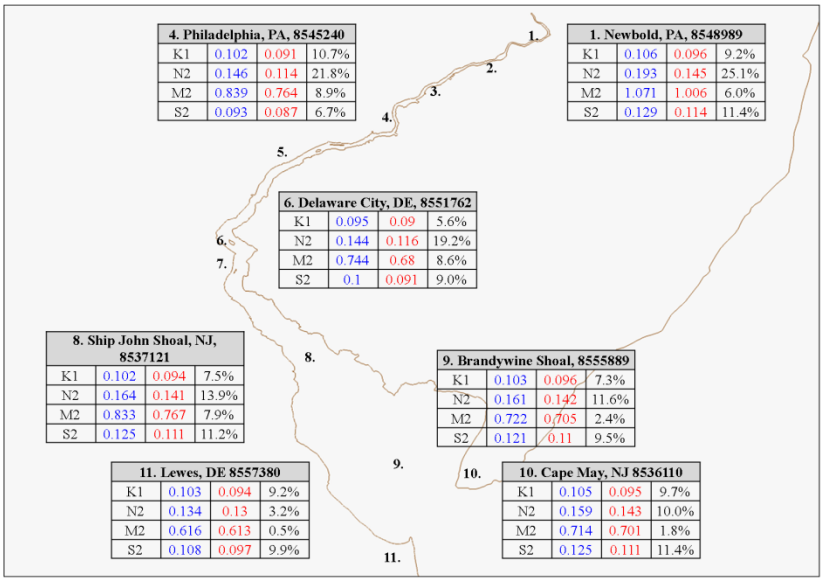

Holocene Grid
Present Day K1,N2,M2,S2 Tidal Constituent Phases (deg)
NOAA Tide Gauge Station vs. **Model, Difference (deg)**

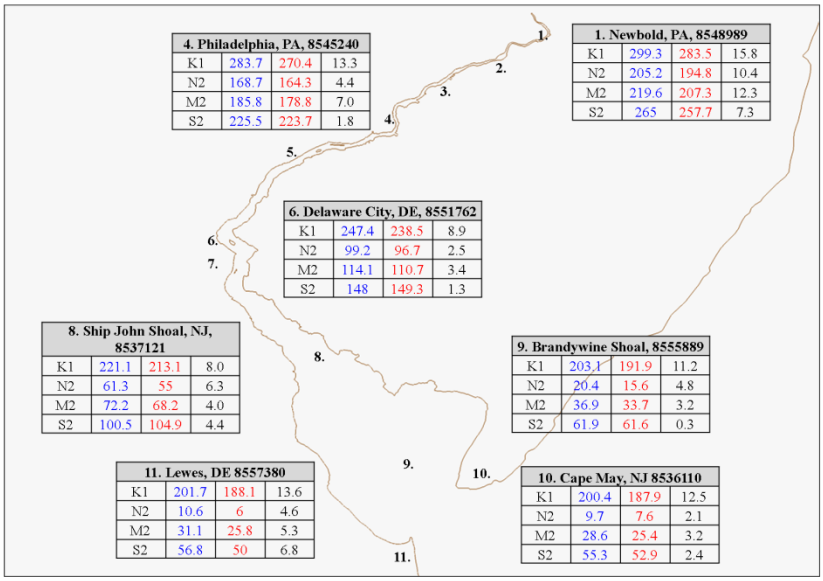

Figure 15: Constituent comparisons of the present day Holocene Grid model (0ka) to NOAA tide gauge constituents at 7 locations throughout the Delaware Bay. Upper panel shows constituent name, NOAA gauge amplitude, model amplitude, and percentage error. Lower panel shows constituent name, NOAA gauge phase, Model phase, and degree difference.

Future Grid
Present Day K1,N2,M2,S2 Tidal Constituent Amplitudes (m)
NOAA Tide Gauge Station vs. **Model, % Difference**

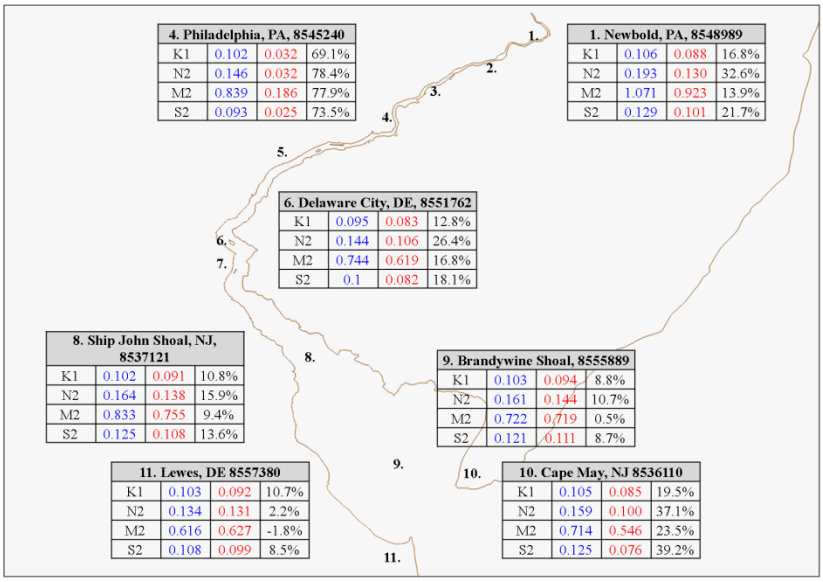

Future Grid
Present Day K1,N2,M2,S2 Tidal Constituent Phases (deg)
NOAA Tide Gauge Station vs. **Model, Difference (deg)**

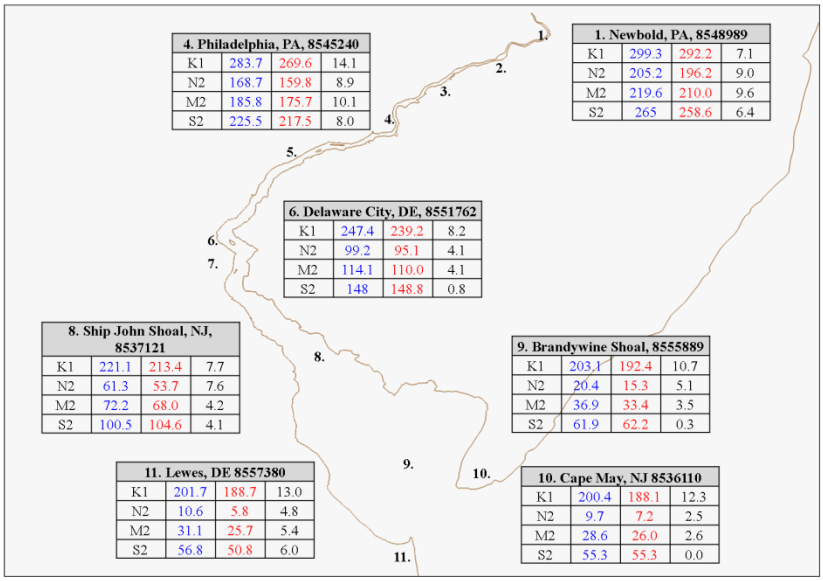

Figure 16: Constituent comparisons of the present day Future Grid model (0ka) to NOAA tide gauge constituents 7 locations throughout the Delaware Bay. Upper panel shows constituent name, NOAA gauge amplitude, model amplitude, and percentage error. Lower panel shows constituent name, NOAA gauge phase, Model phase, and degree difference.

The M_2 constituent is dominant in the semi-diurnal tides of the Delaware Bay (Leorri, et al. 2011), and it provides a strong indicator of tidal behavior. The M_2 constituent was modeled comparably well by the Holocene Grid 0ka run with amplitude differences below 10% and the phases less than 15° off from NOAA data (less than 7° when not counting the upriver Newbold, PA station). In the Future Grid 0ka run, M_2 amplitude errors exceeded 15% at the river stations and in Cape May, NJ, but are below 10% at stations 8, 9 and 11 in the bay. Results were not compared to gauge locations outside the bay; however, on a regional scale, the 0ka Holocene and Future model results are consistent with those described in Hill, et al. (2011) from 6 to 0ka.

4.2 Holocene VM5b Regional

From the Holocene model runs based on the VM5b transformations for 10 to 0ka, regional tidal constituent change was spatially non-uniform with areas of increase, decrease and no-change noted throughout the domain. Presently, the M_2 is the dominant constituent in the macro tidal behavior of the Gulf of Maine/Bay of Fundy (Gehrels, et al. 1995; Ray 2006) and is dampened in the Gulf of Mexico (Mukai, et al. 2002) where the diurnal tidal constituents (i.e. K_1) have greater effects. From 10ka to present day, changes in the M_2 constituent in the western Atlantic Ocean were minimal. The M_2 amplitudes in the Gulf of Mexico and Caribbean Sea were slightly larger in the early Holocene, but remained mostly un-affected by the changing bathymetry (Figure 17). Similarly, the K_1 constituent shows only small changes on a regional scale with decreasing amplitude in the Gulf of Mexico as time is increased through the Holocene; 10 to 0ka (Figure 18).

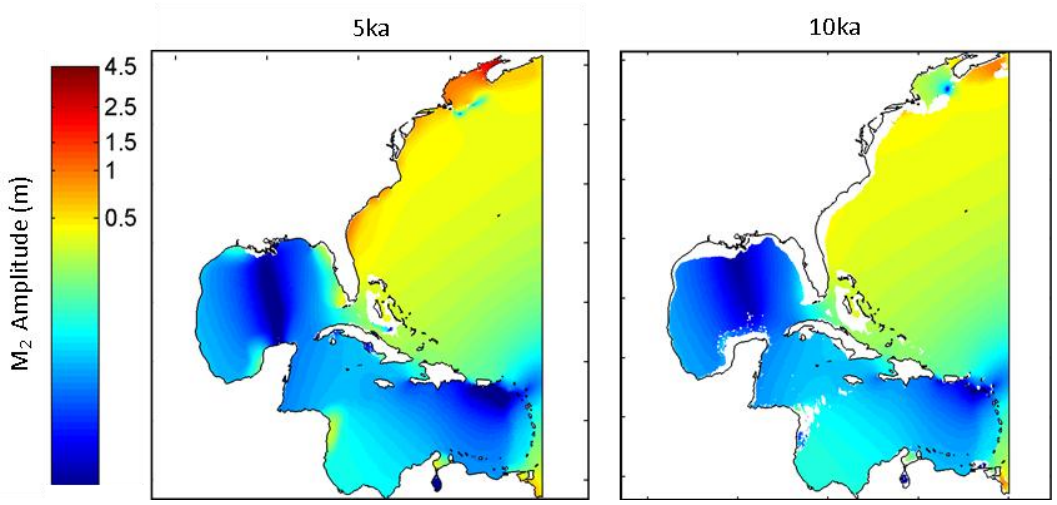

Figure 17: M_2 constituent amplitude at 5 and 10ka.

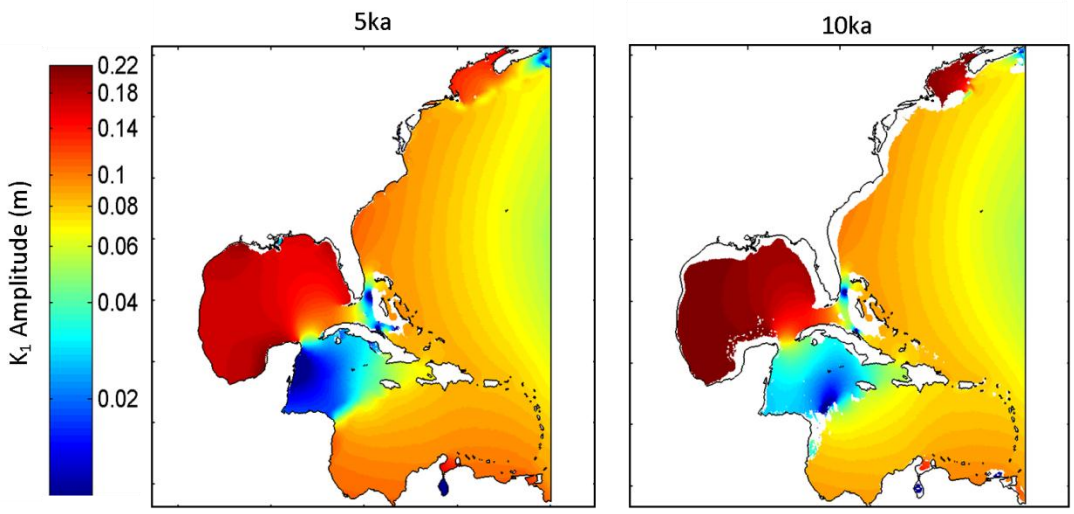

Figure 18: K_1 constituent amplitude at 5 and 10ka.

The great diurnal range in the open Atlantic Ocean is 0.75 to 1m throughout the time slices modeled, showing little change as indicated by the individual constituents. Present day GT in the Gulf of Mexico, ~ 0.6m, is a small but noticeable decrease from the 0.7m range at

10ka, a similar decrease to what was shown in the diurnal constituents (e.g. K_1 in Figure 18). Figure 19 shows the GT change with respect to present day tides as a ratio in the region for 1kyr slices between 5ka and 10ka. Macrotidal behavior in the Gulf of Maine can be seen on this regional scale. The Gulf of Maine began to become resonant between 6 and 5ka, prior to which, blue colors in Figure 19 show that GT was a small fraction of what it is today.

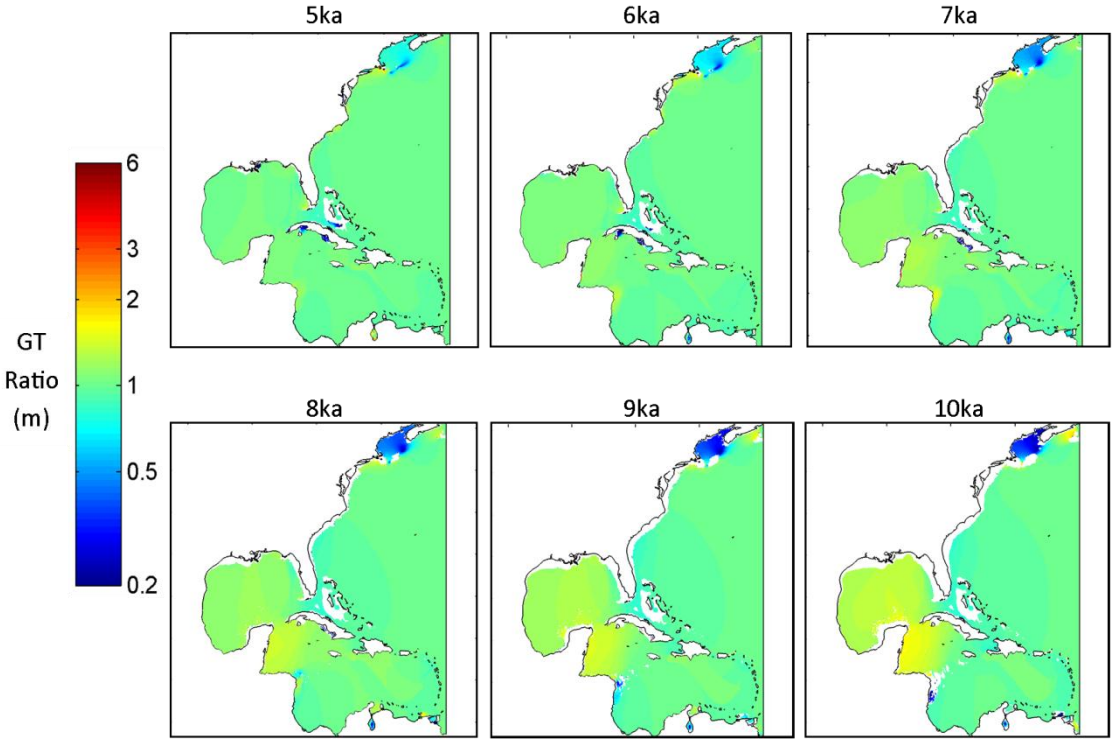

Figure 19: Diurnal range (GT) ratio to present day in the western Atlantic Ocean: 10 to 5ka.

Within the mid-Atlantic coast of the U.S., GT changes vary due to the complicated coastline, offshore shelf bathymetry, and different estuary shapes. Figure 20 shows the M_2 amplitude in the mid-Atlantic higher near the coastline, but with spatial variability. Different M_2 amplitudes are seen along the Long Island Sound, Hudson Canyon, Delaware Bay, Chesapeake Bay, and Outer Banks. The first panel of Figure 20 gives geographical references for further localized results that focus on the Chesapeake Bay (1), Hudson Canyon (2) as well as the main area of concentration in this study, the Delaware Bay (3).

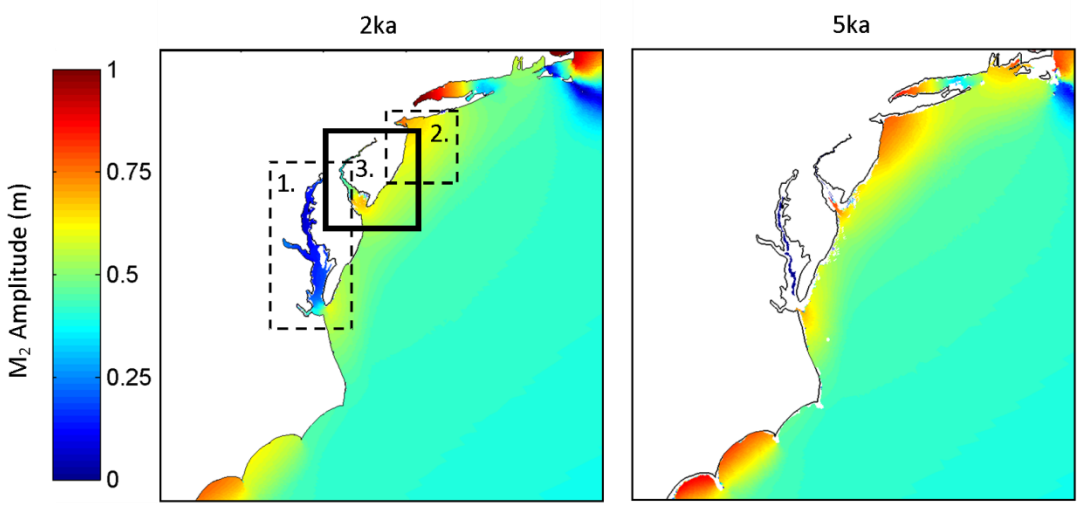

Figure 20: M_2 amplitude in the mid-Atlantic U.S. Coast: 5 to 2ka.

Constituent phases can be resolved at this level and their spatial variability is evident in Figure 21. Major temporal phase changes come in the areas that are directly submerged and inundated; otherwise few areas display notable phase changes. The highest amount of spatial and temporal phase change is noted in the Chesapeake Bay. Within the Chesapeake, M_2 phases are anywhere between 0-360° depending on location. Temporal change occurs mostly near the ends of the truncated tributaries (Figure 21). The Delaware Bay shows distinct 45° (K_1) and 90° (M_2) spatial phase differences between the "upper" or northern portion of the bay above ~39.1° N, and "lower" bay, below 39.1° N. These remain constant in time as shown by a persisting contrast of colors during inundation (Figure 21).

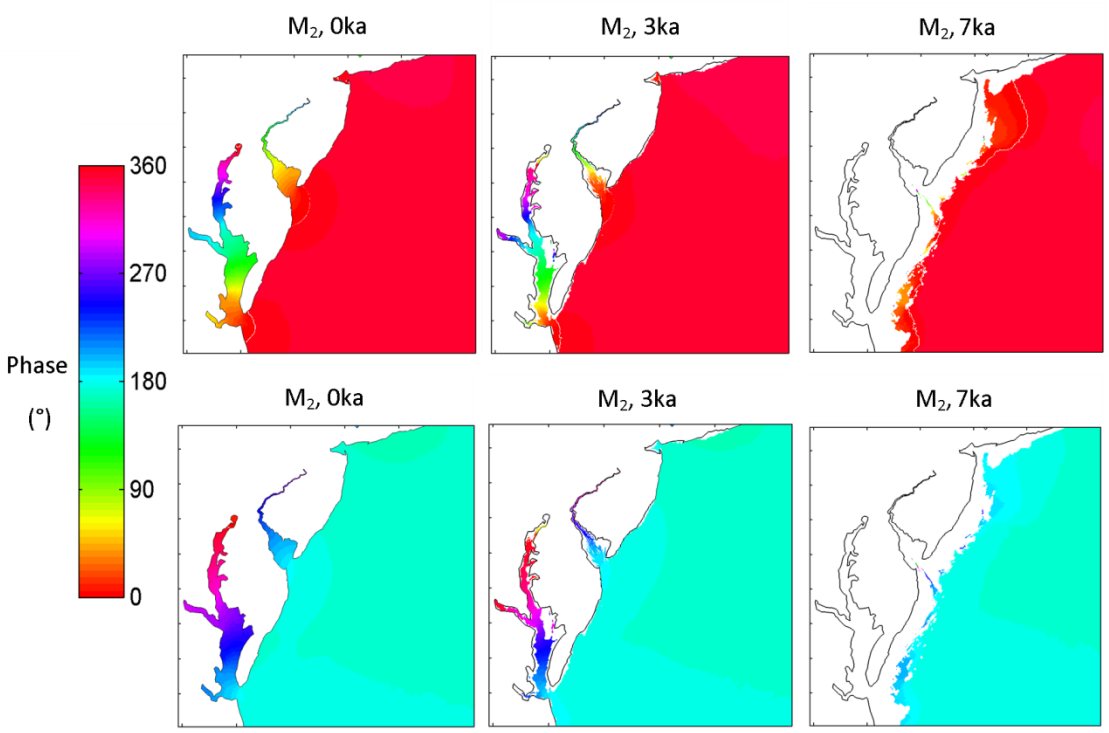

Figure 21: M_2 and K_2 constituent phases in the Mid-Atlantic: 7 to 0ka.

4.3 Holocene VM5b Local

4.3.1 Constituents and great diurnal range outside the Delaware Bay

Within the mid-Atlantic region of the U.S. coast bordering on where the high resolution Delaware Bay grid was added, two areas of distinct tidal changes can be seen over the time intervals modeled.

4.3.1.1 Chesapeake Bay

The Chesapeake is oriented differently than the Delaware Bay and has several larger tributary estuaries that complicate the basin shape. Located in the mid-Atlantic region, the Chesapeake Bay was not covered by the high resolution Delaware Bay portion of the Holocene Grid, but the results are interesting both on their own and for comparison to the Delaware.

Similar to the Delaware Bay, this area was dry prior to 6ka. In the Chesapeake, GT increases with time throughout the bay with the exception of the immediate vicinity of the mouth. The M_2 ratio does not fully describe GT since the tides in the Chesapeake are heavily influenced by diurnal constituents; the damping shown in Figure 20 is reflected in GT behavior. Figure 22 shows the ratio of GT to present day range; here the area of rapid increase is again shown with the plot following closely to that of the M_2 amplitude ratio. Importantly, resent day diurnal ranges in the Chesapeake are mostly below 1m lower than those of the outside shelf area and adjacent Delaware Bay.

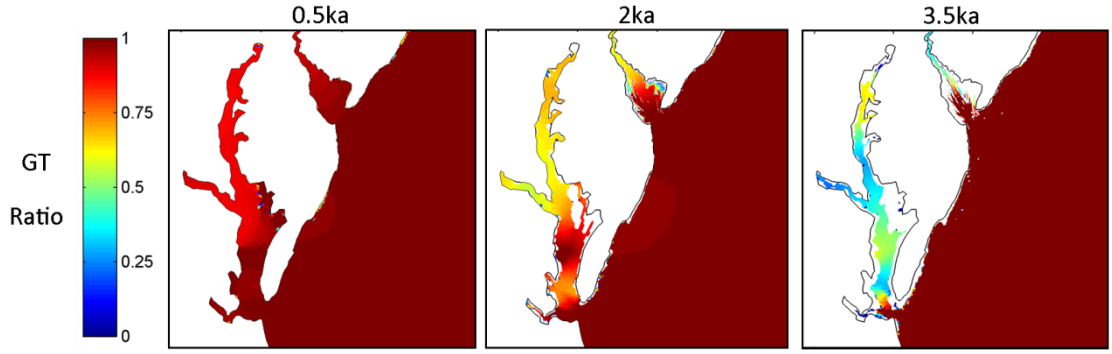

Figure 22: GT ratio to present day in the Chesapeake Bay: 3.5 to 0.5ka.

4.3.1.2 Hudson Canyon

To the north of the Delaware Bay, the Hudson Canyon is a long, narrow, area of deeper water that extends from the mouth of the Hudson River southeast, bisecting the continental shelf. The first indication of notable results in this area came from instabilities in the initial Delaware Bay grid at time slices earlier than 7ka; findings that partially led to the decision to couple the Delaware Bay and WNAT grids to create the Holocene Grid. As a result of its proximity to the previously open boundary, the water surface elevations in the area of the canyon grew exponentially until they exceeded threshold values. After conducting all runs on the Holocene Grid, this area was re-examined based on these initial findings.

The canyon filled in rapidly between 9 and 8ka and immediately began to show higher constituent amplitudes than other surrounding areas. Semi-diurnal constituent

behavior (M_2, S_2) is reflected in the GT ratio to present day in the Hudson Canyon. Here, GT is greatest between 7 and 6ka, showing a noticeable resonance with the shape of the trench as dried from its present day form. The tides at 7ka were 20-30% higher than they are at present day (Figure 23).

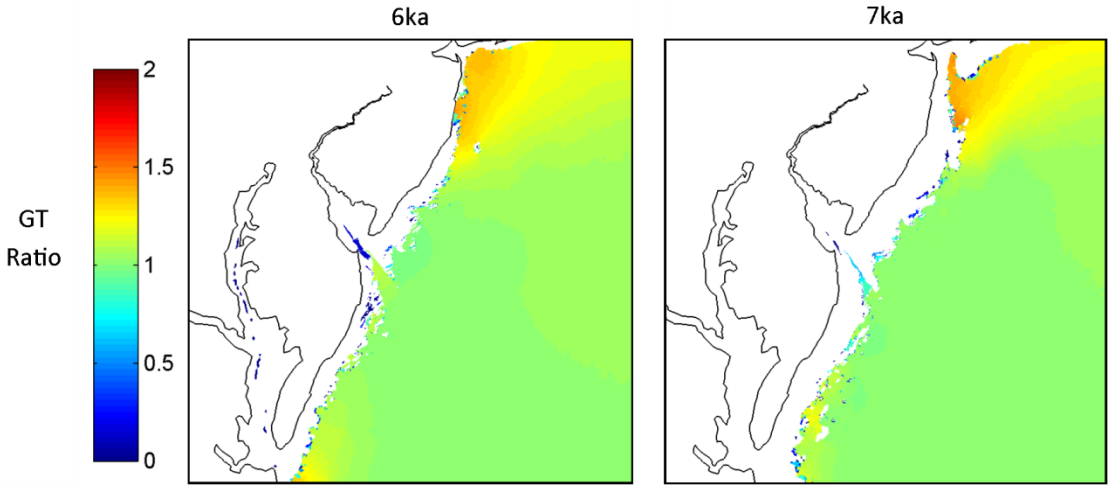

Figure 23: Diurnal Range (GT) Ratio in the Hudson Canyon: 7 to 6ka.

4.3.2 Delaware Bay

Tidal constituent amplitude results within the main area of interest in this study, the Delaware Bay, show notable spatial and temporal variability since the area was inundated at 6-7ka. With these spatially non-uniform changes, different tidal datum results were seen both between the bay and the ocean and within the estuary itself; between the lower, upper and river portions.

Semidiurnal constituents M_2, N_2 and S_2 were the primary contributors with behaviors indicative of GT. Diurnal constituents such as K_1 and O_1 had a small impact. Figure 24 shows the M_2 constituent amplitude ratios throughout the area. On the continental shelf adjacent to the bay, the M_2 amplitude remained relatively constant in time as noted previously. From 6 to 0ka, as the Delaware Bay began to fill in, the M_2 signal in the lower bay area experienced 3 distinct changes. From 6 to 5ka, the M_2 sharply increased from dry (zero value) to an

amplitude 1.5 times that of present day (Figure 24). A time of slow decline in this area was observed between 5 and 2ka. Finally, from 2 to 0ka, the M2 amplitude reached present day values and remained steady. In the upper bay, the M_2 amplitude change was much different displaying an increase throughout all time slices after starting at 50% of present amplitude upon inundation at 4 to 3ka. Even after the Delaware Bay took its characteristic funnel shape between 3 and 2ka, the amplitude ratio of the M_2 constituent was much smaller in the upper bay than in the lower bay.

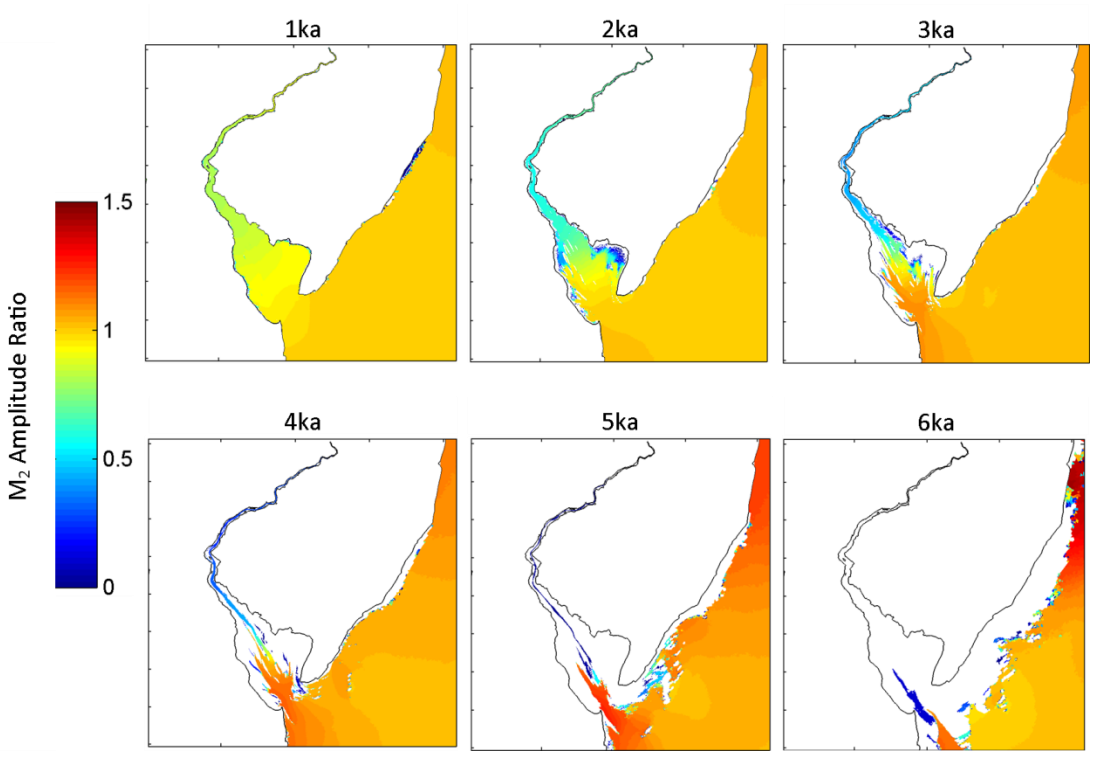

Figure 24: M_2 amplitude ratios within the Delaware Bay: 6 to 1ka.

Present day GTs are greatest in the Delaware River and upper portion of the bay at around 1.8m. Ranges at the mouth in the lower bay are closer to 1.4m further decreasing with distance from the bay mouth moving out onto the shelf. Since 5ka, the tides in the lower bay have been amplified from those of the adjacent continental shelf. The GT in the

lower bay at 5ka was approximately the same as the range in the present day upper bay; it was during these two separate time slices that GT was highest.

Whereas the lower bay became resonant almost immediately upon being inundated, the upper bay filled in before 3ka but had a smaller GT than the lower bay until 1ka. A distinct separation can be seen in the plots between the upper and lower bay. This indicates a sharp increase in GT in the upper bay in recent time slices. To further explore these results, 0.5kyr intervals were used for a higher temporal resolution.

Ratio plots of the Delaware Bay from 3-0.5ka highlight the differences between the GT development in the upper and lower bay (Figure 25). After 3ka the bay had become mostly inundated, yet there was still a strong divide between lower and upper bays in their GT ratios to present day (shown by the red and yellow contrast). The divide persisted and even as late as 0.5ka, the contrast can be seen in the resultant plots. From Figure 25, the GT of the upper bay increased until it surpassed the magnitude of the lower bay. Since 3ka, the GT in the upper bay has increased by 80-100% while the GT in the lower bay has decreased by 5-10%. Predicted tides at present day in the river at 1.8m were of similar magnitude to those in upper bay GT. GT change in the river was also similar to that of the upper bay, with an increase since inundation.

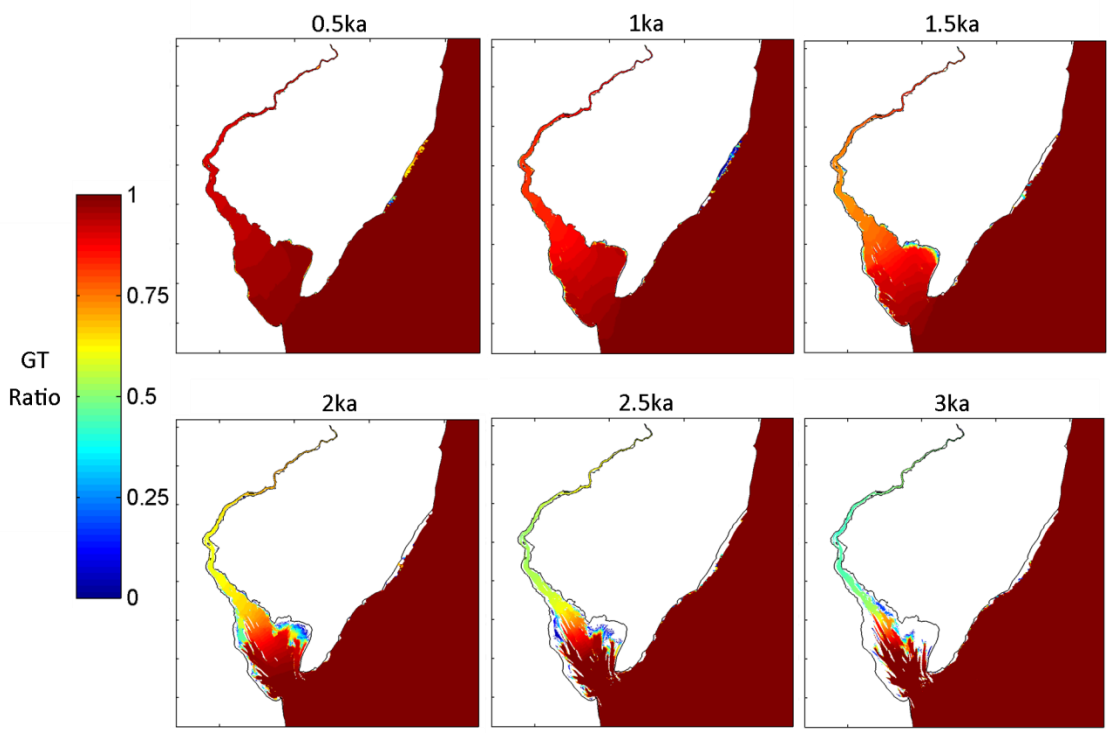

Figure 25: GT Ratio in the Delaware Bay: 3.0 to 0.5ka.

4.4 Holocene VM5a Comparison

4.4.1 Regional

The results obtained from the Holocene Runs conducted using the VM5a bathymetry transformations showed a strong correlation to VM5b results. The rate of sea level change in the VM5a model was faster and the spatial distribution of the transformations was different as noted in chapter 3. Differences in the constituent amplitudes and GT results were noticed.

From a regional perspective, differences in the open ocean GT were small. Figure 26 shows the ratio of the VM5a Holocene GT to that of the VM5b at 5ka, the furthest back that the VM5a depths were modeled. 5ka also shows the greatest difference between the model grid depths on a regional scale. The large green area in Figure 26 shows the GTs modeled by VM5a and VM5b have only small differences; less than 5% of the VM5b range. The red and

blue contours show GT differences greater than 20% in the local regions of inlets and bays; focus remains on the Delaware Bay.

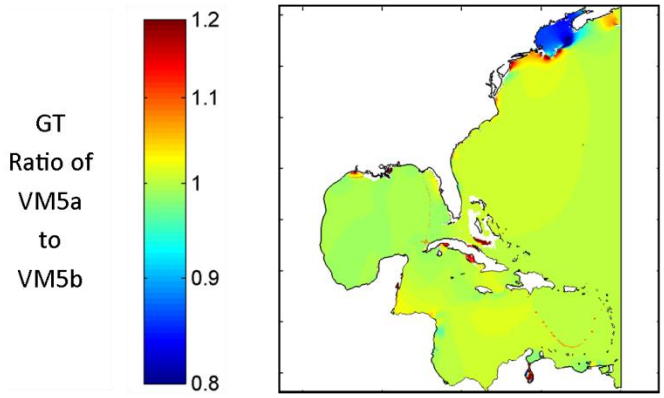

Figure 26: Regional ratio of GT calculated from VM5a to corresponding VM5b model GT: 5ka.

4.4.2 Local

In the Delaware Bay, differences between the GTs of the VM5a and VM5b models are visible when comparing their ratio at each time slice. The VM5a runs are characterized by a 10-15% smaller GT in the upper bay through most of the modeled time slices (Figure 27). An additional 10% larger GT in the lower bay is evident at 4 and 2ka. Outside the bay at the location of the Hudson Canyon, larger VM5a GTs are found at 4ka indicating that the Canyon tidal resonance ended later in the VM5a model.

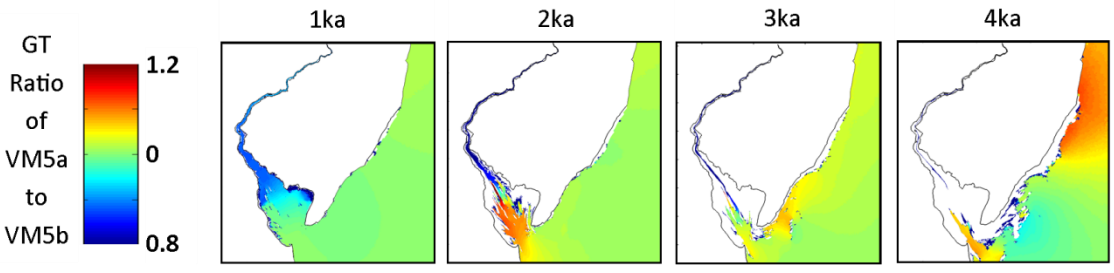

Figure 27: Local ratio of GT calculated from VM5a to corresponding VM5b model GT: 4 to 1ka.

With the bay drying at 5ka in the VM5a model vs. 6ka in the VM5b model, as noted in chapter 3, it was considered that results may line up better when compared at 1kyr time difference. Results of the VM5a model at selected time slices (e.g. 1ka) were compared to VM5b results at time slices of +1kyr (e.g. 2ka). The VM5a 2ka run and VM5b 3ka run model similar GT changes throughout most of the bay and are more closely related than the two 2ka results (Figure 28 compared to 2ka panel of Figure 27). This indicates that the GT differences are mainly due to the temporal changes in the drying of the bay between the VM5a and VM5b model. The VM5a 2ka and VM5b 3k and other +1kyr comparison results are off by small, but varying amounts. While the ratios are very close to 1 in the open ocean, the upper bay is different by 5% (Figure 27), here the spatial differences in the VM5a and VM5b bathymetry transformations may have contributed to GT differences.

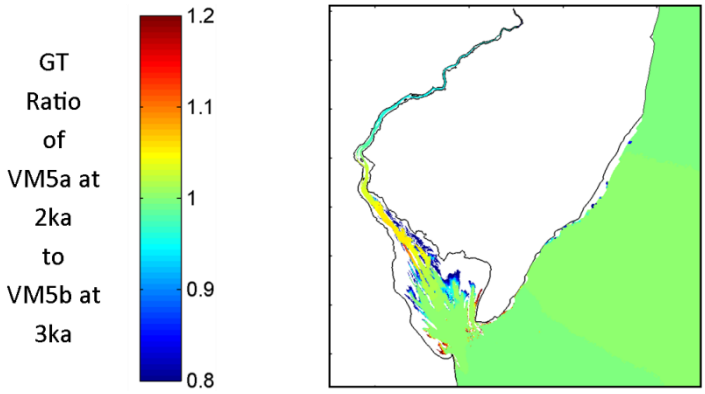

Figure 28: Local ratio of GT calculated from VM5a driven model at 2ka to GT calculated from VM5b driven model at 3ka.

4.5 Future Regional

As shown in chapter 3 and section 4.1, the Future Runs were computed on a grid that added topographic data and did not perform as well as the Holocene Grid in the NOAA water surface elevation and constituent comparison verifications. Subsequently, constituent and GT results were slightly different for runs conducted on the two "0ka" grids where they should have been the same. Figures and further discussion of this are presented in chapter 5.

On a regional level, the output of the 0ka +0.1 and +0.3kyr Future Runs showed similar tidal constituent and range amplitudes to those of present day. Coastline inundation was not significant enough to be shown on the regional plots. Diurnal ranges in the Gulf of Mexico, Caribbean Sea and Gulf of Maine at +0.3kyr do not exhibit differences from present day despite the sea level rise of approximately 3.5m plus variability due to GIA.

4.6 Future Local

4.6.1 Delaware Bay

Constituent phases showed the same spatial variability as the Holocene Runs over the Future Grid at 0ka. At the modeled future time slices, despite large eustatic rises and inundation, minimal changes to constituent phases were observed, with noticeable changes only in the northernmost bend in the Delaware River.

Local future M_2 amplitudes and resulting GT changes (Figure 29) were more apparent and closely tied. With the inundation caused by GIA and eustatic rise at +0.1kyr, GTs at locations in the upper bay remained higher than those in the lower bay. Within the river, GTs dropped in magnitude in the southern end, remaining close to present day range in the northern portion. Tidal flatlands around the edges of the estuary show minimal GT in blue as they were still within the intertidal zone and not fully inundated.

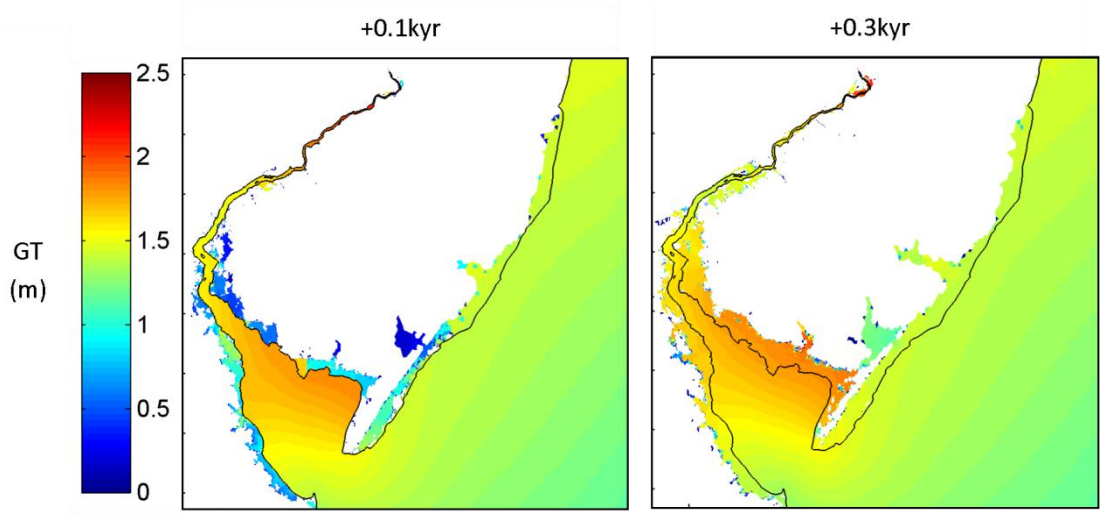

Figure 29: Future GT in the Delaware Bay: 0ka +0.1 and 0ka +0.3kyr.

At +0.3kyr, the change in coverage by the orange color shows that the larger GTs shifted into northeast corner of the bay as the GTs in the northwest corner dropped slightly. The surrounding flatlands in the northwest corner of the bay became local areas of maximum GT immediately after they were inundated. The maximum GT magnitude remained the same within the confines of the bay. The lower river formed a much wider shape, creating a portion of the bay that extends higher to the north. The rest of the river split, with mostly reduced GT in the lower portions; only the bend furthest to the north continued to maintain the highest range.

The Future Runs predicted that GT would decrease with respect to present day magnitude within most of the bay as indicated by the blue color in Figure 30. Note that the scale on Figure 30 only displays +/- 10% of the present day range to show the small trends in the bay. Locations in the intertidal zone at 0ka showed nearly infinite ratios at +0.1 and +0.3kyr (dark red) while areas submerged after 0ka show undetermined values (no data plotted) of GT ratio when compared to present day; these results were ignored as the ratios do not represent meaningful comparisons.

At +0.1kyr, a decrease in GT of about 2% from present day was seen in the bay, with only the portion to the northeast remaining at the same range. The contrast that was seen between the upper and lower bay in the Holocene Run data was not present. In the river, an area of GT decrease coupled with the upper bay transitioned into a GT increase up to 10% in the northern portion of the modeled river.

At +0.3kyr, the decrease in the bay continued but was more pronounced at 9-10% of 0ka GT, this time it encompassed most of the domain except for the fringes of the Holocene 0ka coastline in the northeast bay. The GT in a small portion of the southern river remains the same and moving northward begins to increase again, after falling at +0.1kyr. The upper portion of the river does the opposite and begins to decrease after increasing at +0.1kyr.

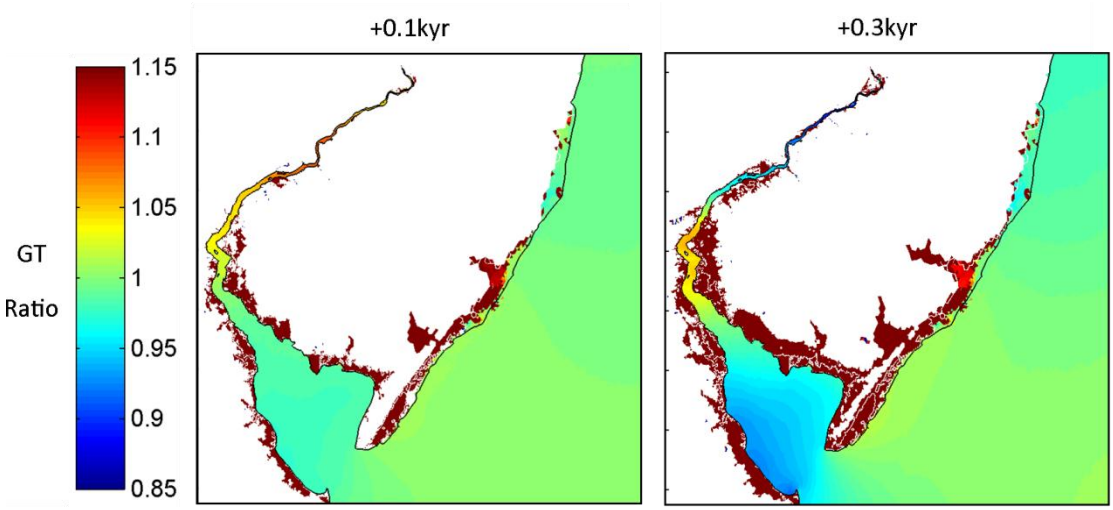

Figure 30: GT ratio in the Delaware Bay: 0ka+0.1 and 0ka+0.3kyr.

4.6.2 Chesapeake Bay

Different from the results in the Delaware Bay, future GT in the Chesapeake Bay increased with SLR, continuing the trend shown in the Holocene Runs. Spatially, these future results were similar to the Holocene trends; the upper and middle portion of the bay shows the largest areas of change while GT at the mouth remains constant. The future changes in the Chesapeake Bay were also of greater relative magnitude than the Delaware Bay. The mid-bay area showed a GT increase of 25% and 50% at +0.1 and +0.3kyr, respectively (Figure 31). The upper Chesapeake Bay showed an increase of up to 75% in 300 years. Figure 31 also showed the coarser resolution of features and fewer areas of inundated land when compared to the future results of the Delaware Bay.

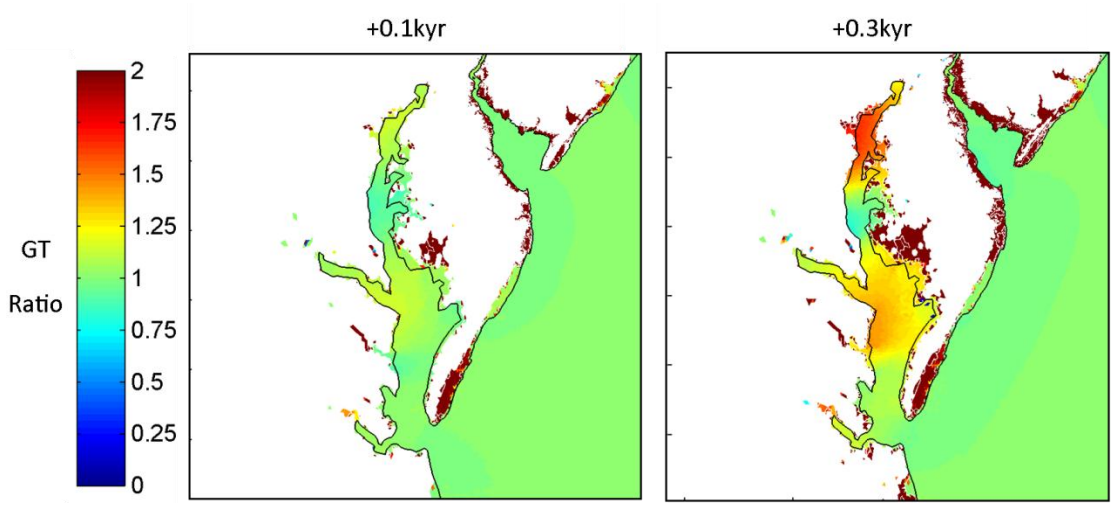

Figure 31: GT ratio in the Chesapeake Bay: 0ka +0.1 and +0.3kyr.

Chapter 5 – Discussion

GT change in the Delaware Bay was spatially variable and responded nonlinearly to sea level changes. This behavior is illustrated in Figure 32, which shows a time series of GT, at single point locations in the Upper Delaware Bay, lower Delaware Bay and the Hudson Canyon from 8ka to present day. Each location began with 0 GT and then became fully inundated at a different time corresponding to the rise in sea level due to GIA. These three locations transitioned to an amplified GT during the course of the modeled time, but their responses to incremented sea level increases were significantly different. Focusing on the behavior just after inundation, GT at locations in the lower bay and Hudson Canyon jumped immediately above present day range before steadily falling. This was contrasted by the GT in the upper bay, which slowly rose after inundation, eventually reaching a maximum at present day.

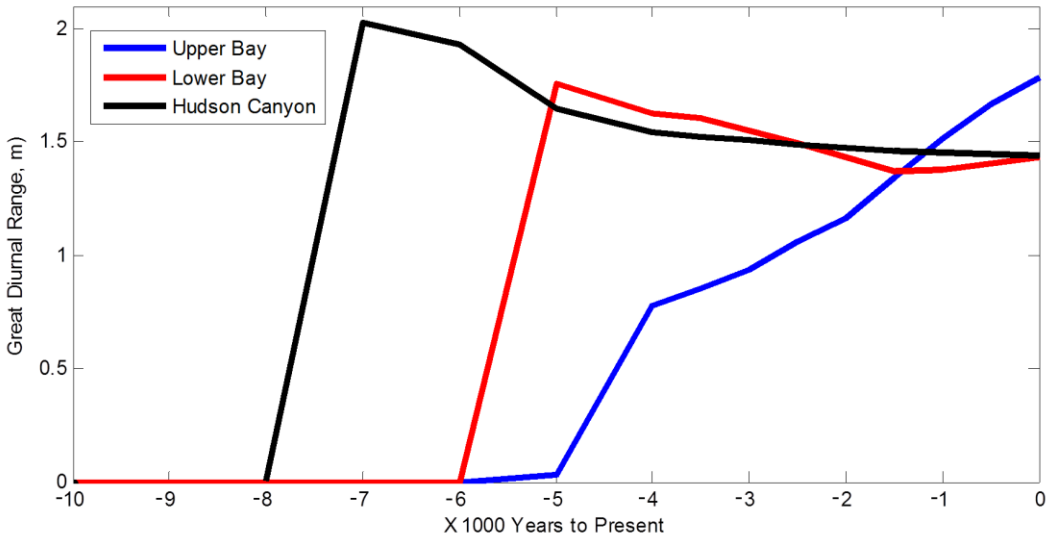

Figure 32: GT time series comparing locations in the upper bay, lower bay, and Hudson Canyon.

These different responses also occurred on different time scales, leading to different behaviors in the bay over a given interval. Between 3 to 0ka, GT in the upper bay and river

steadily increased, doubling to their present day values. During the same time, tidal range in the already inundated lower bay remained much steadier, decreasing then increasing slightly. In future scenarios, small decreases were seen in GT at all locations except in the river, where further spatial and temporal variability was observed. Figure 33 shows this temporal variability through time series plots of GT at select locations in the Delaware Bay during the interval of 3ka to +0.3kyr. Based on the spatial and temporal variability of both the bathymetric and GT changes, mechanisms for tidal range change can be examined.

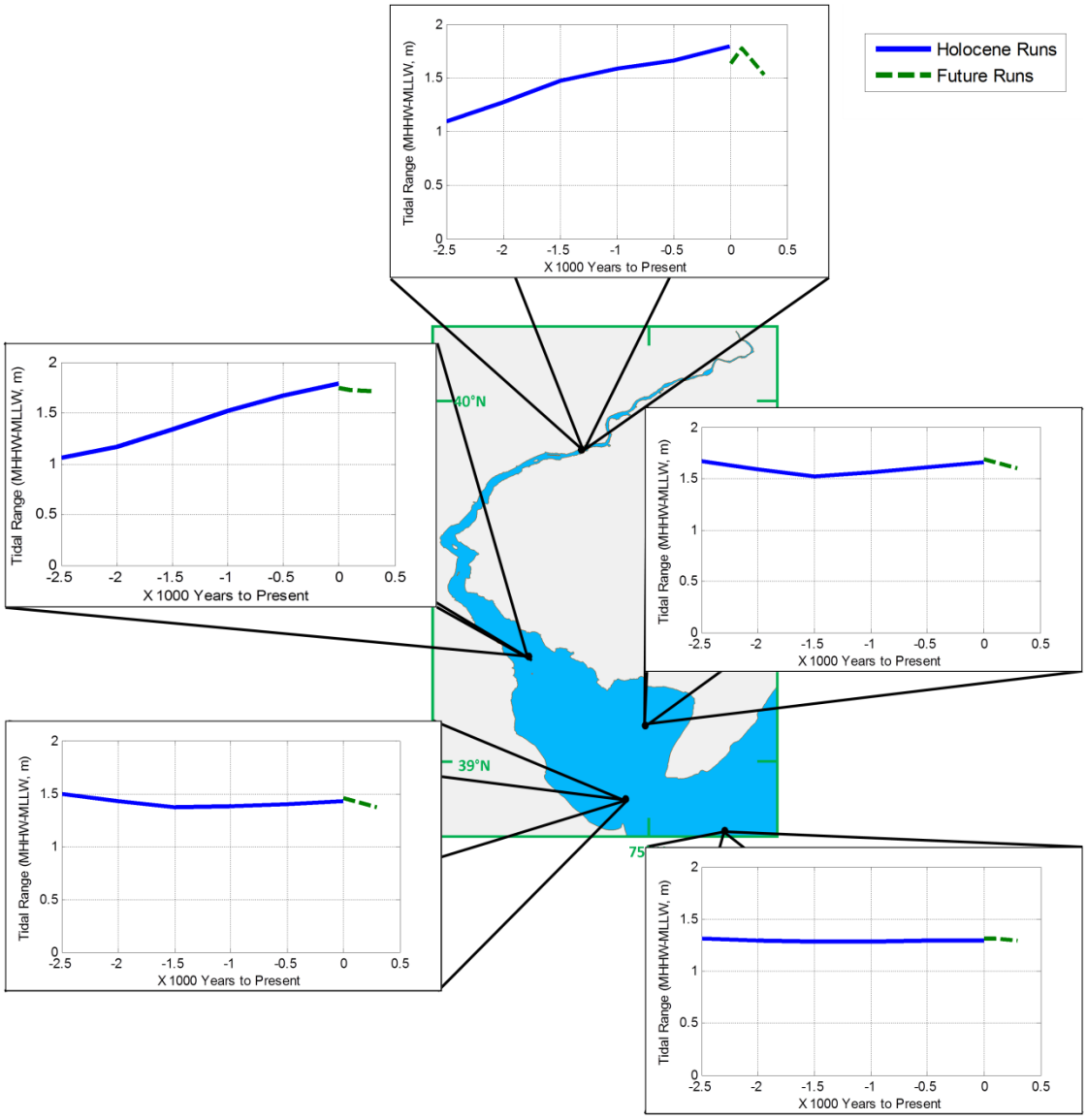

Figure 33: GT trends at selected locations in the Delaware Bay.

5.1 Mechanisms

5.1.1 Frictional Dissipation

Some combination of dissipation and resonance likely caused the tidal range changes modeled in the Delaware Bay. Damping due to the increased role of bottom friction can be explored from model results where the areas of shallow water added as the bay was

inundated could have caused more frictional damping and reduced tidal range (e.g. Zhong, Li and Foreman 2008). This behavior on a larger scale was noted in global models of the wetting of continental shelves since the LGM (e.g, Green 2010). This may have contributed to the spatial variability of GT throughout the bay in the Holocene and may be prominent in the Future scenarios, explaining the net decrease in GT.

Plots of cross sectional bathymetry with time slice waterlines show inundated length and depth changes over certain time intervals. Figure 34 shows cross sections of the bathymetry at 3ka, 0ka and +0.3kyr developed using the GIA models as described in chapter 3. In this figure, the bottom profile remains fixed while dashed lines represent bathymetry changes relative to the 0ka condition. Four spatially representative cross sections (A-D) are shown. Since the dashed lines at 3ka and +0.3kyr are relative to 0ka, the mostly flat surfaces show that there is little variability in the GIA signals from the west to east bay; only location C at +0.3kyr shows a small declining slope moving from west to east. The significant variability in GIA is north-south in the bay, between the sections of the bay shown in Figure 3.

From the cross section of location D, the narrow channel to the southeast can be seen along with shallower depths to the northwest. The slopes of the banks on either side are relatively steady and steep, so there is only a small amount of gained inundation length at each successive sea level rise interval. Contrast that with location C where, with much more gradual banks, between 3 and 0ka the inundation length nearly doubled, providing a wide cross section of shallower water. Location B shows some significant increase in depth over the wetted area between 3 and 0ka, then inundation over shallower tidal flats between 0ka and +0.3kyr. Location B represents the upper bay, where GT increased between 3 and 0ka while location D is within the lower bay where GT remained the same or decreased slightly over the same period. In both locations, between 0 and +0.3kyr, GT decreased as the inundation length and area of shallow water appeared to increase. The gently sloped areas that make up present day tidal flats can be seen to inundate between 0ka and +0.3kyr in the other locations as well. These represent the significant shallow water areas that are added in Future Runs, presumably dissipating energy and causing a net reduction in GT. These plots also highlight the fact that cross-shore beach profiles remained unchanged aside from the

waterline, a factor that, while necessary from this approach based on time and spatial scale, probably represented an unrealistic representation of the nearshore.

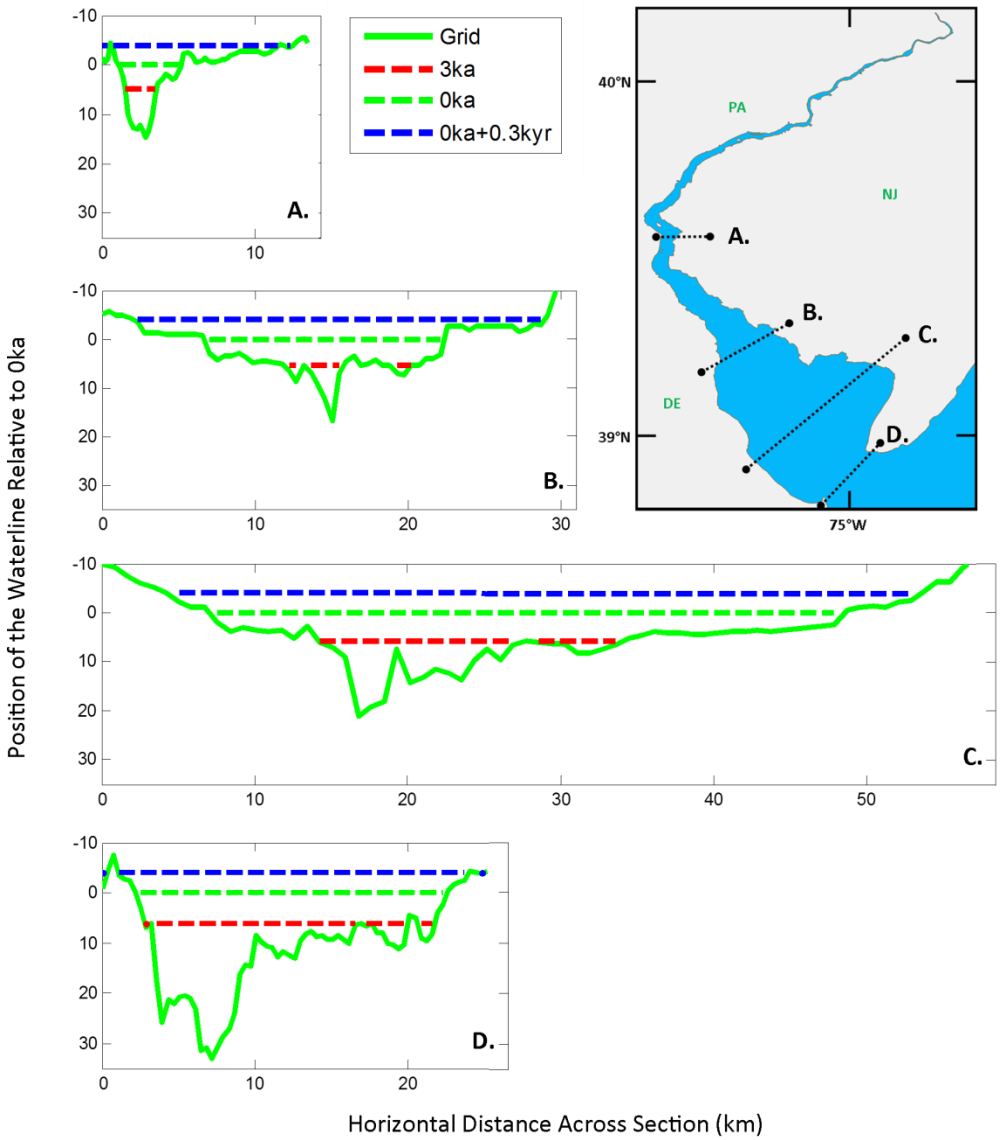

Figure 34: Cross-sectional bathymetries and water levels at 3ka, 0ka and +0.3kyr.

For cross-sections between selected successive time slices (6 to 5ka, 5 to 4ka, 4 to 3ka, 3 to 2ka, 2 to 1ka, 1 to 0ka, and 0ka to +0.3kyr), the inundated horizontal length was

quantified and normalized by the distance at 0ka. The additional land is generally of shallower water (Figure 34), so a greater ratio of added land should correlate to higher damping from bottom friction and lower GT. Figure 35 plots that ratio with respect to GT calculated adjacent to the west bank of the bay. Overall, GT and inundation distance along the cross section are non-linear but very weakly correlated. The bathymetries are complicated and different at each cross section as they represent real soundings at a high resolution; the position of the channels and tidal flats also change across the north-south orientation. Significant increases in inundated land (i.e. above 50% of present day), however, do correlate to GT decrease in all cases, while smaller inundation lengths vary in their GT response but generally show increase. Within the scenarios of significant increases in inundated land, the shallow water damping of tidal energy can then be tied to a decrease in GT.

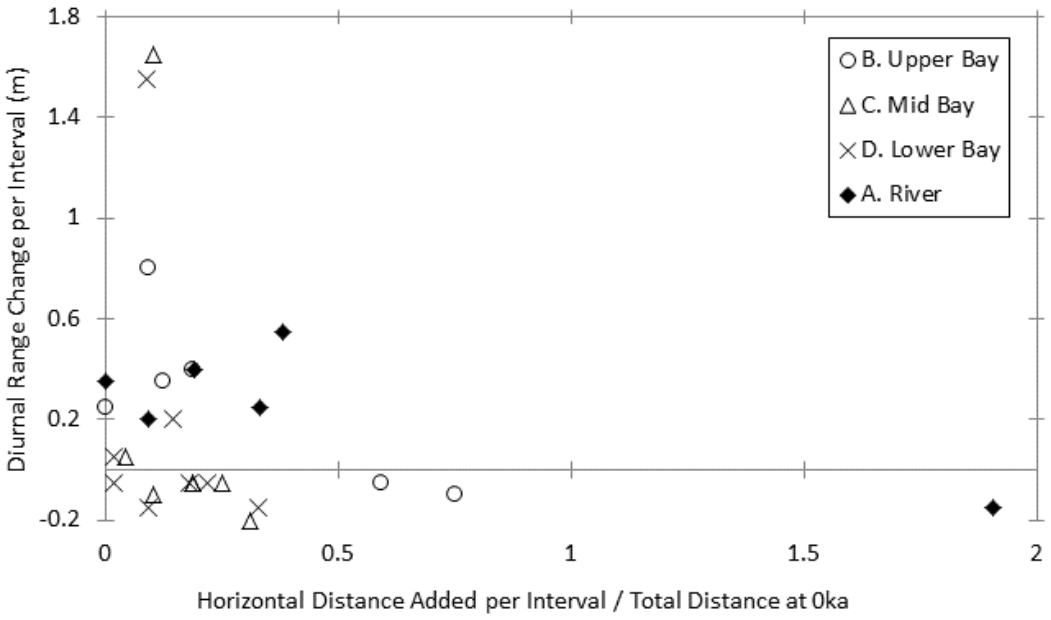

Figure 35: Plot of inundation length relative to length at 0ka vs. GT for time intervals for four cross sections from 3ka to +0.3kyr.

5.1.2 Resonance

Resonance as a mechanism for tidal range change can be explored through changes to the natural period of the bay caused by overall length and depth, as well as the width of the estuary where the shape dictates relative spatial differences in tidal range. Walters (1997) used a frequency response model for the present day Delaware Bay, finding periods of resonance of 9 hours in the lower bay and 6 hours in the river. Semidiurnal constituents (i.e. M_2, S_2) with periods of ~12hrs are then closer to resonance while diurnal constituents (i.e. K_1) with periods of ~24hrs are not. The quarter-diurnal tides (such as the M_4 overtide with a period of about 6hrs) are nearly in resonance with the river. The Merian formula for calculating basin resonance states that the period is proportional to length and inversely proportional to the square root of the depth (Dean and Dalrymple 1991). From 0ka to 3ka, the estuary depth decreased by 5-6m, while the north-south length only decreased slightly (Figure 10). In a simple approximation, this relative change would cause the resonance period of the whole bay to increase, bringing it closer to that of the M_2 tide.

Parker (1991) noted that an analytical model of an exponentially decreasing estuary width was able to describe the M_2 amplitude behavior of the present day Delaware Bay, where the amplitude, and therefore the tidal range, increased with decreasing bay width. Figure 10 showed a decrease in width throughout the length of the bay, going back in time as the estuary transitioned from a funnel shape at 0ka to a constant width at 3ka. In accordance with Parker (1991), this transition in width should have caused the relative GT in the upper estuary to decrease.

These concepts can potentially explain the upper and lower bay GT behavior as highlighted in Figure 32. An initially close, but diverging resonance period with the M_2 tide as depth increased in time could have led to the high GT seen in the lower bay at 5ka that decreased. Separately, when the bay was initially inundated with a constant width and slender shape, the upper bay GT was smaller relative to that of the lower bay. Subsequently filling out into a funnel shape could have increased the GT where the width remained narrow in the upper bay, providing for a difference between the two locations.

5.1.3 Non-Linear Response

Of the important higher order constituents, the M_4 occurs due to the nonlinear interaction of the M_2 tide with itself and the M_6 represents the non-linear response of the M_2 tide to frictional dissipation. Given the changes in bay shape throughout time, both constituents can be used to show the importance of non-linearity in the changing tidal behavior (Parker 1991). Figure 36 shows the ratio of the M_4 and M_6 to M_2 amplitude at specific locations in the upper and lower bay. In the upper bay, the higher order harmonics make up less than 8% of the M_2 constituent as opposed to less than 5% in the lower bay. Here, nonlinearity is more significant in the upper bay, but neither is very large relative to M_2. While nonlinear responses did change, it was the effect of the M_2 tide that accounted for the majority of the GT change. It is important to note that the points selected were in channels to enable further exploration in changes with time. Presumably, the percentages would be higher at locations in shallower water, especially for the M_6/M_2 ratio.

From the time series, the upper and lower bay display different patterns in their nonlinearity. In the upper bay, the M_4 constituent is steady with respect to the M_2 constituent for the period of initial wetting to 2ka, where it begins to decrease until 0ka and beyond. The M_6 tide also decreases in importance after 3.5ka. This seems to oppose the rise of the M_2 tide in the same location, indicating that nonlinearity becomes less important the as the M_2 tide resonates with the upper bay. The lower bay is marked with less steady trends of increase and decrease in non-linear response, the maximum non-linear influence from both M_4 and M_6 at this location occurs at 1.5ka, which coincides with the minimum value of M_2 amplitude and GT.

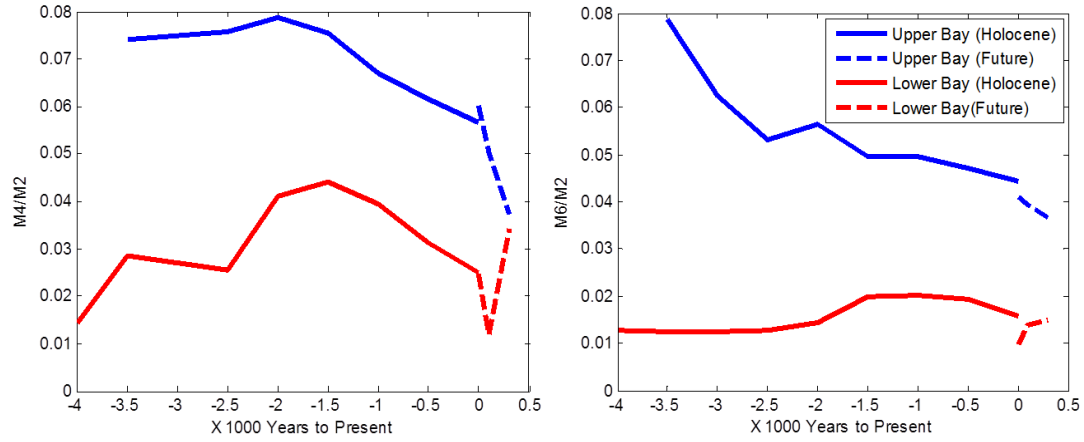

Figure 36: Time series of M_4 and M_6 higher order constituents normalized by M_2 for upper and lower bay locations.

5.2 Comparisons

5.2.1 Hill, et al. (2011)

With this study employing constant offshore tidal forcing, tidal range changes were attributed exclusively to changes in regional and local bathymetry, removing the influence of global tides. These results can be used to further explain the mechanisms behind changes noted by Hill, et al. (2011), which used temporally variable open boundary forcing as forced from global models. Hill, et al. (2011) also used the VM5a/ICE-5G coverage model vs. VM5b/ICE-6G in this study. Engelhart, Peltier and Horton (2011) showed little difference between the ICE-5G and ICE-6G models along the U.S. Atlantic coast while comparisons of results from the VM5a and VM5b models in this study showed slight changes in the magnitudes of GT, with the major differences being in the timing. With these differences in GIA estimates only causing minimal changes in GT, and since a similar regional grid was used, the differences between Hill, et al. (2011) and this study can be attributed to the respective variable and constant boundary forcing used.

As mentioned previously, the relatively steady tides in the Atlantic Ocean since 6ka modeled in Hill, et al. (2011) provided our justification for not varying open boundary tidal forcing in time since the Delaware Bay was dry prior to that time. At these time slices, results

from both studies were in agreement. Prior to that, Hill et al. (2011) saw a rise in Atlantic Ocean tides around 9ka, while tides in this study remained constant, indicating that this behavior was dependent on the global temporally varying forcing. Other similarities to Hill, et al. (2011), and therefore, results driven by regional bathymetric changes were seen in in the Gulf of Maine system and other estuaries where tidal range of the past experienced non-linear increases forward in time.

5.2.2 Flick, et al. (2003)

For locations in Cape May, NJ and Lewes, DE, GT change rates obtained from the Flick, et al. (2003) analysis of tide gauges are shown with rates obtained in this study in Table 4 (for location reference, see Figure 5). The three rates from this study are obtained with respect to present day from results of two Future Run cases and one Holocene Run case. Comparisons of the Future Run GT change rates from 0ka to +0.1kyr and 0ka to +0.3kyr to tide gauge data showed trend agreement. A very close match of magnitude and trend was found between the gauge data and +0.1kyr calculation at the Lewes, DE station. Both the model and observation at this location suggested a significant downward trend in GT. Comparing the gauge data and Holocene GT change rates from 0.5ka to 0ka, showed very different magnitudes and directions. This rate represents only the change modeled by GIA without a eustatic rise, where changes in bathymetry based on the VM5b model amount to about 20cm in 0.1kyr. This suggests that the observations of Flick, et al. (2003) reflect the GT changes caused by a eustatic rise in sea level coupled with a GIA signal, instead of just the GIA signal. Other gauge observations at locations within the Western Atlantic domain were compared to results in the model, but trends in GT showed no correlations in any other areas except in the Chesapeake Bay.

Flick, et al. (2003) compiled measurements of water surface elevations from the mid to late 20th century. Presumably, the sea levels during this time would have been affected by a recent increase in global temperatures. However, the sea level rise that was used to model +0.1kyr in this study is non-linear, based on a further *future* increase of 1.8°C in global temperature and associated acceleration in the rate of sea level rise. Based on unknown SLR accelerations, potential gauge measurement error and unaccounted-for model processes tidal change trends were not expected to line up this closely for the time periods. This

disparity in temperature change mechanisms as well as having only two gauge stations within the modeled Delaware Bay area (with none in the upper bay) makes a high confidence in the correlation with Flick, et al. (2003) difficult to justify. Nevertheless the existing results are in alignment where both model and gauge data suggest that the tidal range in the lower Delaware Bay is presently decreasing.

Table 4: Comparison of rates of GT change from Flick, et al. (2003), modeled Future Runs (0ka-0.1kyr and 0ka-0.3kyr), and modeled Holocene Runs in this study (0.5-0ka).

		MHHW-MLLW Change Rate			
	Location	Measured (Flick et al. 2003)	Modeled 0-0.1kyr	Modeled 0-0.3kyr	Modeled 0.5-0ka
10	Cape May, NJ				
	(mm/100yr)	-51	-22	-24	8
	(%/100yr)	-3	-1.4	-1.5	0.5
11	Lewes, DE				
	(mm/100yr)	-33	-32	-40	5
	(%/100yr)	-2	-2.2	-2.8	0.4

5.2.3 Zhong, Li and Foreman (2008)

Although the Chesapeake Bay was modeled with lower resolution grid spacing on the order of multiple km, the 0ka and +0.1kyr tidal range results from this other location corroborate the study of Zhong Li and Foreman (2008), showing increases in tidal range. This increase occurs in the lower-mid and upper portions of the bay in this study, while other adjacent areas, such as the mouth, show little change. Figure 31 showed GT changes in these areas of the Chesapeake were on the order of 25% with the +0.1kyr sea level increase on the order of 1m. These were among the largest changes noted within the grid over the 100 year period. According to Zhong, Li and Foreman (2008), the GT increase is due to the large relative increase to the otherwise shallow depth causing a lower resonance with diurnal constituents as well as reduced shallow water dissipation. These authors did note that

landward inundation would be needed to better understand the tidal range change mechanisms, which was incorporated in this study. Here, the shallow water dissipation caused by shoreward inundation, which likely accounted for the GT decrease in the Delaware, did not prevent the tidal range from increasing in the Chesapeake. Furthermore, results of Flick, et al. (2003) gauge data show an increasing GT in upper bay locations in Baltimore and Annapolis, MD with decreases at stations at the mouth of the bay. Although the gauge locations were not fully resolved by the grid of this study and the magnitudes are different, the Flick, et al. (2003) results show qualitative trend agreement with both model studies. While this response appears of greater future concern than the Delaware Bay, it is also important to note the lower present day tidal amplitudes. Through the results of these different studies, the Chesapeake Bay shows a notable relative response to future sea level rise suggesting that higher resolution studies would be beneficial in determining potential future impacts of tidal range change.

5.2.4 Leorri, et al. (2011)

The Holocene Runs within the Delaware Bay offer a comparison to the methods and results of Leorri et al. (2011). These authors used a uniform sea level decrease of 5.33m from present day to simulate the water levels of 4ka, and forcing a tidal model with the M_2 constituent over 0ka and 4ka bathymetries. Using the VM5b from this study for sea level transformation, 3ka results show a sea level decrease of 4.5m in the river, 6.1m in the lower bay, and 5m in the upper bay. Noting this difference in temporal sea level change with their 4ka scenario matching better to our 3ka scenario, the M_2 amplitude changes over these intervals between Leorri, et al. (2011) and this study can be compared to evaluate the contribution of the use of other tidal constituents and GIA spatial variability in this model.

Qualitative comparisons of the spatial M_2 amplitude plots between these two studies show good agreement. Given the different time intervals, the area of large amplitude increase in the river and upper bay that contrast an area of steady amplitudes in the lower bay is visible in both results. Table 5 shows this comparison in terms of the ratio to present day M_2 amplitude for the upper and lower bay locations. Leorri, et al. (2011) argued that the M_2 constituent would show nearly the same behavior as the tidal range in the Delaware Bay. Models of this study show that M_2 constituent makes up about 50% of the tidal amplitude in

the bay, the S_2 and N_2 are about 10% each and the K_1 accounts for around 6%. Despite the significant contribution of other constituents, the results of the relative M_2 constituent amplitudes are in very close agreement with the GT ratio parameter (Table 5, last column).

Comparing M_2 ratios at a location in the upper bay, it can be seen that the similar depth change of ~5m had the same effect on M_2 amplitude in both studies; causing an amplitude of 50% of present day. The M2 amplitude in the lower bay in this study experienced less change than that in Leorri, et al. (2011). A difference of 11% in the M_2 ratio between the two studies in the lower bay shows how the two sea level changes at this location (5.33m in Leorri, et al. 2011 vs. 6.1m in this study) affected the tidal range differently. Looking at the two locations relative to each other as an indication of their effect on sea level rise estimates, the incorporation of GIA at this time slice slightly decreases the difference between the tidal range changes at the two locations noted in Leorri, et al. (2011). With this difference being less, tidal range change difference would also have less of an impact on the different sea level rise rate estimates between these two locations.

While this study offers a more robust model of multiple time slices in the Delaware Bay, the spatially variable tidal range change trend noted by Leorri, et al. (2011) is shown. With general agreement at this location, the difference in results between this study and that of Leorri, et al. (2011) is attributable to the spatial variability in bathymetry change and difference in temporal SLR caused by implementing the VM5b GIA model.

Table 5: Comparison of M_2 amplitude ratio results of Leorri, et al. (2011) to M_2 amplitude and GT ratios from this study.

	M_2 Amplitude Ratio		GT Ratio
	Leorri et al. (2011)	This Study	This Study
% of Present Day	4 to 0ka	3 to 0ka	3 to 0ka
Upper Bay	0.50	0.51	0.53
Lower Bay	1.20	1.09	1.09

5.3 Accuracy

5.3.1 Holocene Runs

Model resolution represents a significant contributor to the accuracy of tidal range change models (Hinton 1996, Müller et al. 2011). Of the previous studies of tidal range change, the 80-175m spacing in this study provides the highest resolution grid in the local area. This study also is the highest temporal resolution study of the paleo-tidal Delaware Bay and the first attempt at simulating future tidal scenarios in the location.

Holocene and Future baseline grids appear to accurately model the tidal constituent behavior as separately verified by NOAA within the majority of the Delaware Bay. The largest constituent errors towards the river and in the Future Grid were on the order of 20% of NOAA values. On the regional scale of both grids, tide gauge comparisons would not likely yield good results given the placement of gauges in harbors unresolved by the grids.

For the Holocene Runs, it is argued that errors in the model parameters and the structure of the grid chosen do not substantially contribute to the spatial differences in tidal behavior within the Delaware Bay. While verifications were conducted, they could only have been done for 0ka since tidal range in the Delaware is not well documented prior to 100 years ago. Bottom friction and eddy viscosity mixing terms, the major parameters contributing to model solution, are not likely to vary in time within the location, so the values from 0ka should be good throughout the time slices modeled. For the selected results chosen in the bay from 3 to 0ka, there are sufficient elements in the wetted grid to provide useful solutions in the upper bay; Figure 37 shows that there are greater than 30 (much greater than the required three) elements spanning the width of the river at 3ka, allowing full communication and solutions among the nodes. Only in the northernmost section of the river do element constraints potentially have an effect at 3ka.

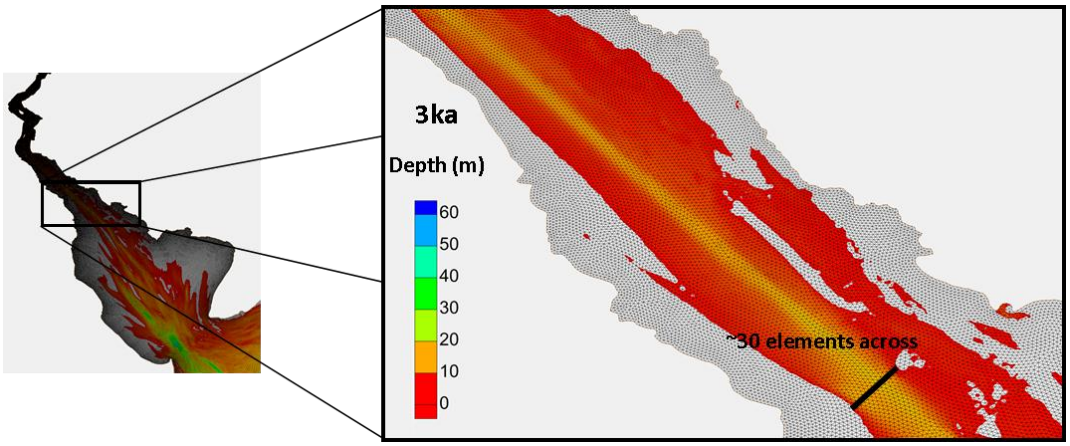

Figure 37: Depths plotted over elements showing that there is sufficient resolution in the narrow features of the Upper Bay at 3ka.

5.3.2 Future Runs

Future scenarios were taken from forward extrapolated GIA estimates and sample SLR predictions of eustatic rise from one source (Rahmstorf, Perrette and Vermeer 2011). The GIA signal made up to 15% of SLR in some areas in the +0.1kyr case, so GIA was not insignificant compared to eustatic rise. The rises in sea level of the Future scenarios were similar in magnitude to the Holocene rises of 1000yr intervals despite being on the order of 100yr. Given a wide range of SLR rate predictions made in other studies (e.g. 20cm to 2m in 0.1ky), future scenarios are perhaps even more unknown than past conditions. The results here provide only a potential case and the resultant tides. Due to the non-linear results found, other cases of SLR and inundation could lead to very different tidal results.

Figure 33 showed a discontinuity between the Holocene and Future Runs at each location in the 0ka GT results, while from the 0ka grid verifications, it was seen that the Future Grid produced larger errors compared to NOAA gauge data Figure 16. While mostly the same, there were certain portions of the Holocene Grid that were removed in the interest of fitting the best possible coastline. For the Future Grid, topographic data were obtained from the NED (USGS 2011) a different source that, although transformed to the same datum, could have had disagreements with the NGDC data (NOAA 2011b). These

complications resulted in the addition of small areas of the Future Grid that were below the waterline of the Holocene coastline at 0ka.

All model tuning was done to the 0ka Holocene Grid, with the same parameters used in the 0ka Future Grid. Here, keeping the same bottom friction for the 0ka Holocene and Future run grids may have been the parameter that contributed the most to the different results. When inundated at 0ka, the Future Grid contained more shallow water areas, over which more energy could have been dissipated due to bottom friction. Additionally, the Future Grid element resolution was not tuned to fit in all of the small (~<80m) features in the additional topographic data. Figure 38 shows the ratio of GT in the 0ka Future Grid to that calculated in the Holocene Grid. Within the lower and mid bay regions, the grids provide a similar answer. A departure between the grids occurs in the upper bay and river where the calculated GT by the Future Grid is up to 10% smaller. It appeared that the bottom friction term that was tuned to the Holocene grid was too high for the Future Grid in the river. It is possible that a better dissipation term could have improved the accuracy of the 0ka Future Grid solution had it been specifically tuned to this grid. Creating one 0ka grid from bathymetry and topography, tuning it to present day, and using it for Holocene *and* Future Runs would help for future studies.

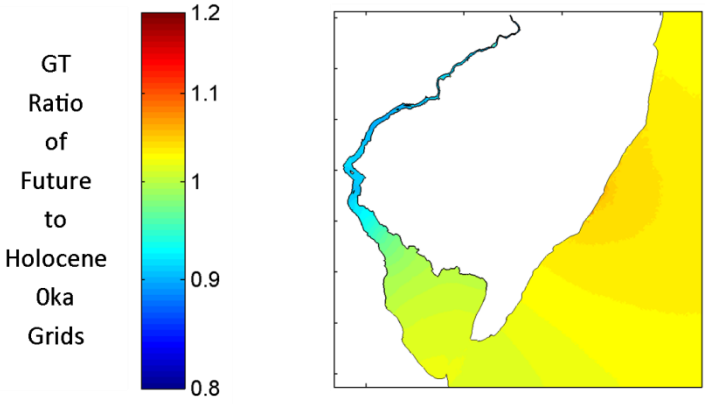

Figure 38: Ratio of GT calculated from the Future 0ka grid to that calculated from the Holocene 0ka grid.

5.3.3 Processes Not Modeled

While the hydrodynamics were able to be verified, the grids over which the forcing was run provide a source of potentially significant error. The sediment transport and geomorphology of the estuary due to interaction with the waves, tides, river currents and atmospheric effects represent physical processes that were not modeled. Other sediment transport processes such as estuary infill from tidal distortion, or river influence represent additional change mechanisms that may have a more significant impact on time slice bathymetries. An additional source of error is in the direct anthropogenic interference of the past century that was ignored in the Holocene Runs. These changes could also affect the future cases as shoreline modifications are carried out to limit change in locations of interest (i.e. dredging, sea walls, etc.).

These events occur on decadal and lower time scales; 500 year intervals are too large to resolve these processes. It may be possible to apply simple transformations based on estimated effects of these processes, however verification would not be presently possible and non-physics based estimates would lead to more unknowns. Given the amount of time required to run these models, more scenarios of shoreline and bathymetric change are not practical. It is therefore argued that, while recognizing the associated inaccuracy, the use of the VM5b and sea level rise estimates are currently the best available means of simulating paleo-bathymetries of this temporal and spatial scale.

5.4 Tidal Range Corrections in Holocene SLR Estimates

As noted in Engelhart et al. (2009), and in Figure 4, SLIP generated Holocene SLR rates were higher in the upper bay location than in the lower bay. Corrections for both GIA and tidal range changes can be implemented using data from this study with the goal of explaining this spatial difference. Using the VM5b, upper and lower Delaware Bay locations at 3ka were modeled with a 5.25m and 6m decrease in water depths, respectively. Subtracting the maximum GIA signal difference (0.75m) from the RSLR estimates, the upper bay location is ~0.75m higher than the lower bay location in 3kyr. Implemented as a correction, this would decrease the difference between the rates at the two locations.

Figure 39 shows sample GT change corrections from this study implemented to SLIP data from a location in Sea Breeze, NJ located 6km from the site of the upper bay

measurements (Nikitina et al., in press). With the large temporal changes in tidal range noted in this study in the upper bay, the changes can be seen to more heavily affect the SLIP boxes further back in time. Qualitatively, the red boxes in Figure 39 form a milder slope, indicating that the rate of sea level rise would be less with tidal corrections at this location. Given GT results showing less change at the lower bay, it is expected that corrections would have less of an effect on the SLR rate at that location. Effectively based on the trends, these tidal range corrections would bring the lower and upper bay SLR rates closer to each other by some amount in addition to with GIA. Initial estimates indicate that there would still be a remaining difference in SLR rates at the two locations after both corrections, but further analysis would be required using SLIP data from each location to develop a quantitative answer. Furthermore, since the VM models are tuned to coincide with SLIPs, and changes in the VM model affect GT, the process of incorporating GT changes should be iteratively solved for more accurate results (Leorri, et al. 2011).

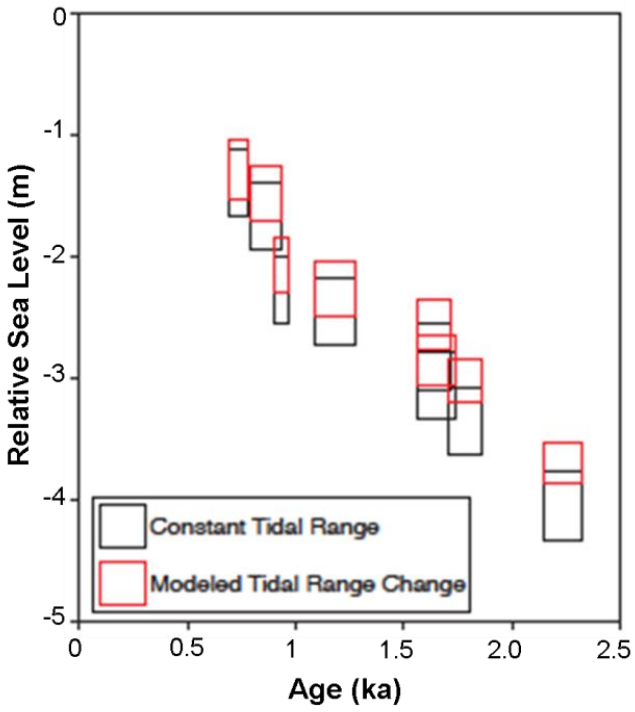

Figure 39: Sea level index points (SLIPs) from Sea Breeze, NJ with and without correction for tidal range from this study, (Nikitina, et al. in press).

5.5 Future Impacts

In the Future scenarios presented here, tidal range change magnitudes fell within the potential error bounds of the associated sea level rise estimates within the Delaware Bay. Looking exclusively at the potential changes in water levels, it is then difficult to distinguish the compounding impacts of tidal range change from the impacts of SLR. Greater relative magnitudes of GT change, with an increasing trend, were noted in the lower resolution model of the Chesapeake Bay that may be shown to be of greater significance when compared to SLR. The nonlinearity of GT change results in response to sea level should be noted in addition to the unknowns involved in the models of future bathymetry presented previously. One set of sea level rise scenarios is inadequate to describe potentially highly variable changes in tidal range, but a statistically based range of possibilities and outcomes would be highly computationally intensive.

If the trend in tidal range is downward as modeled in the Delaware Bay, the change could act in a small capacity against higher water levels associated with sea level rise; however, a reduced tidal range could have other secondary effects. Associated transport currents may be impacted and cause changes if brought below a certain threshold. Chemical, biological and ecological processes may be affected, presumably less so than if the tidal range change were greater, but these would be largely speculative.

Changes in tidal behavior may be indicated by parameters other than GT. One example is in constituent properties that indicate the strength and direction of distortion of the tidal wave where an estuary can be dominated by currents in the flood or ebb direction (Parker 1991). Figure 40 showed the M_4 to M_2 ratio for two locations within the bay going forward in time to display non-linear response. This ratio is also representative of the magnitude of the tidal distortion (Parker 1991). Looking at the Future Run results (0 to +0.3kyr), large changes in this magnitude are seen over the short periods; the ratio in the upper bay decreases while the lower bay increases.

The relative elevation phase of $2(M_{2\ Phase})–M_{4\ Phase}$ indicates the tendency towards tidal flood or ebb dominance at a given location, this phase difference can be analyzed from model data as well. Figure 40 shows this relative elevation phase plotted for the two

locations in the upper and lower bay. Based on this phase difference, criteria from Friedrichs and Aubrey (1988) can be used to classify the Holocene upper bay as having strong flood dominance, marked by a shorter duration of higher currents during the tidal flood stage when compared to the ebb stage. This correlates well with present day time series observations from tide gauges at upper bay locations where steeper flood waves are noticeable in the upper bay and river. The lower bay has shifted between ebb to flood and presently back to ebb dominance with weaker tendencies. The Future cases in both locations do show a steep change towards tidal symmetry between 0ka and +0.1kyr (represented by 180°, meaning neither flood not ebb dominated), steadying out between +0.1 and +0.3kyr at different relative phases than in the past.

The high currents in flood (ebb) dominated areas lead to sediment transport in the direction of the flood (ebb), causing estuary infill (draining) (Friedrichs and Aubrey 1988). Within the Delaware Bay, there is great spatial variability in sediment transport with the primary determinant being the small scale irregularities instead of the large scale tidal ranges and estuary shapes (Phillips 1986). However, a coexistence of flood and ebb dominated areas can also be the cause of complicated sediment transport patterns (Brown and Davies 2007). Small shifts in flood or ebb dominance can lead to large differences in sediment transport patterns within estuaries (Mirfenderesk and Tomlinson 2009). Future shifts noted at the two locations in this study show general decreasing flood dominance in the upper bay with decreasing ebb dominance in the lower bay indicating that the tidal distortion at the two locations would become more closely related. These transport patterns can also affect salinity, heat, biological and other chemical transports associated with an estuary. As previously noted, the effects of past changes in flood and ebb dominance on sediment transport were not modeled in the past bathymetries. However, the Future changes noted here may result in larger scale changes to the local coastal shapes and environment in the future. These patterns would result in some new equilibrium condition that could also affect the shape of the estuary. It has been proposed that increased depth would lead to increased flood dominance in an estuary until a new equilibrium is found (Brown and Davies 2007). This model shows a more complicated and spatially variable response of flood and ebb dominance.

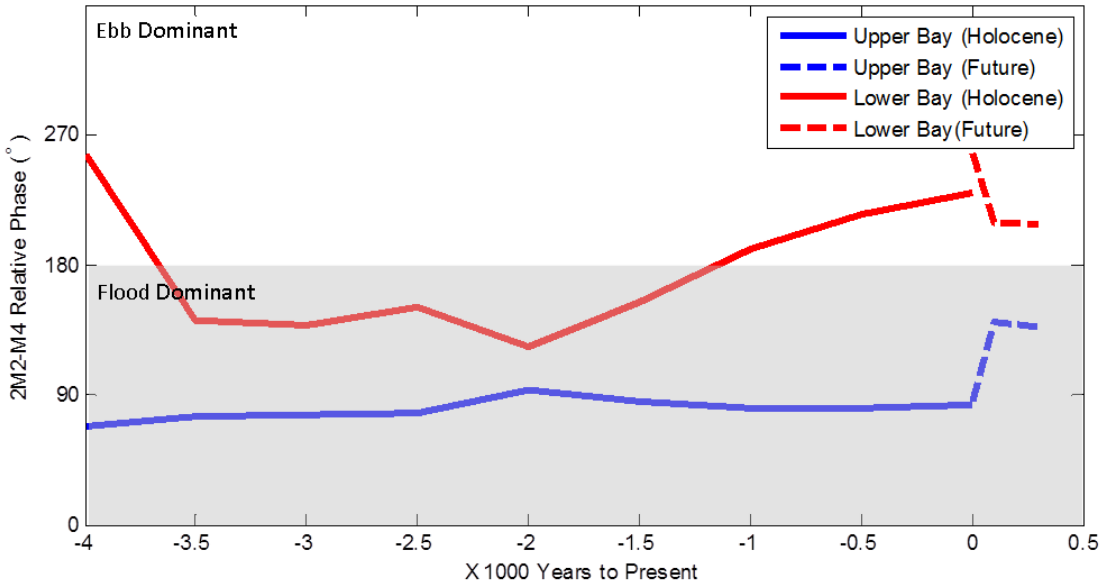

Figure 40: Time series of 2M2-M4 relative tide elevation phase with classifications as flood and ebb dominant from Friedrichs and Aubrey 1988.

Chapter 6 – Conclusion

This study explored tidal changes in an estuary as caused by glacial isostatic adjustment and eustatic sea level rise, focusing in the Delaware Bay, USA. Two finite element grids were built with a regional coverage of the northwestern Atlantic Ocean bathymetry of present day, increasing resolution in and around the Delaware Bay. A Holocene Grid containing only present day bathymetric data, and a Future Grid with additional topographic data were used as baseline conditions. Additional grids representing time slices between 10ka in the past and +0.3kyr into the future were created by applying a combination of GIA and predicted future eustatic sea level changes to these baselines. The ice coverage/mantle viscoelastic response model ICE-6G/VM5b was selected for the GIA transformation based on its applicability to the U.S. east coast (Engelhart, Peltier and Horton 2011). Subsequent comparisons of results with the ICE-6G/VM5a model (Toscano, Peltier and Drummond 2011) showed nearly the same trends but on different timelines. Usage of a GIA model provided a best estimate for paleo-bathymetries given the associated spatial and temporal scale. The addition of eustatic components in addition to GIA for Future Runs provided scenarios that representative of some mid-level estimates of sea level change due to global temperature increase. An ADCIRC model was then forced with present day tidal constituents over each time slice grid. Comparisons of each successive run's results produced temporal trends showing that GT responded nonlinearly to changes in bathymetry, spatially varying throughout locations in the constructed grid.

Regional GTs showed little temporal change as basin shape remained relatively constant and the open boundary forcing was not temporally varied. Significant GT changes were noted in areas along the coast and within the continental shelf. While this study was conducted to highlight results in the Delaware Bay, the Gulf of Maine, Hudson Canyon, and Chesapeake Bay also showed areas of significant GT change. Comparisons to Hill, et al. (2011), which used variable open boundary forcing over a similar regional area, showed that GT changes in these nearshore bays and estuaries were caused by local variations in bathymetry instead of larger scale changes in open boundary forcing.

Within the Delaware Bay, the significant spatial variability in Holocene GT change was north-south, divided between the upper and lower areas of the bay. GT in the lower bay

decreased after initial inundation while GT in the upper bay steadily climbed between 4ka and 0ka. Over the time period of 3ka to 0ka, the lower bay GT decreased 8% by while the upper bay increased by 91% where this spatial difference in tidal behavior is important due to its effect on sea level rise estimates. This spatial variability is similar to that seen in Leorri, et al. (2011), but the incorporation of the GIA model shows a smaller difference in tidal range behavior between the upper and lower bay, suggesting slightly less of an impact on sea level measurements. Among possible mechanisms for this change in resonance appears likely as the shape of the bay as it transitioned from a narrow channel to a funnel may have caused the increasing relative GT in the upper bay.

Future results of GT in the Delaware Bay showed different trends, marked by a decrease during scenarios of +0.1 and +0.3kyr in both the lower and upper bay. GT in the Delaware River meanwhile was more spatially varied, showing areas of increase and decrease. This decrease in tidal range may be tied to shallow water dissipation as significant energy was damped in the newly inundated tidal flatlands surrounding the bay. GT trends noted at locations in Lewes, DE and Cape May, NJ corresponded to those noted from 20th century tide gauge records in Flick, et al. (2003). This suggests that the measured trends in tidal range change correspond to local bathymetric changes as driven by modern global eustatic sea level rise. GT change within the Delaware Bay was less than 10% of present day magnitude in 0.3kyr, as opposed to GT changes noted in the Chesapeake Bay of up to 75%. While the Chesapeake Bay was modeled at lower resolution, trend agreement was also noted here with measurement results of Flick, et al. (2003) and model results of Zhong, Li and Foreman (2008), potentially providing an example location where GT change could become significant, should sea levels continue to rise. Future changes in both areas can impact water levels, providing higher high and lower low tides that would impact the coastal environment. Results of the behavior in the Delaware were also used to show potential changes in tidally driven transport in the bay where through shifts in flood and ebb dominance were seen.

Bibliography

ADCIRC. *ADCIRC related utility programs.* 2011. http://www.unc.edu/ims/adcirc/Utility_programs.html (accessed March-September 2011).

Arbic, Brian K., Richard H. Karsten, and Chris Garrett. "On tidal resonance in the global ocean and the back-effect of coastal tidses upon open-ocean tides." *Atmosphere-Ocean* 47, no. 4 (2009): 239-266.

Argus, Donald F., and W. Richard Peltier. "Constraining models of postglacial rebound using space geodesy: a detailed assessment of model ICE-5G(VM2) and its relatives." *Geophysical Journal International* 181 (2010): 697-723.

Brown, J. M., and A. G. Davies. "Flood/ebb tidal dominance in an estuary: sediment transport and morphology." *River, Coastal and Estuarine Morphodynamics: RCEM 2007, Two Volume Set. Proceedings of the 5th IAHR Symposium on River, Coastal and Estuarine Morphodynamics,.* Enschede, NL, 2007. 779-787.

Cazenave, Anny, and William Llovel. "Contemporary Sea Level Rise." *Annual Review of Marine Sciences* 2 (2010): 145-173.

Dean, Robert G., and Robert A. Dalrymple. *Water Wave Mechanics for Engineers and Scientists.* Singapore: World Scientific, 1991.

Dietrich, J. C., R. L. Kolar, and R. A. Luettich. "Assessment of ADCIRC's Wetting and Drying Algorithm." Edited by C. T. Miller, M. W. Farthing, W. G. Gray and G. F. Pinder. *XV International Conference on Computational Methods in Water Resources (CMWR).* 2004. 1767-1778.

Egbert, G. D., and R. D. Ray. "Significant dissipation of tidal energy in the deep ocean inferred from satellite altimeter data." *Nature* 405 (2000): 775-778.

Egbert, Gary D., Andrew F. Bennett, and Michael G.G. Foreman. "TOPEX/POSEIDON tides estimated using a global inverse model." *Journal of Geophysical Research* 99, no. C12 (1994): 24821-24852.

Egbert, Gary D., Richard D. Ray, and Bruce G. Bills. "Numerical modeling of the global semidiurnal tide in the present day and in the last glacial maximum." *Journal of Geophysical Research* 109, no. C03003 (2004).

BIBLIOGRAPHY (continued)

Engelhart, S. E., W. R. Peltier, and B. P. Horton. "Holocene relative sea-level changes and glacial isostatic adjustment of the U.S. Atlantic coast." *Geology* 39, no. 8 (2011): 751-754.

Engelhart, Simon E., Benjamin P. Horton, Bruce C. Douglas, W. Richard Peltier, and Torbjorn E. Tornqvist. "Spatial variability of late Holocene and 20th century sea-level rise along the Atlantic coast of the United States." *Geology* 37, no. 12 (2009): 1115-1118.

Fletcher, Charles H., Harley J. Knebel, and John C. Kraft. "Holocene evolution of an estuarine coast and tidal wetlands." *Geological Society of America Bulletin* 102, no. 3 (1990): 283-297.

Flick, Reinhard E., Joseph E. Murray , and Lesley C. Ewing. "Trends in United States tidal datum statistics and tide range." *Journal of Waterway, Port, Coastal, and Ocean Engineering-ASCE* 129 (2003): 155-164.

Friedrichs, Carl T., and David G. Aubrey. "Non-linear Tidal Distortion in Shallow Well-mixed Estuaries: a Synthesis." *Estuarine, Coastal and Shelf Science* 27 (1988): 521-545.

Gehrels, W. Roland, Daniel F. Belknap, Bryan R. Pearce, and Bin Gong. "Modeling the contribution of M2 tidal amplification to the Holocene rise of mean high water in the Gulf of Maine and Bay of Fundy." *Marine Geology* 124 (1995): 71-85.

Gerritsen, Herman, and Cas W.J. Berentsen. "A modelling study of tidally induced equilibrium sand balances in the North Sea during the Holocene." *Continental Shelf Research* 18 (1998): 151-200.

Green, Johan A. Mattias. "Ocean tides and resonance." *Ocean Dynamics*, 2010: 1243-1253.

Griffiths, Stephen D., and W. Richard Peltier. "Modeling of Polar Ocean Tides at the Last Glacial Maximum: Amplification, sensitivity and climatological implications." *Journal of Climate* 22 (2009): 2905-2924.

Hill, D. F., S. D. Griffiths, W. R. Peltier, B. P. Horton, and T. E. Tornqvist. "High-resolution numerical modeling of tides in the western Atlantic, Gulf of Mexico, and Caribbean Sea during the Holocene." *Journal of Geophysical Research* 116, no. C10014 (2011).

Hinton, A.C. "Tides in the Northeast Atlantic: Considerations for modelling water depth changes." *Quaternary Science Reviews* 15 (1996): 873-894.

BIBLIOGRAPHY (continued)

Houston, J. R., and R. G. Dean. "Sea-level acceleration based on U.S. tide gauges and extensions of previous global-gauge analyses." *Journal of Coastal Research* 27, no. 3 (2011): 409-417.

Jay, David A. "Evolution of tidal amplitudes in the eastern Pacific Ocean." *Geophysical Research Letters* 36, no. L 04603 (2009).

Kolar, R. L., and W. G. Gray. "Shallow Water Modeling in Small Water Bodies." *Proceedings in 8th International Conference on Computational Methods in Water Resources (CMWR).* 1990. 39-44.

Leorri, E., R. Martin, and P. McLaughlin. "Holocene environmental and parasequence development of the St. Jones Estuary, Delaware (USA): Foraminiferal proxies of natural climatic and anthropogenic change." *Palaeogeography, Palaeoclimatology, Palaeoecology* 241 (2006): 590-607.

Leorri, Eduardo, Ryan Mulligan, David Mallinson, and Alejandro Cearreta. "Sea-level rise and local tidal range changes in coastal embayments: An added complexity in developing reliable sea-level index points." *Journal of Integrated Coastal Zone Management* 241, no. 3-4 (2011): 307-314.

Luettich, Richard A., and Johannes J. Westerink. "A solution for the vertical variation of stress, rather than velocity, in a three-dimensional circulation model." *International Journal for Numerical Methods in Fluids* 12 (1991): 911-928.

Luettich, Rick, and Joannes Westerink. "Formulation and Numerical Implementation of the 2D/3D ADCIRC Finite Element Model Version 44.XX." Theory Report, 2004.

Milne, Glenn A, W. Roland Gehrels, Chris W Hughes, and Mark E Tamisiea. "Iidentifying the causes of sea-level change." *Nature Geoscience*, 2009: 471-478.

Mirfenderesk, Hamid, and Rodger Tomlinson. "Interaction between Coastal Development and Inland Estuarine Waterways at the Short–Medium Timescale." *Journal of Coastal Research* 25, no. 4 (2009): 969-980.

Mofjeld, Harold O., Angie J. Venturato, Frank I. Gonzalez, Vasily V. Titov, and Jean C. Newman. "The Harmonic Constant Datum Method: Options for Overcoming Datum Discontinuities at Mixed–Diurnal Tidal Transitions." *Journal of Atmospheric and Oceanic Technologies* 21 (2004): 95-104.

BIBLIOGRAPHY (continued)

Mukai, A. Y., J. J. Westerink, R. A. Luettich, and D. Mark. *Eastcoast 2001, a tidal constituent database for western North Atlantic, Gulf of Mexico and Caribbean Sea.* Coastal Inlets Research Program, Vicksburg, MS: U.S. Army Corps of Engineers Engineer Research and Development Center, 2002.

Muller, M., B. K. Arbic, and J. X. Mitrovica. "Secular trends in ocean tides: Observations and model results." *Journal of Geophysical Research* 116, no. C05013 (2011).

NOAA. *ETOPO1 Global Relief Model.* 2011e. http://www.ngdc.noaa.gov/mgg/global/global.html (accessed September 2011).

—. *National Oceanic and Atmospheric Assiocaition (NOAA) National Geophysical Data Center (NGDC) Coastline Extractor.* 2011a. http://www.ngdc.noaa.gov/mgg/coast/ (accessed November 2011).

—. *NOAA NGDC Hydrographic Survey Data.* 2011b. http://www.ngdc.noaa.gov/mgg/bathymetry/hydro.html/ (accessed July 2011).

—. *Tides & Currents.* 2011d. http://tidesandcurrents.noaa.gov/ (accessed March-July 2011).

—. *Vertical Datum Transformation.* 2011c. http://vdatum.noaa.gov/ (accessed March-September 2011).

NSF. *National Science Fund (NSF) Extreme Science and Engineering Discovery Environment (XSEDE).* 2011. https://portal.xsede.org/ (accessed July-November 2011).

Officer, Charles B. *Physical Oceanography of Estuaries (And Associated Coastal Waters).* New York: J. Wiley, 1976.

Parker, Bruce B. "The relative importance of the various nonlinear mechanisms in a wide range of tidal interactions (review)." In *Tidal Hydrodynamics*, by B.B. Parker, 237-268. New York: J. Wiley, 1991.

Peltier, W. R. "Closure of the budget of global sea level rise over the GRACE era: the importance and magnitudes of the required corrections for global glacial isostatic adjustment." *Quaternary Science Reviews* 28 (2009): 1658-1674.

Peltier, W. R. "Global glacial isostasy and the surface of the ice-age earth: the ICE-5G(VM2) model and GRACE." *Annual Review of Earth and Planetary Sciences* 32 (2004): 111-149.

BIBLIOGRAPHY (continued)

Peltier, W. R. "Global sea level rise and glacial isostatic adjustment." *Global and Planetary Change* 20 (1999): 93-123.

Peltier, W. R. "Global sea level rise and glacial isostatic adjustment: an analysis of data from the east coast of North America." *Geophysical Research Letters* 23 (1996): 717-720.

Peltier, W. R. "Ice Age Paleotopography." *Science* 265, no. 5169 (1994): 195-201.

Peltier, W. R., and Rosemarie Drummond. "Rheological stratification of the lithosphere: A direct inference based upon the geodetically observed pattern of the glacial isostatic adjustment of the North American continent." *Geophysical Research Letters* 35, no. L16314 (2008).

Phillips, Jonathan D. "Spatial analysis of shoreline erosion, Delaware Bay, New Jersey." *Annals of the Association of American Geographers* 76, no. 1 (1986): 50-62.

Pickering, M. D., N. C. Wells, K. J. Horsburgh, and J.A.M. Green. "The impact of future sea-level rise on the European Shelf tides." *Continental Shelf Research* 35 (2012): 1-15.

Pugh, D.T. *Tides, Surges and Mean Sea-Level: A Handbook for Engineers and Scientists.* New York: J. Wiley, 1987.

Rahmstorf, Stefan, Mahe Perrette, and Martin Vermeer. "Testing the robustness of semi-empirical sea level projections." *Climate Dynamics*, 2011: 1-15.

Ray, R.D. "Secular changes of the M2 tide in the Gulf of Maine." *Continental Shelf Research* 26 (2006): 422-427.

Ray, Richard D. "Secular changes in the solar semidiurnal tide of the western North Atlantic Ocean." *Geophysical Research Letters* 36, no. L19601 (2009).

Scott, David B., and David A. Greenberg. "Relative sea-level rise and tidal development in the Fundy tidal system." *Canadian Journal of Earth Sciences* 20 (1983): 1554-1564.

Shennan, I., et al. *Modelling western North Sea palaeogeographies and tidal changes during the Holocene.* Vol. 116, in *Holocene Land-Ocean Interaction and Environmental Change around the North Sea*, by I. Shennan and J. Andrews, 299-319. London: Geological Society, 2000.

Shennan, Ian. "Flandrian sea level changes in the Fenland II: Tendencies of sea-level movement, altitude changes and local and regional factor." *Journal of Quarternary Sciences* 1 (1986): 155-179.

BIBLIOGRAPHY (continued)

Shennan, Ian, and Ben Horton. "Holocene land- and sea-level changes in Great Britain." *Journal of Quarternary Science* 17 (2002): 511-526.

Shennan, Ian, et al. "Integration of shelf evolution and river basin models to simulate Holocene sediment dynamics of the Humber Estuary during periods of sea-level change and variations in catchment sediment supply." *The Science of the Total Environment* 314-316 (2003): 737-754.

Sterl, A., H. van den Brink, H. de Vries, R. Haarsma, and E. van Meijgaard. "An ensemble study of extreme storm surge related water levels in." *Ocean Science* 5 (2009): 369-378.

Thomas, Maik, and Jurgen Sundermann. "Tides and tidal torques of the world ocean since the last glacial maximum." *Journal of Geophysical Research* 104, no. C2 (1999): 3159-3183.

Toscano, Marguerite A., W. Richard Peltier, and Rosemarie Drummond. "ICE-5G and ICE-6G models of postglacial relative sea-level history applied to the Holocene coral reef record of northeastern St Croix, U.S.V.I.: investigating the influence of rotational feedback on GIA processes at tropical latitudes." *Quaternary Science Reviews* 30 (2011): 3032-3042.

TPXO. *The OSU/TOPEX Global Inverse Solution (TPXO 7.2).* 2011. http://volkov.oce.orst.edu/tides/global.html (accessed August 2011).

Tushingham, A. M., and W. R. Peltier. "ICE-3G_ A New Global Model of Late Pleistocene Deglaciation Based Upon Geophysical Predictions of Post-Glacial Relative Sea Level Change." *Journal of Geophysical Research* 96 (1991): 4497-4523.

Tushingham, A. M., and W. R. Peltier. "Validation of ICE-3G model of Wurm-Wisconsin deglaciation using a global data base of relative sea level histories." *Journal of Geophysical Research* 97 (1992): 3285-3304.

Uehara, Katsuto, James D. Scourse, Kevin J. Horsburgh, Kurt Lambeck, and Anthony P. Purcell. "Tidal evolution of the northwest European shelf seas from the Last Glacial Maximum to the present." *Journal of Geophysical Research* 111, no. C09025 (2006).

USGS. *National Elevation Dataset.* 2011. http://ned.usgs.gov/ (accessed October 2011).

Van De Plassche, Orson. *Sea-Level Research: A Manual for the collection and Evaluation of Data.* Norwich, U.K.: Geobooks, 1986.

BIBLIOGRAPHY (continued)

Walters, Roy A. "A model study of tidal and residual flow in Delaware Bay and River." *Journal of Geophysical Research* 102, no. C6 (1997): 12689-12704.

Wong, Kuo-Chuin, and Christopher K. Sommerfield. "The variability of currents and sea level in the upper Delaware estuary." *Journal of Marine Research* 67 (2009): 479-501.

Woodworth, P. L. "A survey of recent changes in the main components." *Continental Shelf Research* 30 (2010): 1680-1691.

Zhong, Liejun, and Ming Li. "Tidal energy fluxes and dissipation in the Chesapeake Bay." *Continental Shelf Research* 26 (2006): 752-770.

Zhong, Liejun, Ming Li, and M. G.G. Foreman. "Resonance and sea level variability in Chesapeake Bay." *Continental Shelf Research* 28 (2008): 2565-2573.

Appendix A – Model Instabilities

In addition to the chosen model input parameters that were the same every run, several individual adjustments were made to certain Holocene Grids that allowed for the successful completion of the 90 day harmonic analysis. These adjustments were made in response to the runs becoming unstable at time steps and specific locations. While a 3 second time step was successful for some grids, an analysis of the 0ka baseline condition showed that a 2 second time step was the maximum allowable timestep when a Courant number (CFL) of 0.6 was imposed. Based on results from several unstable trials, the 1, 2, 3, 4, 7 and 8ka domains were run with a 2 second time step while the others were run with 3 seconds. In order to keep the results of the 2 and 3 second runs as similar as possible, the sampling density of the harmonic analysis output was forced to be the same by changing the fort.15 in ADCIRC.

Even with a 2 second timestep, the 7 and 8ka Holocene Grids remained unstable. While interesting instabilities were also noted in just the Delaware Bay Grid around this same point in time, these instabilities here occurred in portions of the WNAT mesh that were far away from the area of concern in the mid-Atlantic U.S. The instabilities in the 7ka grid occurred in the region that represents the mouth of the Mississippi River in Louisiana. After the application of the vm5b transformation across the model, a section of the river remained below sea level but was not connected to the main body of water (Figure A-1). Likely due to the tidal potential forcing in this small, deep basin, this area became unstable quickly, achieving unreasonable water surface elevations in excess of 1000m within 1-2 days of model time, causing the model to shut down. To correct for this, the depth values for the nodes in the Mississippi (represented by the box in Figure A-1) were manually changed to a uniform 5 meters above sea level so that they would appear dry and therefore no longer produce results.

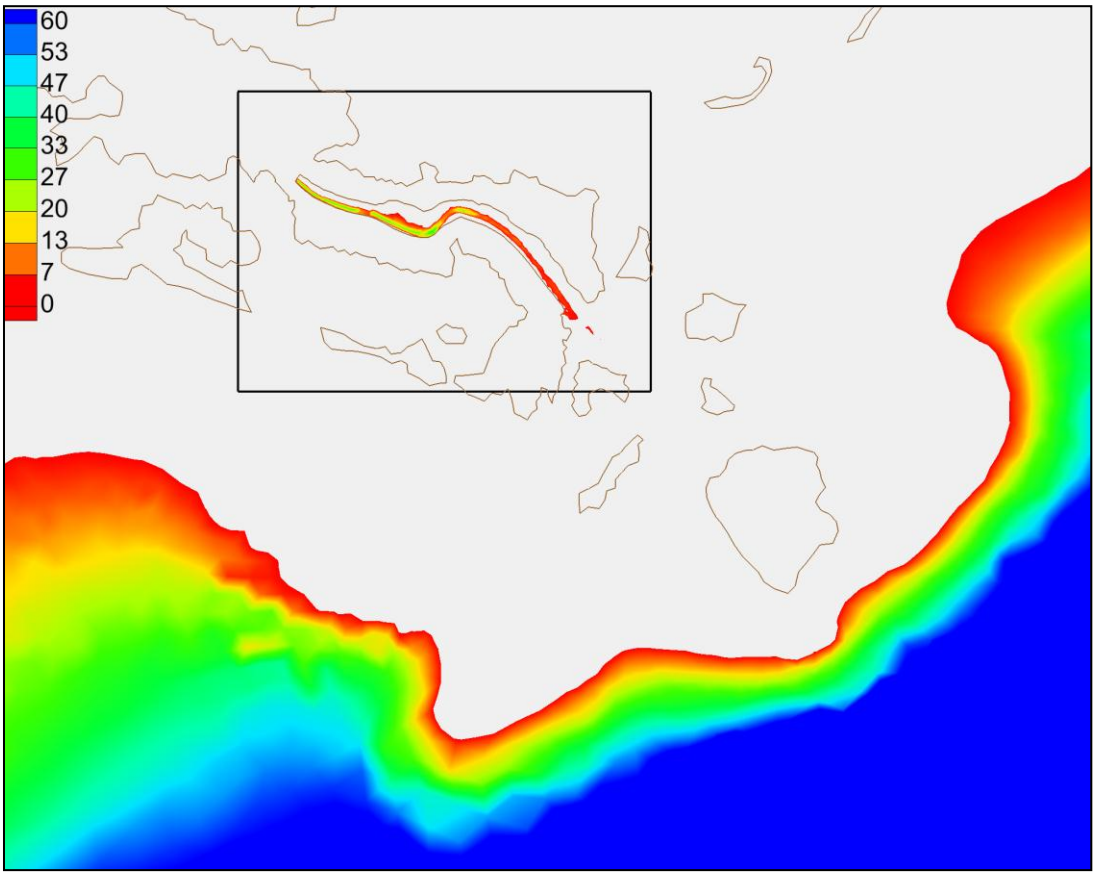

Figure A-1: 7.5ka depths (m) in the lower Louisiana, USA. Note that the Mississippi River is cut off from communication with the open ocean, yet this area produced exceedingly high tides in original model runs.

A similar effect occurred for the 8ka grid on the representation of the northeast section of the island of Cuba where a section of the Bay of Dogs was cut off from the open ocean yet experienced some forcing that caused excessive water heights in the model. Similarly, the depths of the local nodes in this area were manually changed to be 5 meters above sea level, and the subsequent model completed a full 90 day run. Since the unstable behavior outside the main body of water at a distance from the area of concern in the Delaware Bay, these depth changes would have had minimal, if any effect on tidal range results had the original runs been stable.

Tidal Range Changes in the Delaware Bay: Past Conditions and Future Scenarios

by

George F. Hall

A THESIS

submitted to

Oregon State University

in partial fulfillment of

the requirements for the

degree of

Master of Science

Presented May 21, 2012

Commencement June 2012

Tidal Range Changes in the Delaware Bay: Past Conditions and Future Scenarios

by

George F. Hall

A THESIS

submitted to

Oregon State University

in partial fulfillment of

the requirements for the

degree of

Master of Science

Presented May 21, 2012

Commencement June 2012

Tidal Range Changes in the Delaware Bay: Past Conditions and Future Scenarios

by

George F. Hall

A THESIS

submitted to

Oregon State University

in partial fulfillment of

the requirements for the

degree of

Master of Science

Presented May 21, 2012

Commencement June 2012